2008

Cluster kinetics modeling of glassforming materials

Lisa Ann Brenskelle
Louisiana State University and Agricultural and Mechanical College

CLUSTER KINETICS MODELING OF GLASSFORMING MATERIALS

A Dissertation

Submitted to the Graduate Faculty of the
Louisiana State University and
Agricultural and Mechanical College
in partial fulfillment of the
requirements for the degree of
Doctor of Philosophy

in

The Gordon A. and Mary Cain Department of Chemical Engineering

by

Lisa Ann Brenskelle
B.S. Carnegie Mellon University, 1989
B.A. Carnegie Mellon University, 1989
May 2008

ACKNOWLEDGEMENTS

Early work on this research was funded by Grant No. DGE–9987603 from the National Science Foundation. This work could not have been successfully completed without the guidance of Dr. Benjamin J. McCoy, Professor Emeritus, in the Department of Chemical Engineering and Materials Science at the University of California at Davis, the assistance of Dr. Martin A. Hjortsø, George H. Nusloch, II, Professor, in the Gordon A. and Mary Cain Department of Chemical Engineering at the Louisiana State University and Agricultural and Mechanical College, and the aide and support of my beloved husband, Elmer Ledesma.

TABLE OF CONTENTS

ABSTRACT

In this work, a new model relating temperature and pressure to dielectric relaxation or viscosity of a glassformer is developed. The model is based upon cluster kinetics, reaction-like mechanisms describing interactions between glassformer monomers and their clusters. Mathematical solutions of population balance equations for monomer and cluster lead to molar concentrations in terms of rate coefficients of the reaction-like mechanisms. These are then related to viscosity or dielectric relaxation time through free volume theory. The resulting equations are tested against data for a variety of pure glassformers, fragile, non-fragile, large, and small molecules over a wide range of temperatures, pressures, and dielectric relaxation times. It is found that the parameters of the cluster kinetics model are invariant to temperature and pressure and can be used to predict dielectric relaxation at other conditions. The parameters can thus be considered properties of the glassformer compound. Given this understanding of the parameters, the cluster kinetics model is then demonstrated to predict binary glassformer dielectric relaxation times for mixtures exhibiting a single relaxation in response to temperature, by application of a simple mixing rule to determine mixture parameters from the pure component parameters. For binary mixtures exhibiting two distinct relaxations in response to temperature, the pure component parameters are demonstrated to have predictive ability for the mixture. The same is demonstrated for glassformer solutions. Thus, the cluster kinetics model is shown to have broad applicability and to successfully predict dielectric relaxation behavior for pure glassformers, glassformer mixtures, and glassformer solutions.

CHAPTER 1
GLASS AND THE GLASS TRANSITION

1.1 Glass and the Glass Transition Definition

Glass is a long-lived metastable state of matter[1] exhibiting the mechanical properties of a solid, but, like a liquid, lacking long-range order[2]. As such, it is sometimes referred to as an amorphous solid[3], having no crystal structure. It does not constitute an equilibrium phase, because glassy materials are metastable. Glasses are also dynamically heterogeneous from a spatial perspective[2]. In general, it can be said that glass is a molecularly disordered, dense, and highly viscous form of matter formed when a fluid is cooled or compressed in a manner that avoids nucleation and crystallization[4]. Widespread in nature and technology, glassy materials are ordinarily formed when organic or inorganic liquids are cooled sufficiently rapidly that nucleation cannot occur. Such materials are characterized by a huge increase in viscosity as temperature decreases. Many disparate compounds exhibit a glassy form. It is frequent among polymers, but smaller compounds such as sorbitol, toluene, and propylene carbonate are also glassformers[5-7]. The glassy state is important to food processing, stabilization of labile biochemicals, insect life preservation under extreme conditions of cold or dehydration, geology, polymers in engineering plastics, optical fibers, the metals industry, photovoltaic cells, and for understanding the glassy state of water in outer space[8]. From a purely scientific perspective, glassy materials and the transition to glass from fluid are an active area of research[7]. Developing a quantitative understanding of glassforming transitions during supercooling or compression is a serious challenge in condensed matter science.

The glass transition, as observed experimentally, is a kinetic not thermodynamic phenomenon, characterized by the time scale for molecular rearrangements becoming longer

than the experimental time scale[9]. The glass transition is accompanied by a dramatic increase in viscosity or dielectric relaxation time for a decrease in temperature (or an increase in pressure). This dynamic slow-down is typically more than 10 orders of magnitude[2]. This occurs without any change in molecular configuration, as both the liquid and glassy states lack long-range order and are distinguished by their dynamic, not static, properties[9]. The mechanisms that underlie this transition are a subject of controversy and continue to be the topic of vigorous scientific debate[9]. A number of properties of glassforming materials change significantly at the glass transition, such as the coefficient of linear thermal expansion, the heat capacity, and the specific volume. Thus, there are a number of different ways to determine the glass transition temperature, T_g. Some methods that have been used include: differential thermal analysis, differential scanning calorimetry, thermochemical analysis, electric conductivity analysis, mechanical analysis, dielectric spectroscopy, and dilatomatry[10,11]. Figure 1 shows the glass transition induced by temperature, indicating the inflexion point where the specific volume V versus temperature T curve changes slope as the glass transition temperature. Differential scanning calorimetry, DSC, is perhaps the most commonly-applied method to determined T_g, and this T_g is termed the calorimetric T_g. In this approach, a plot such as Fig. 2 is used to determine T_g. Due to the variety of graphical approaches used, the glass transition temperature is often a range of values, with the midpoint of the range being assigned the designation glass transition temperature, T_g[12]. In fact, for polymers, the reported range for T_g is often around 20 ºC[10]. Some sources have reported that the value of T_g determined by these techniques is influenced by the starting state of the material[12], and it is known to depend on the rate of cooling[12,13]. Thus, to fully define a glass transition temperature, the cooling rate must be specified. Due to the inconsistencies of graphical approaches, the use of the dielectric T_g (as determined by dielectric spectroscopy)

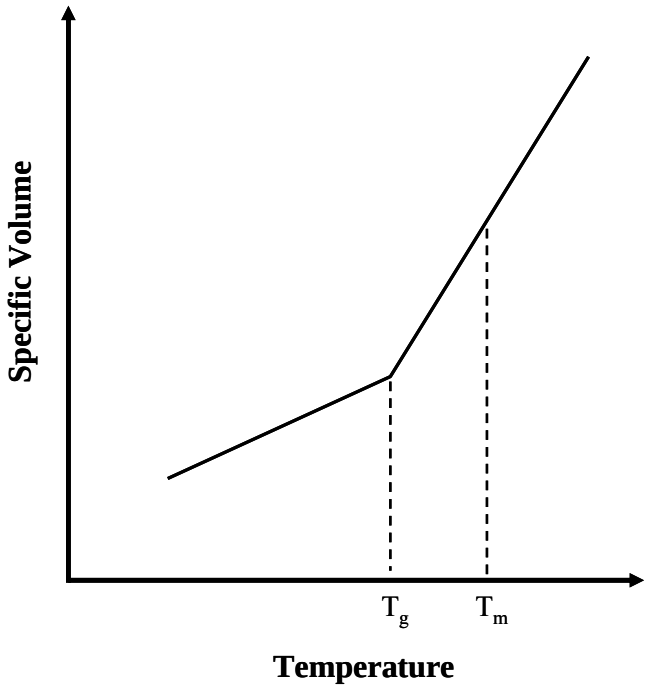

Figure 1 Plot of specific volume versus temperature used to determine the glass transition temperature, T_g. T_m is the melting point.

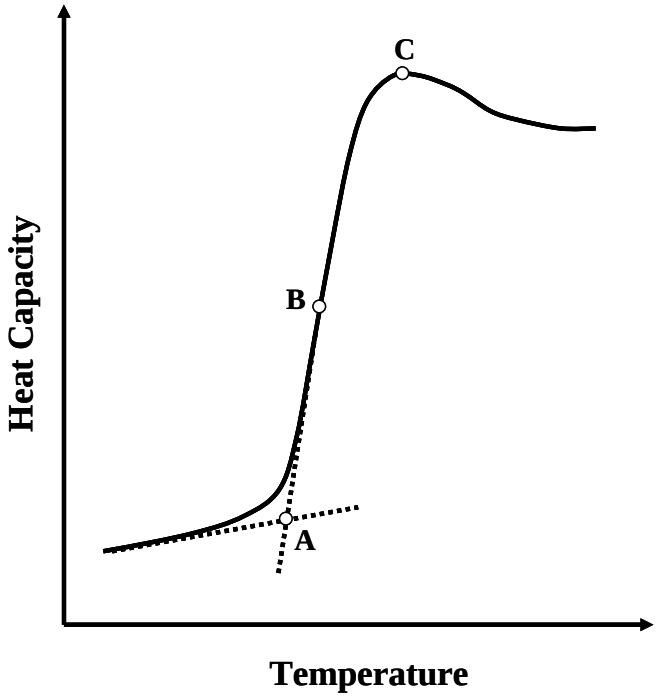

Figure 2 Plot of heat capacity versus temperature resulting from differential scanning calorimetry. Point A (the intersection of lines drawn through the two straight portions of the plot) is normally used to represent the calorimetric glass transition temperature, although points C (the maximum in the plot) and B (average of the methods for points A and C) are also found in the literature[11].

has become common in the literature. In this approach, a particular value of the dielectric relaxation time (values of 1 second, 10 seconds, and 100 seconds are often seen in the literature[5,14-16]) is designated as "glass" and the corresponding temperature or pressure as the dielectric T_g or P_g. For some glassformers, a dielectric relaxation time of 100 seconds corresponds to the glass transition temperature as determined by DSC[17,18], while for others τ = 1000 sec. corresponds to the calorimetric T_g[19]. Thus, there are various ways to determine the glass transition temperature, creating various definitions of T_g and more than one value of T_g or a range of values for a single compound. The majority of the literature data employed in this research has been generated by dielectric spectroscopy, and the dielectric T_g as defined at a dielectric relaxation of one second is used throughout.

The dielectric relaxation time, τ, can normally be related to the viscosity, although this relation has been reported to break down under certain conditions[20]. Thus, measuring the dielectric relaxation is akin to measuring viscosity, and designating a dielectric relaxation time as glass is similar to stating that glass occurs at a particular value of viscosity. The dielectric relaxation time is also employed because viscosity is a function of molecular weight for polymers, and many glassformers that are studied are polymers.

1.2 Measurements Related to the Glass Transition

Dielectric spectroscopy allows measurement of the movement of ionic species, as well the reorientation of dipolar molecules. It is the second measurement ability that is employed to determine the dielectric relaxation time. An impedance analyzer is used to determine dielectric loss in a compound versus frequency at different pressure and temperature combinations. The frequency at the maximum in the dielectric loss curve can be related to the dielectric relaxation time by

$$\tau = 1/(2*\pi*f_{max}) \qquad (1)$$

where f_{max} is the frequency at the maximum dielectric loss. The dielectric relaxation that is associated with the glass transition is the segmental (or α) relaxation, motions occurring on a 2-10 nm length scale[21]. The logarithm of the segmental dielectric relaxation is frequently plotted against the scaled inverse temperature in what is termed a fragility plot. Figure 3 is an example of such a graph. Fragility is quantified by taking the slope of this plot at the glass transition temperature[22]. This measure is termed the steepness index. The greater this index, the more fragile the compound is said to be. If the relation of the scaled inverse temperature to the logarithm of the dielectric relaxation time is essentially linear, it is termed Arrhenius behavior. For pressure-induced glass formation, a similar plot can be drawn using the scaled pressure in place of the scaled inverse temperature.

1.3 Modeling the Temperature and Pressure Response of Glassformers

As mentioned in the previous section, the nature of the glass transition is a subject of intense scientific investigation. The parameterization of experimental data related to the glass transition is the objective of a number of models developed to describe the behavior of glassforming materials in the vicinity of the glass transition, relating dielectric relaxation or viscosity to temperature and/or pressure. These models can be grouped into several types: phenomenological, free volume-based, and entropy-based. When tested over a broad range of temperatures and pressure, validation of a model is possible. Unfortunately, many models have failed to interpret the data in a consistent and precise manner.

1.3.1 Phenomenological Models

Among the phenomenological models, the most commonly-applied is that of Vogel, Fulcher, Tammann and Hesse (VFTH equation)[23],

$$\tau_\alpha(T) = \tau_0 \exp[B/(T - T_0] \qquad (2)$$

where τ_0, B, and T_0 are fitting parameters, with τ_α representing the segmental dielectric

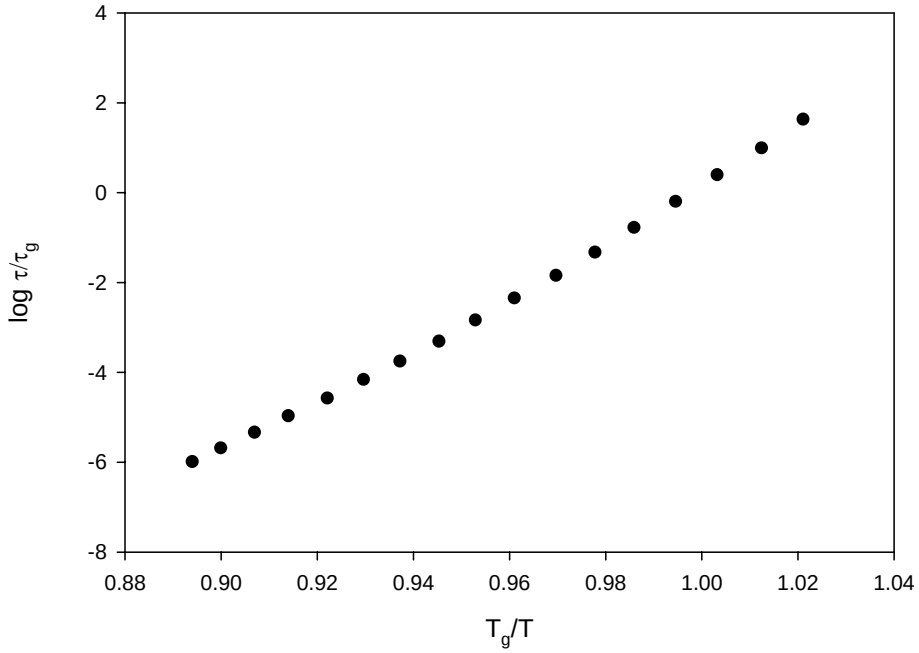

Figure 3 Fragility plot for salol[16], of scaled dielectric relaxation vs. scaled inverse temperature.

relaxation time and T representing temperature. This model, while widely used, has failed to fit higher temperature data for orthoterphenyl (OTP)[24]. In fact, it has been stated that, for fragile and intermediate glassforming compounds, the VFTH equation cannot describe the experimental data over a broad temperature range and two sets of VFTH parameters are required[25]. Equation (2) is the original model formulation. It has since been re-formulated for pressure-induced glass formation, using P instead of T in Eq. (2). Other authors have modified Eq. (2) with additional parameters[9], relating dielectric relaxation to temperature and pressure. Some of these formulations suffer from incorrect mathematical representations of observed phenomena (for example, one equation requires a linear relation of log τ_α to pressure, which is almost never seen in glassformers) or have limited application, particularly for data with varying pressure[9]. One of the models[26] based on the VFTH equation could not fit data for polymethyltolylsiloxane (PMTS) as precisely as other models.[27] Another model based upon Eq. (2), while successful in fitting some dielectric relaxation versus pressure data, has four additional fitting parameters[28], making it significantly more complex than the original VFTH equation.

1.3.2 Free Volume Models

Free volume models are based upon the concept that the motion of a molecule will depend on the open space in its vicinity (i.e. the free volume). The earliest free volume model, that of Cohen and Turnbull[29], was a formalization of the empirical Doolittle equation[30],

$$\eta = a_D \exp(b_D V_\infty / V_f) \qquad (3)$$

where η is viscosity, V_f is the free volume, V_∞ is the occupied volume, and a_D and b_D are constants. Recent research has shown that free volume shrinkage cannot account for the segmental relaxation time decrease for polyvinylacetate[31]. Other research indicates that

volume is not a dominant control variable for dielectric relaxation or viscosity[9]. Other models relating dielectric relaxation to T and P by using the fractional free volume, V_f/V_∞, have also been developed, but given the research data suggesting volume is not a controlling variable, and the model's neglect of thermal energy contributions to glass formation which are known experimentally to be quite significant, any free volume approach is likely to ultimately fail[9]. A model that relates conceptually to the free volume model is the hole model[32], which envisions each monomer trapped by its surroundings, with an activation energy necessary for it to leave the trap, and holes being the means by which it leaves. This model formulation, essentially an equation of state, is complex, and when used to determine the free volume, leads to the result that the compressibility of the occupied volume is almost as large as the free volume compressibility, a counter-intuitive result[33,34]. Among the models related to the free volume concept is the dynamic lattice liquid model[35,36], wherein molecules are assigned to sites in a lattice. In this model formulation, which relates the probability of local molecular rearrangements to temperature and the activation energy, rearrangement of the molecules is thermally activated, with an activation energy dependent on local density. In evaluating the activation energy parameter in the model, E, results are found that are either at odds with experimental data or in poor agreement with them[9,37]. A fourth free-volume related model is that of Cohen and Grest[38-41], which allows for a dynamically heterogeneous system. In this model, which relates dielectric relaxation to temperature, diffusion is dominated by the free volume. This equation has one more fitting parameter than Eq. (2), but also can fit experimental data over a wider range of temperature, which would require two different VFTH equations to fit. Although the original model was modified to include pressure effects, it cannot describe dielectric relaxation data at high pressure[42-44]. It has also failed

to fit data for polymethyltolylsiloxane (PMTS) as precisely as other models[27]. Another dynamic free-volume related model is the defect diffusion model[45-47]. In this formulation, a molecule can move when it encounters a "defect", a region of local free volume. In the defect diffusion model, which relates dielectric relaxation with temperature and pressure, the defects cluster as the pressure is raised or the temperature lowered. This model has five fitting parameters and fits dielectric relaxation data vs. pressure or temperature quite well. However, a feature of the defect diffusion model is that is predicts a strict correlation between the fragility and the breadth of the dielectric relaxation function and this correlation has been found to not hold experimentally at high pressure[48-50].

1.3.3 Entropy-based Models

The entropy-based models include the Avramov model[51], whose hypothesis is that the cooperative motions underlying the glass transition are thermally-activated. The Avramov model has failed to fit experimental data for polymethyltolylsiloxane (PMTS) as precisely as other models[27] and for 1,1'-di(*p*-methoxyphenyl)cyclohexane (BMPC) a fit of the Avramov model resulted in large errors in the fitting parameters, which were found to be interrelated[52]. This model formulation, which relates viscosity to activation energy and entropy, predicts that the fragility is independent of pressure, which is contrary to experimental results[49,50,53]. Given this inconsistency, the model was revised to agree with experimental findings[50]. The parameters in the Avramov model are measurable thermodynamic properties, but, in the case of polyvinylacetate, the parameter values obtained from fitting dielectric relaxation data did not agree with values deduced from the thermodynamic properties, calling this model into question[17]. The most commonly-applied of the entropy-based models is that of Adam and Gibbs[54]. This model envisions cooperatively-rearranging regions (CRR) that grow in size as the temperature is lowered,

but do not interact with one another. The size of the CRR is dependent on configurational entropy for this model. Thus, the dielectric relaxation slow-down is due to the increasing size of the CRR. The original Adam Gibbs model formulation is given by

$$\tau_\alpha = \tau_{AG} \exp(C_{AG} * \Delta\mu / T * S_c) \quad (4)$$

where C_{AG} is a constant, $\Delta\mu$ is the free energy barrier to rearrangement (per molecule), and S_c is defined as the entropy of the liquid minus the vibrational contribution. In practice, S_c is actually taken as the excess entropy. This model has been extended to account for pressure effects upon dielectric relaxation[55]. Various aspects of this model have been debated in the literature as inconsistent with experimental findings[56-59].

1.4 Conclusion

As described above, glassy materials are quite significant both industrially and scientifically and are considered an outstanding challenge in condensed matter physics[60]. Several models have been developed in the literature to describe dielectric relaxation or viscosity behavior of a glassformer as it approaches the glass transition, either by compression or rapid cooling, but all of these have deficiencies, such as failure to fit data for certain compounds or mathematical formulations that are complex or do not agree with experimental observations. Therefore, a better model that fits a broader range of dielectric relaxation or viscosity data versus temperature and pressure and whose mathematical formulation does not contradict observed behavior is needed. To develop such a model is the aim of this work.

CHAPTER 2
POPULATION BALANCE

2.1 Description of the Population Balance Equation and Its Applications

The population balance is equivalent to a statement of continuity for particulate systems. It is frequently applied to chemical engineering problems in granular processing. However, it can be applied to any system with discrete particles of varying sizes, such as polymerization reactions and soot formation[61,62]. Population balances have also been applied to phase transitions, biological systems, human dynamics, crystal growth and dissolution, gelation reactions, and spinodal decomposition[63-64], to name just a few applications. Its application in this work to the glass transition is based on reaction-like mechanisms of monomers (single molecules in random thermal motion) and clusters (a distribution of variably-sized groups of bonded molecules moving cooperatively) forming the conceptual basis for an understanding of the glass transition. This conceptual basis for understanding of the glass transition allows use of the population balance model to describe it, as it involves discrete particles of varying sizes, whether they be monomers or clusters. In general, when there is a distribution of particles of varying molecular weights, defined as $P(x)$, the molar concentration in the range $(x, x+dx)$ is given as $P(x)dx$. The properties of the distribution are defined by moments: The zeroth moment $P^{(0)} = \int_0^\infty P(x)dx$ is equivalent to total molar concentration, for example. The first moment, $P^{(1)} = \int_0^\infty P(x)xdx$ is equivalent to the mass concentration (i.e. total mass/volume). The average particle mass is the ratio, $P^{avg} = P^{(1)}/P^{(0)}$. A measure of polydispersity derives from the second moment. The general moment equations are determined by applying the operation $P^{(n)} = \int_0^\infty P(x)\, x^n\, dx$. Note that the distribution of

particle sizes for the cluster kinetics approach to the glass transition involves reaction-like mechanisms such that the distribution changes with time. Thus, for the problem at hand, *P* is not only a function of *x* (mass for the cluster kinetics approach to the glass transition), but also of *t* (time), *P(x, t).* In general, a distribution may be a function of both time and position, *P(x, t, $\underline{v}$).* The population balance equation is given by[61]:

$$\frac{\partial P}{\partial t} + \underline{\nabla} \cdot \left(\underline{v} P\right) + \frac{d}{dx}\left(\frac{dx}{dt} \cdot P\right) = B - D \tag{5}$$

where B is an accumulation term (particle birth) and D is a loss term (particle death). The above can be thought of as a particle balance. To define *dx/dt*, a rate expression is required. Eq. (5) is a microscopic population balance equation. There are also discrete forms of the population balance equation. For the case of the cluster kinetics development in Chapter 3, no spatial dependence is assumed as this a non-flow system (eliminating the second term in Eq. (5)). The third term in Eq. (5), which includes *dx/dt*, is also taken as zero (i.e. no change in mass with time) because of a requirement for local equilibrium conditions to define viscosity. Neglecting spatial dependence is frequent in applications of the population balance equation, as average properties throughout the volume of interest are all that is generally required[69]. Thus, the final population balance equation applied in this work reduces to:

$$\frac{\partial P}{\partial t} = B - D \tag{6}$$

Since average properties will be considered in this work, the moments of the particle distribution will be considered. Applying the moment operation to Eq. (5) gives:

$$\frac{\partial P^{(n)}}{\partial t} + \underline{\nabla} \cdot \left(\underline{v} P^{(n)}\right) + \int_0^{\infty} [dx \cdot x^{(n)} \frac{\partial}{\partial x}\left(\frac{dx}{dt} \cdot P\right)] = B^{(n)} - D^{(n)} \tag{7}$$

Given the assumptions listed above for this work, the moment equation will be reduced to:

$$\frac{\partial P^{(n)}}{\partial t} = B^{(n)} - D^{(n)} \tag{8}$$

Equations (6) and (8) will be applied in Chapter 3 for the model development.

CHAPTER 3
DEVELOPMENT OF THE CLUSTER KINETICS MODEL

3.1 Introduction

Chapter 1 has explained the importance of glassy materials and listed a number of models developed to relate the dielectric relaxation or viscosity of a pure compound to temperature and pressure at or near the glass transition. These existing models have all been demonstrated to have deficiencies. Thus, a more broadly-applicable model, whose parameters have meaning, and that can be readily applied to a variety of cases is needed.

The study of simple models is important to developing an understanding of glass.[70] An explanation commonly applied to glassy heterogeneous dynamics is based on the two–state concept. Angell *et al.*[71] reviewed how reaction-like mechanisms between the two states, A $\leftrightarrow$ B, had previously been used to devise an equilibrium constant K_{eq} = [A]/[B], which was related to free energy, and hence to enthalpy and entropy differences for the reaction. McCoy[72]observed, however, that the simplified two–state model does not distinguish cluster–cluster and monomer–cluster interactions. When such interactions are included, the concept provides a realistic and quantitative interpretation of the temperature dependence of glassformer viscosity.

The cluster-kinetics model developed below is based upon the concept that molecules cluster together as they approach the glass transition, and that this is the underlying physical phenomenon that explains glass formation. The clustering concept did not originate with this work[72-74], only the formal development of the concept into a model for the temperature and pressure effects on dielectric relaxation or viscosity. While this clustering behavior has not been confirmed by experimental evidence except in colloidal glassformers[60,75,76], it is conceptually attractive as an explanation and would explain the spatial dynamic

heterogeneities observed near the glass transition as well as the lowering of the glass transition temperature that has been observed in nano-confined materials[77]. In addition, evidence of a growing length scale when approaching the glass transition has been reported[78], which could certainly be explained by clustering. The cluster kinetics approach is also consistent with related models for nucleation, crystal growth, and subsequent ripening.[79] These phase transition steps are avoided if the glass–forming process is more rapid than the nucleation rate.

Although temperature effects for glassy materials have received more attention, the influence of pressure is also practically and theoretically important.[80] Computer experiments with particles having repulsive or attractive interactions reveal glasslike behavior when pressure increases and particles are forced to cluster together.[81] The volume dependence of energy landscapes was also reported to be significant in pressure–induced glassy behavior.[82]

The objective of this work is to explore the temperature and pressure–induced vitrification of a metastable liquid. Cluster kinetics of glass formation is extended, via transition state theory, to include activation energies and volumes in the rate coefficients for monomer–cluster addition–dissociation and cluster aggregation–breakage. The glass formation kinetics are based on the dynamics of hypothesized cluster–monomer distributions in liquids. The consequences of this hypothesis for metastable liquids that do not nucleate are interpreted in terms of fragility plots for the pressure and temperature effects on dielectric relaxation time, and thus on viscosity. On the basis of free volume ratios the proposed model provides activation volume and activation energy values that allow representation of the viscosity. Given values of pressure and temperature at the glass transition and when the material is fluid, two parameters, a volume–difference parameter and an energy-difference parameter are needed to complete the correlation.

3.2 Model Development

The underlying concept of the cluster kinetics model is that a glassformer exhibits clustering behavior as it is supercooled and approaches the glass transition. The formulation includes monomers in the fluid, which are separately in random thermal motion, and clusters, groups of bonded molecules moving cooperatively. Let x and x_m be the masses of clusters and monomer, respectively. Reversible addition of monomer $\boldsymbol{M}(x_m)$, to a cluster $\boldsymbol{C}(x)$ is represented by

$$\boldsymbol{C}(x) + \boldsymbol{M}(x_m) \underset{k_d}{\overset{k_g}{\leftrightarrows}} \boldsymbol{C}(x + x_m), \tag{9}$$

with rate coefficients k_g and k_d for growth and dissociation, respectively. The clusters may aggregate with rate coefficient k_a or fragment with breakage rate coefficient k_b,

$$\boldsymbol{C}(x) + \boldsymbol{C}(x') \underset{k_b}{\overset{k_a}{\leftrightarrows}} \boldsymbol{C}(x + x'). \tag{10}$$

The above reaction-like equations represent fluctuating heterogeneous structures within the metastable liquid. The four rate coefficients are considered independent of x, and all have temperature and pressure dependence given by transition–state theory. Population dynamics equations for the monomer and cluster can be formulated[72] and solved for moments of the distributions, where zero moments are total molar concentrations. The balance equations (11) and (12) that govern the distribution of the clusters, $c(x,t)$, and of the monomer, $m(x,t)$, are based on mass conservation (population balance) equations for the processes represented by Eqs. (9) and 10):

$$\partial c/\partial t = -k_g c\int_0^{\infty} m(x')dx' + k_g\int_0^{x} c(x\text{-}x')m(x')dx' - k_d\, c + k_d\int_x^{\infty} c(x')\,\delta[x\text{-}(x'\text{-}x_m)]\,dx' -$$

$$2k_a c\int_0^{\infty} c(x')dx' + k_a\int_0^{x} c(x')c(x-x')dx' - k_b\, c + 2k_b\int_x^{\infty} c(x')dx'/x' + I\,\delta(x-x^*) \quad (11)$$

and

$$\partial m/\partial t = -\,k_g m(x)\int_0^{\infty} c(x')dx' + k_d\int_x^{\infty} c(x')\,\delta(x-x_m)dx' - I\delta(x-x^*)x^*/x_m \qquad (12)$$

Explanatory comments on each term in Eqs. (11) and (12) can be found in the Appendix. Nucleation, represented as a source term in Eq. (11), is a sink term in Eq. (12) where the nuclei of mass x^* are composed of monomers of mass x_m. Integral forms of the rate expressions in the population balances lend themselves to calculations by moments, defined as integrals over x,

$$c^{(n)}(t) = \int_0^{\infty} c(x, t)x^n\, dx. \qquad (13)$$

The zeroth moment, $c^{(0)}(t)$, is the time-dependent molar concentration, and the first moment, $c^{(1)}(t)$, is mass concentration (mass/volume) of clusters. The average cluster (particle) mass is the ratio, $c^{avg} = c^{(1)}/c^{(0)}$, and with cluster mass density could be used to define a length scale for temperature dependent inhomogeneity[83](cluster size). A measure of polydispersity derives from the second moment. The general moment equations are determined by applying the operation $\int_0^{\infty}[\,]\,x^n\,dx$,

$$dc^{(n)}/dt = -(k_d + k_g m^{(0)})c^{(n)} + \sum_{j=0}^{n} \binom{n}{j} x_m^{n-j}\, c^{(j)}[(-1)^{n-j}\, k_d + k_g m^{(0)}] - 2k_a c^{(0)}c^{(n)} +$$

$$k_a\sum_{j=0}^{n} \binom{n}{j} c^{(j)}\, c^{(n-j)} - k_b c^{(n)} + 2k_b c^{(n)}/(n+1) + I\, x^{*n} \qquad (14)$$

and

$$dm^{(n)}/dt = [k_d\, x_m^{\,n} - k_g m^{(n)}]c^{(0)} - I\, x^{*n}x^*/x_m \qquad (15)$$

It follows that the cluster moment equations for $n = 0$ and 1 are

$$dc^{(0)}/dt = [k_b - k_a c^{(0)}]\, c^{(0)} + I \tag{16}$$

$$dc^{(1)}/dt = x_m c^{(0)}[-k_d + k_g m^{(0)}] + I\, x^* \tag{17}$$

Equations (15) and (17) together satisfy the mass balance, $dc^{(1)}/dt + x_m dm^{(0)}/dt = 0$. In the absence of nucleation (I = 0), for $n = 0$, Eqs. (15) and (16) are equivalent to Eqs. (18) and (19) below. The first and zero moments of the size distribution give an average mass of cluster, which with a cluster density provides an average cluster volume. This interpretation suggests how to define the elusive length parameter for glass materials. As a local equilibrium condition is required for the representation of viscosity, the rate expressions can be written directly according to the mass action principle for Eqs. (9) and (10), yielding the same result as the population balance, shown in Eqs. (18) and (19) below. In terms of the molar concentrations of fluidized monomer and clusters, $m^{(0)}(t)$ and $c^{(0)}(t)$, respectively, the rate expressions[72] are

$$dm^{(0)}/dt = (k_d - k_g m^{(0)})\, c^{(0)} \tag{18}$$

and

$$dc^{(0)}/dt = (k_b - k_a c^{(0)})\, c^{(0)}\ . \tag{19}$$

Growth and aggregation processes are second–order rate expressions in terms of concentrations, whereas dissociation and breakage are first–order according to Eqs. (9) and (10).

Each rate coefficient in Eqs. (9) and (10) is assumed to have temperature and pressure dependence given by transition state theory,[84,85] and is thus proportional to $\exp(-E/k_BT - P\mathcal{V}/k_BT)$. The activation energy E is the difference in energies of reactant and transition state; the activation volume $\mathcal{V}$ is the difference in volumes of reactant and transition state (Fig. 4).

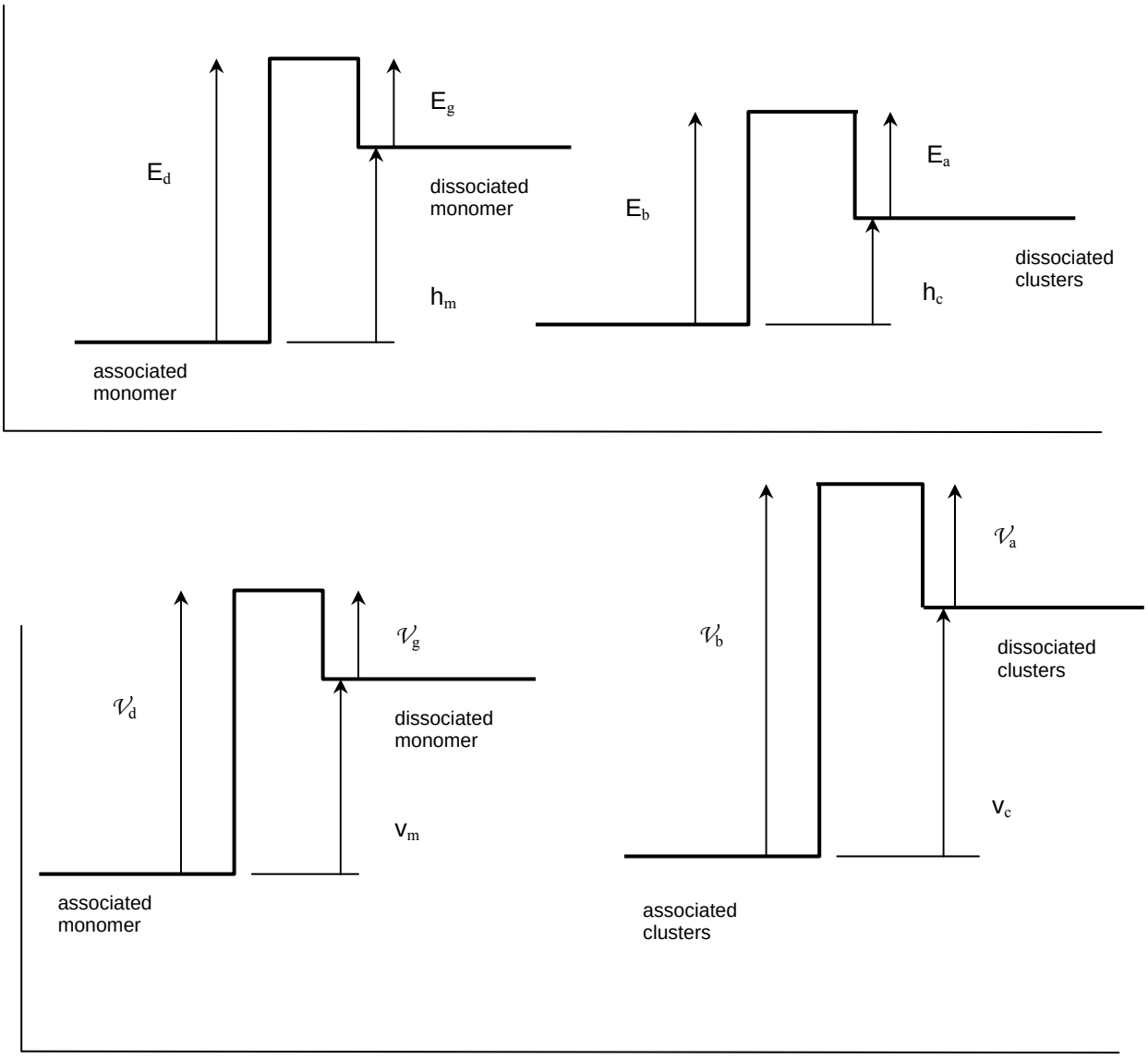

Figure 4 Elements of the energy landscape. Energy and volume barriers are based on transition state theory for reversible monomer–cluster growth and dissociation and cluster–cluster association and breakage [Eqs. (17) and (18)]. Energies and volumes of transformation are differences in activation energies and volumes: $h_m = E_d - E_g$, $h_c = E_b - E_a$, $v_m = \mathcal{V}_d - \mathcal{V}_g$, and $v_c = \mathcal{V}_b - \mathcal{V}_a$.

Localized thermodynamic equilibrium conditions are determined by setting the time derivatives in Eqs. (18) and (19) to zero. The equilibrium values of monomer and cluster concentrations are then ratios of the rate coefficients,

$$m^{(0)}_{eq} = k_d/k_g = \kappa_m \exp(-h_m/k_BT)\exp(-Pv_m/k_BT) \quad (20)$$

and

$$c^{(0)}_{eq} = k_b/k_a = \kappa_c \exp(-h_c/k_BT)\exp(-Pv_c/k_BT) \; . \quad (21)$$

The volumes $v_m = \mathcal{V}_d - \mathcal{V}_g$ and $v_c = \mathcal{V}_b - \mathcal{V}_a$ are differences in activation volumes[85] for Eqs. (9) and (10) and represent volumes of transformation for reversible growth and aggregation. The energies $h_m = E_d - E_g$ and $h_c = E_b - E_a$ are differences in activation energies for Eqs. (9) and (10) and represent heats of transformation. The coefficients κ_m and κ_c are proportionality constants. The dimensionless parameters h_m/k_BT and h_c/k_BT, and Pv_m/k_BT and Pv_c/k_BT, are thus measures of the sensitivity of the metastable liquid to temperature and pressure, respectively. Activation energies for the forward (association or aggregation) processes of Eqs. (9) and (10) are less than reverse (dissociation or breakage) processes. The reaction progress of a dynamic system undergoing cooling and compression represents fluctuations among a large number of monomers and clusters as they proceed over peaks and through valleys to lower energies. Such a process can be interpreted as an excursion over an energy landscape in a large dimensional hyperspace. Unlike other suggested abstract energy landscapes, however, the current picture is unambiguously defined by the energy transformation parameters h_m and h_c, and the volume transformation parameters v_m and v_c. Rather than the stochastically varying peaks and valleys pictured in some theories, the proposed energy landscape has a regular and readily defined character that, as will be demonstrated, realistically represents observed features of glass formation.[72] Eqs. (20) and (21) can be used to construct all the local thermodynamic quantities for metastable liquids.

Cluster dynamics can be related to observable kinetics of vitrification through free volume theory.[86] The Turnbull–Cohen theory[87] is consistent with the empirical Doolittle[88] equation, which allows quantitative representation of the relative effects of clusters and solute on viscosity,[72, 86]

$$\eta = a \exp(b'V) , \tag{22}$$

where V is the ratio of cluster and monomer volumes $V = m^{(0)}_{eq} / c^{(0)}_{eq}$, and a and b' are constants. This relation for V is valid if $m^{(0)}_{eq}$ is taken as moles of monomer/volume of monomer, and $c^{(0)}_{eq}$ as moles of clusters per volume of clusters. Substituting Eqs. (20) and (21), and combining with Eq. (22) to obtain for the viscosity,

$$\eta = a \exp(b\Phi) \quad . \tag{23a}$$

Here, b is a parameter to be determined by the viscosity of the fluid phase, and Φ is an exponential function of T and P,

$$\Phi = \exp[(h + Pv)/k_B T], \tag{24}$$

where

$$h = h_c - h_m = E_b - E_a - (E_d - E_g) \tag{25}$$

and

$$v = v_c - v_m = \mathcal{V}_b - \mathcal{V}_a - (\mathcal{V}_d - \mathcal{V}_g). \tag{26}$$

Note that using the inverse of V merely causes the terms on the right hand side of Eqs. (25) and (26) to be reversed.[72] As shown previously,[72] the double exponential in Eq. (23a) denotes a viscosity temperature dependence stronger than exponential, except for the special case $(h + Pv)/k_B T << 1$, when Arrhenius dependence holds. Avramov[51] also proposed a double–exponential relation for η, but with viscosity related to the double exponential of entropy. In Eq. (23a), the entropic contribution to viscosity is in the pre–exponential parameter b.

As the viscosity is proportional to the dielectric relaxation time τ, its pressure and temperature dependence can also be determined. For polymers the viscosity η is largely controlled by molecular weight, and dielectric relaxation is preferable to viscosity to determine the glass or fluid state.[89] Although the proportionality has been reported to break down for some substances,[20] for many materials Eq. (23a) can be re-written as

$$\tau = \alpha \exp(b\Phi). \tag{23b}$$

A goal is to determine a scaled equation for the temperature and pressure dependence of viscosity or dielectric relaxation time in terms of glass and fluid conditions. In general, scaled expressions for any two conditions of temperature and pressure can be derived, for example, let

$$\eta(T=T_1, P=P_1) = \eta_1 \text{ and } \eta(T=T_2, P=P_2) = \eta_2 \tag{27a}$$

or

$$\tau(T=T_1, P=P_1) = \tau_1 \text{ and } \tau(T=T_2, P=P_2) = \tau_2. \tag{27b}$$

It is straightforward to eliminate a and b in Eq. (23a), or α and b in Eq. (23b), to obtain,

$$\ln(\eta/\eta_2)/\ln(\eta_1/\eta_2) = (\Phi - \Phi_2)/(\Phi_1 - \Phi_2) = \ln(\tau/\tau_2)/\ln(\tau_1/\tau_2), \tag{28}$$

where Eq. (24) defines Φ,

$$\Phi_1 = \exp[(h + P_1 v)/k_B T_1], \tag{29}$$

and

$$\Phi_2 = \exp[(h + P_2 v)/k_B T_2]. \tag{30}$$

The above scaled Eq. (28) with Φ defined in Eq. (24) can be applied at a constant pressure P to determine the temperature effect, or at a constant temperature T to determine the pressure effect on viscosity or dielectric relaxation time.

For a constant pressure P the glass transition temperature, $\eta(T=T_g) = \eta_g$ or $\tau(T=T_g) = \tau_g$, and the fluid temperature, $\eta(T=T_f) = \eta_f$ or $\tau(T=T_f) = \tau_f$, can be substituted into Eq. (28) to give the scaled equation,

$$\ln(\eta/\eta_g)/\ln(\eta_f/\eta_g) = (\Phi - \Phi_g)/(\Phi_f - \Phi_g) = \ln(\tau/\tau_g)/\ln(\tau_f/\tau_g), \quad (31)$$

where η_g and η_f are of the order 10^{14} and 10^{-1} poise, respectively. For constant pressure this expression provided quite good agreement with experimental data[72] when $h_p = h + Pv$ was used as a fitting parameter. This result was compared with experimental measurements by means of the empirical equation of Cohen and Grest.[38]

Equation (28) shows how in the absence of nucleation it is possible for the viscosity of a glassformer to increase to that of a higher density glass under cold isothermal compression. Such an unnucleated collapse can be explained qualitatively with an abstract potential energy landscape.[89] Here quantitative means to interpret the phenomenon by means of activation volumes in cluster–fluctuation rate expressions is provided.

Similarly to the constant pressure case, for a constant temperature near T_f, the glass transition pressure can be defined as $\tau(P=P_g) = \tau_g$, and the fluid pressure as $\tau(P=P_f) = \tau_f$. Equation (28) becomes

$$\ln(\tau/\tau_g)/\ln(\tau_f/\tau_g) = (\psi - \psi_g)/(\psi_f - \psi_g), \quad (32)$$

where

$$\psi = \exp(Pv/k_BT),\ \psi_g = \exp(P_gv/k_BT), \text{ and } \psi_f = \exp(P_fv/k_BT). \quad (33)$$

The energy terms cancel in the scaled equation, leaving only the volume terms in v.

Applying the identity $\psi = \psi_g^{P/Pg}$, fixing τ_f by the limit condition $\tau(P\rightarrow 0) = \tau_f$, and letting $\tau_g = 1$ s, $\log_{10}(\tau)$ can be expressed as a function of P/P_g according to

$$\log_{10}(\tau/\tau_g) = [(\psi_g^{P/Pg} - \psi_g)/(1 - \psi_g)] \log_{10}(\tau_f/\tau_g). \quad (34)$$

As with temperature–dependent viscosity, Eq. (34) can be displayed as a plot of $\log_{10}(\tau/\tau_g)$ versus P/P_g. The result, Fig. 5, is similar to temperature fragility plots, except that P/P_g replaces T_g/T, and τ replaces η. The parameter in Fig. 5 is ψ_g, such that $\ln \psi_g = vP_g/k_BT$ varies as 0.001, 0.693, 1.39, 2.303, 3.40, and 4.605.

It is clear that $\ln \Phi_g = h_p/k_BT_g$ and $\ln \psi_g = vP_g/k_BT$ play similar roles in determining the glass fragility; thus, if $vP_g/k_BT << 1$ the pressure dependence of $\log \tau$ is linear. The symmetry of the fragility plots stems from the symmetry of the underlying cluster processes [Eqs. (9) and (10)], which is also reflected in the symmetric mathematical description, e.g., Eq. (28).

As indicated by Eqs. (27) and (28), the model with constant v and h applies for any two conditions denoted by subscripts 1 and 2. A material at zero pressure may be a fluid only if the temperature is near T_f. Thus Eq. (32) can be written in terms of the glass pressure, P_g, and any other intermediate pressure, P_{f*}. In this case, P_{f*} is not assumed to be zero, and Eq. (34) takes a slightly more complex form:

$$\log_{10}(\tau/\tau_g) = [(\psi_g^{P/Pg} - \psi_g)/((\psi_g^{Pf*/Pg} - \psi_g)] \log_{10}(\tau_{f*}/\tau_g). \quad (35)$$

If a similar identity is applied to the constant pressure case, $\Phi = \Phi_g^{Tg/T}$, an equation of the same format is obtained:

$$\log_{10}(\tau/\tau_g) = [(\Phi_g^{Tg/T} - \Phi_g)/((\Phi_g^{Tg/Tf*} - \Phi_g)] \log_{10}(\tau_{f*}/\tau_g). \quad (36)$$

Eq. (36) is valid regardless of the second temperature used with T_g.

3.3 Conclusion

An interpretation of glass transition and metastable liquid has been presented that includes both temperature and pressure influences. The simple model presumes that fluctuations are cluster–based, dynamic restructuring processes in the metastable liquid. The

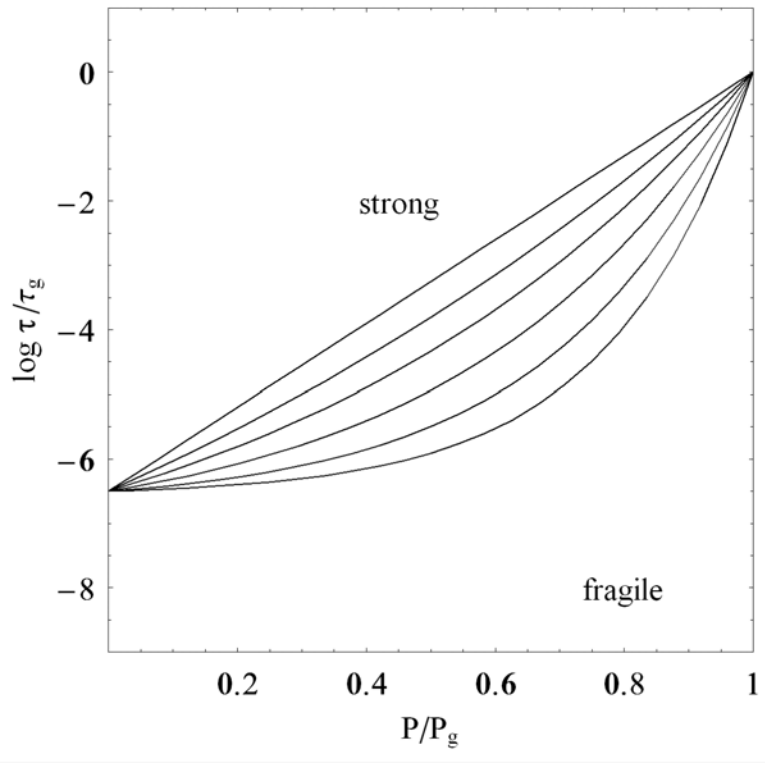

Figure 5 Fragility plot for dielectric relaxation increase during pressure–induced glass formation. The parameter $\ln \psi_g = vP_g/k_BT$ varies as 0.001, 0.693, 1.39, 2.303, 3.40, and 4.605 (left to right) and $\log \tau_f$ is set to –6.5.

model for fluctuations combines reversible growth and aggregation of solid clusters from monomer solute. The model development made use of population balance equations for monomer and cluster, which were solved for molar concentrations of monomer and cluster in terms of the rate coefficients. Thus, rate equations for the cluster and monomer concentrations for the reaction-like processes lead to local equilibrium equations in terms of rate coefficients. Transition–state expressions for temperature and pressure effects provide activation energies and volumes. The free–volume theory shows how these rate expressions combine to yield a scaled equation for viscosity or dielectric relaxation. In the absence of nucleation, the amorphous "phase" transition behavior described by this kinetics approach appropriately correlates the temperature and pressure dependence of the glass transition and provides representations of metastable liquids exhibiting strong or fragile character.

CHAPTER 4
APPLICATION OF THE CLUSTER KINETICS MODEL TO PURE COMPOUNDS

4.1 Introduction

Developing a quantitative understanding of glassforming transitions during supercooling or compression is a serious challenge in condensed matter science. The objective of this chapter is to explore the temperature or pressure–induced vitrification of a metastable liquid, using the cluster kinetics model developed in Chapter 3. Equations (35) and (36) will be applied to a total of ten compounds in the sections that follow, including those (OTP, BMPC, and PMTS) that other glass transition models failed to adequately represent, as noted in Chapter 1. The cluster kinetics model will be shown to quantitatively describe a variety of glassformers of varying molecular weights and differing fragilities. The range of experimental data to be modeled for pressure, temperature, and relaxation time includes pressures and temperatures above and below the dielectric glass transition and relaxation times that vary over nearly twelve decades. The parameters h and v (difference of activation energy and activation volume differences) will be demonstrated to be invariant to pressure and temperature; parameters determined at one set of conditions will successfully be applied at other temperatures and pressures to predict the dielectric relaxation, given T_g , P_g, T_{f^*} , P_{f^*},and log τ_{f^*}/τ_g at the new conditions. This evidence supports the contention that h and v are properties of the compound, and not merely fitting parameters, and have physical meaning as described in Chapter 3. The subsequent sections of this chapter demonstrate the broad applicability and ease of use of the cluster kinetics model.

4.2 General Method

In general, the method of application of the cluster kinetics model begins with the selection of two data points, fluid and glass, from either a constant pressure or a constant

temperature data set. The fluid point is generally taken as the highest temperature in a constant pressure data set, or as the lowest pressure in a constant temperature data set. The glass point is defined at $\tau = 1$ second. These two data points are substituted into Eq. (35) for a constant temperature data set or into Eq. (36) for a constant pressure data set and a regression of the experimental data is performed. The regression yields ψ_g (for Eq. (35)) or Φ_g (for Eq. (36)). From ψ_g the value of v is calculated, and given this value, from Φ_g the value of h is calculated. If no constant temperature data set is available for a given compound, h_p can be determined instead of h and v.

4.3 Application of the Cluster Kinetics Model to Eight Pure Compounds at or Near 293 K

Published experimental data[15,25,27,90-94] (Figs. 6, 7) for dielectric relaxation times measured for different compounds with variable pressure and constant temperature at or near 293 K is considered first. For each compound, a value of ψ_g is determined by fitting the data to Eq. (35), (Figs. 6 and 7). For plots of log τ/τ_g versus P/P_g, all curves intersect at the common point $\tau(P/P_g = 1)/\tau_g = 1$. Full names and parameter values for the compounds are provided in Table 1. Once ψ_g was calculated, the activation volume parameter v was determined from Eq. (33). Table 1 gives the values of P_g and log τ_{f*}/τ_g used in Eq. (35) and values obtained for ψ_g and v. The estimates of the uncertainty in ψ_g, calculated as 1.96 × standard error, are fairly small, with maximum uncertainty ~ 12%. Also given is the curve–fit correlation coefficient R^2, indicating that the data were fitted quite well by Eq. (35). In some cases, the range of experiments was limited and before the data could be fitted, it was necessary either to extrapolate or interpolate a P_g versus T_g plot to obtain P_g (the pressure at which $\tau = \tau_g = 1$ s). In the case of PMTS and PBD, plots of P_g versus T_g were available in the literature,[15,27] and a linear interpolation between two given data points was sufficient to determine P_g at $T = 293$ K and 293.2 K, respectively. For DGEB, a plot of P_g versus T_g was

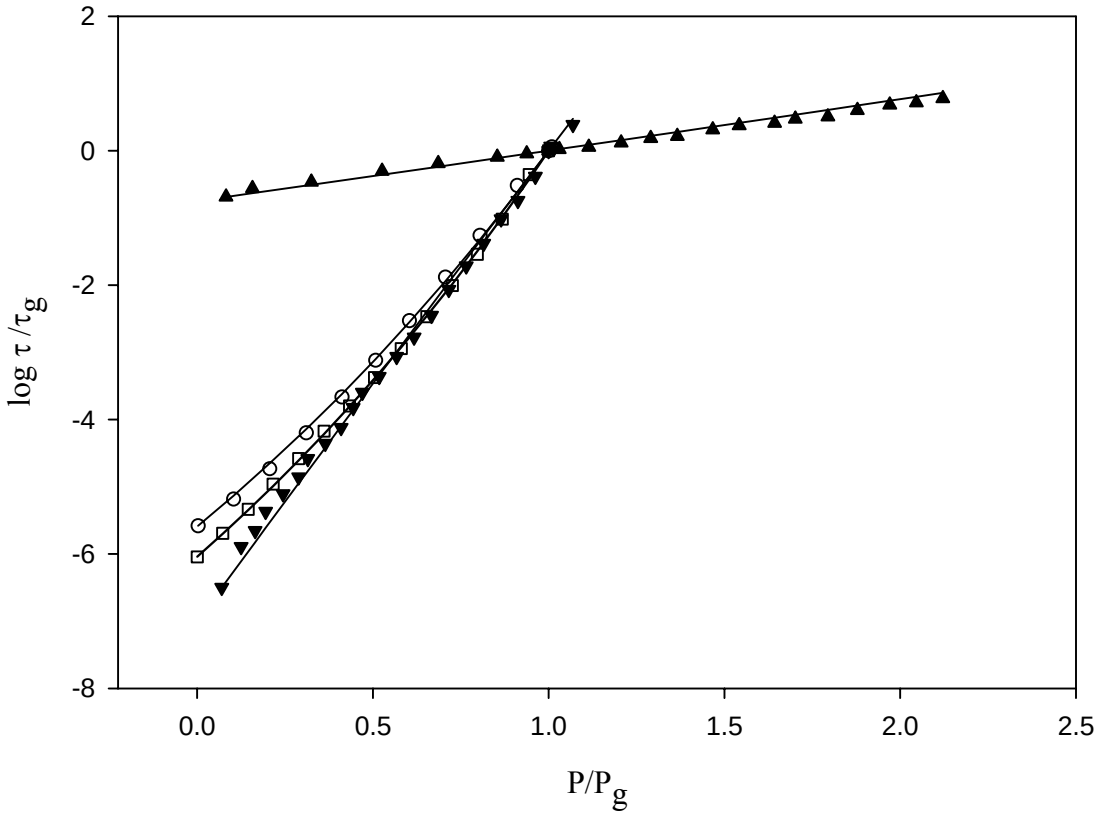

Figure 6 Plot of the log of scaled dielectric relaxation time versus scaled pressure for PBD (□), IPCB (▲), PGEC (○) and DAR (▼) at ~ 293 K. Model fits are shown as lines with parameters of Table 1 and experimental data [15, 90, 91, 94] as points. The defined point at log $\tau_{f^*}/\tau_g = 0$ at $P/P_g = 1$ has been added to the data sets.

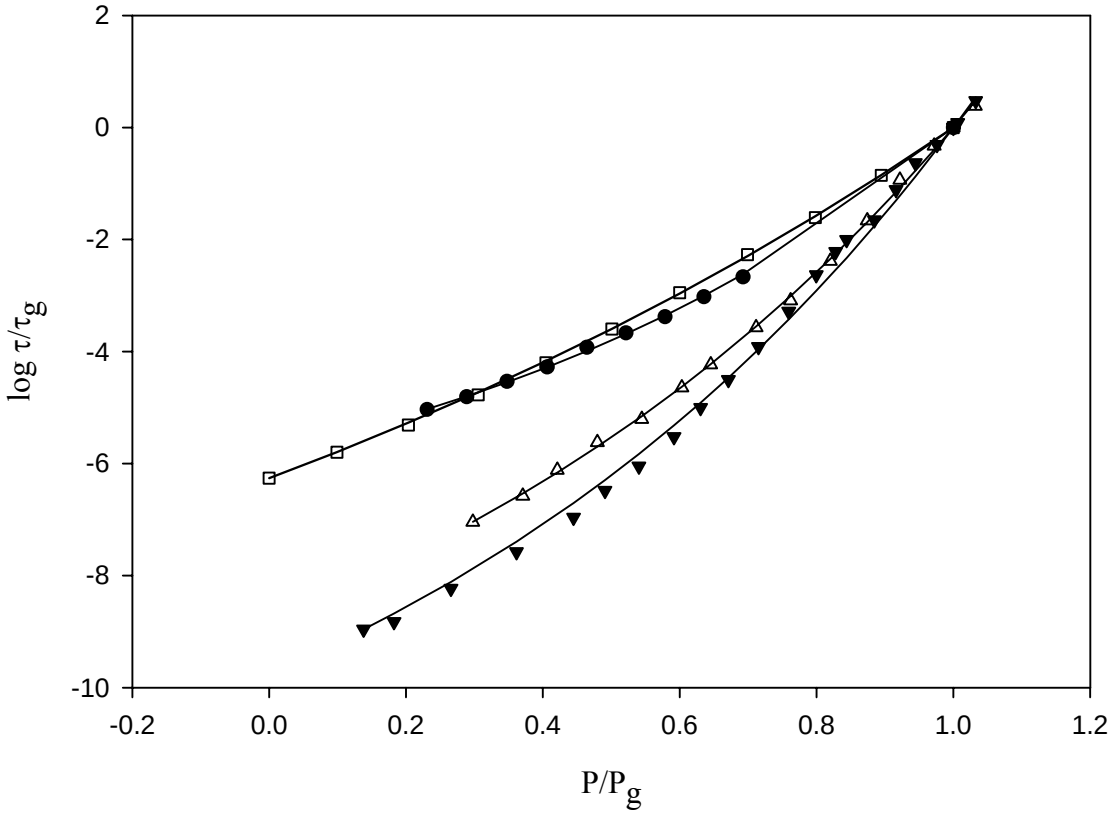

Figure 7 Plot of the log of scaled dielectric relaxation time versus scaled pressure for PMTS (□), PPG (△), DGEB(●) and DEP (▼) at ~ 293 K. Model fits are shown as lines with parameters of Table 1 and experimental data [27,25,92,93] as points. The defined point at log $\tau_{f*}/\tau_g = 0$ at $P/P_g = 1$ has been added to the data sets.

Table 1 Parameters ψ_g and v evaluated for experimental data by regression with Eq. (35). T, P_g, and log τ_{f*}/τ_g are given for each data set, with P_g values determined from extrapolation of a P_g vs. T_g plot designated by *. The correlation coefficient R^2 demonstrates the quality of the fit and ± 1.96 × the standard error estimates the uncertainty in ψ_g.

Chemical	T (K)	P_g (MPa)	log τ_{f*}/τ_g	ψ_g	R^2	v / 10^{-29}m^3
DAR[a]	293	1263	-6.50	0.961 ± 0.093	0.996	-0.0127
(dendrimeric alkyd resin)						
PPG[b]	293	859	-7.04	3.01 ± 0.24	0.999	0.517
(poly–propylene glycol)						
PMTS[c]	293	102	-6.26	1.83 ± 0.049	0.999	2.40
(polymethyltolylsiloxane)						
PGEC[d]	293.5	200	-5.58	1.65 ± 0.11	0.999	1.01
(polyphenyl glycidal ether coformaldehyde)						
PBD[e]	293.2	275	-6.04	1.69 ± 0.052	0.999	0.777
(1,2–polybutadiene)						
IPCB[f]	293	59.4	-0.69	1.02 ± 0.023	0.998	0.161
(isopentylcyanobiphenyl)						
DGEB[g]	293	217*	-5.03	3.66 ± 0.23	0.998	2.42
(diglycidal ether of bisphenol A)						
DEP[h]	293.65	1124	-8.96	3.09 ± 0.38	0.996	0.407
(diethyl phthalate)						

[a]Reference 91.
[b]Reference 93.
[c]Reference 27.
[d]Reference 90.
[e]Reference 15.
[f]Reference 94.
[g]Reference 92.
[h]Reference 25.

determine P_g at T = 293 K and 293.2 K, respectively. For DGEB, a plot of P_g versus T_g was not available, but was obtained by determining P_g and T_g for nine data sets found in the literature.[92] A linear extrapolation then provided P_g at T = 293 K. The value of τ at which P = 0 was chosen as τ_{f*}, or if the data set did not include this pressure, then τ at the lowest pressure was selected as τ_{f*}. The lowest pressure varied widely between data sets, from ~ 0 MPa to 200 MPa.

The compounds represent widely varying molecular weights, from polymers to much smaller molecules. In addition, the range of experimental data, for both pressure and relaxation time is quite broad. Pressures above and significantly below the glass transition are included, and relaxation times vary over nearly eleven decades (10^{-9} – 10 s). The compounds also reflect a range of fragilities, from linear (Arrhenius) behavior to more fragile behavior, with ψ_g varying from less than one to nearly four. Of the eight compounds, DAR and IPCB show an essentially linear relation of log τ/τ_g to pressure, reflected by a zero or nearly zero value of v (Table 1), whereas the others all have nonzero v. It should be noted that the data for IPCB cover an especially broad range of pressures, from fluid to well beyond the glass transition. In Table 1, a measurement at zero pressure, which seems to deviate from the linear relation, was eliminated from the data set prior to fitting with Eq. (35). Rejecting the point gives ψ_g = 1.024 and $v = 0.161 \times 10^{-29}$ m^3 whereas if this point is retained, the fit yields ψ_g = 0.895 and $v = -0.755 \times 10^{-29}$ m^3.

4.4 Determination of Sensitivity to Selection of Fluid Point

To test if Eq. (35) would give the same results for ψ_g, and thus for the parameter v, regardless of the pressure and dielectric relaxation time selected as P_{f*} and τ_{f*}, the Eq. (35) fit was repeated with measurements from the data sets of τ_{f*} at pressures other than the lowest. For the same compounds, results are shown in Table 2, indicating that ψ_g did not vary much

Table 2 Parameter ψ_g evaluated for experimental data by regression with Eq. (35), using various pressures as P_{f*}. P_{f*}/P_g and log τ_{f*}/τ_g for each regression are given.

Chemical	ψ_g	P_{f*}/P_g	log τ_{f*}/τ_g	R^2
DAR[a]	0.961 ± 0.093	0.070	-6.50	0.996
	1.22 ± 0.10	0.125	-5.89	0.998
	1.21 ± 0.11	0.165	-5.66	0.998
	1.32 ± 0.16	0.195	-5.37	0.997
PPG[b]	3.00 ± 0.24	0.298	-7.04	0.999
	2.87 ± 0.30	0.371	-6.58	0.999
	3.14 ± 0.40	0.421	-6.11	0.999
	3.04 ± 0.54	0.480	-5.62	0.998
PMTS[c]	1.83 ± 0.049	0	-6.26	0.999
	1.82 ± 0.060	0.0989	-5.80	0.999
	1.79 ± 0.082	0.203	-5.31	0.999
	1.83 ± 0.10	0.305	-4.77	0.999
PGEC[d]	1.65 ± 0.11	0.0027	-5.58	0.999
	1.56 ± 0.11	0.103	-5.18	0.999
	1.53 ± 0.16	0.207	-4.73	0.999
	1.60 ± 0.16	0.311	-4.20	0.999
PBD[e]	1.69 ± 0.052	0.0004	-6.04	0.999
	1.72 ± 0.060	0.073	-5.69	0.999
	1.73 ± 0.068	0.146	-5.33	0.999
	1.75 ± 0.085	0.216	-4.96	0.999
IPCB[f]	0.895 ± 0.033	0.082	-0.688	0.995
	1.02 ± 0.032	0.157	-0.561	0.997
	0.985 ± 0.032	0.325	-0.464	0.997
	1.08 ± 0.054	0.526	-0.303	0.995
DGEB[g]	3.66 ± 0.23	0.231	-5.03	0.998
	3.65 ± 0.29	0.289	-4.81	0.998
	3.84 ± 0.35	0.348	-4.53	0.998
	3.79 ± 0.37	0.406	-4.28	0.998
DEP[h]	3.09 ± 0.38	0.138	-8.96	0.996
	2.78 ± 0.33	0.182	-8.83	0.997
	2.73 ± 0.38	0.266	-8.23	0.997
	2.62 ± 0.43	0.362	-7.58	0.997

[a]Ref. 91, [b]Ref. 93, [c]Ref. 27, [d]Ref. 90, [e]Ref. 15, [f]Ref. 94, [g]Ref. 92, [h]Ref. 25.

when pressures other than the lowest were used to determine τ_{f^*} in Eq. (35). These results also indicate that excellent fits of the data were obtained, based on the R^2 value, regardless of the measurements chosen as τ_{f^*} and P_{f^*}. In some cases, it can be seen that the uncertainty in ψ_g increases as values further from the lowest pressure are used as P_{f^*}, but all values of ψ_g obtained are nearly equivalent.

4.5 Prediction of Dielectric Relaxation at Other Temperature Conditions

For PGEC, DGEB, and PMTS, data at other conditions of temperature were available. With the value of v determined at or near T = 293 K, log τ could be predicted for another temperature by Eq. (35), given the value of P_g, P_{f^*}, and log τ_{f^*}/τ_g at the new temperature. Predictions of Eq. (35) with a constant value of v given by Table 1 were applied to DGEB data at T = 267 K and T = 279 K, to PGEC data at T = 274.5 K and T = 303.4 K, and to PMTS data at T = 277 K, 283 K, 303 K and 313 K. Figures 8, 9, and 10 show log τ/τ_g versus experimental values for DGEB, PGEC, and PMTS. For the PGEC data at T = 303.4 K, an extrapolation was made to determine P_g by fitting the data to Eq. (35) and solving for P_g. For PMTS at T = 283 K, interpolation of a P_g versus T_g plot was used to determine P_g. The value of ψ_g, and thus of v, is sensitive to inaccuracies in P_g. A reduction in P_g of less than 5 MPa ($\cong$ 5 %) for PMTS at T = 293 K yields an increase in ψ_g of 0.62 (> 30%), and nearly doubles the value of v (to $v = 3.73 \times 10^{-29}$ m^3). Thus, any extrapolation introduces error into the final computed results. Of course, errors in the experimental data could potentially cause similar effects.

Figures 8, 9, and 10 confirm the assumption that v is constant across varying conditions of temperature and pressure, since a constant value of v fitted all the data. This is in contrast to earlier work that indicated an activation volume that varies with temperature.[93]

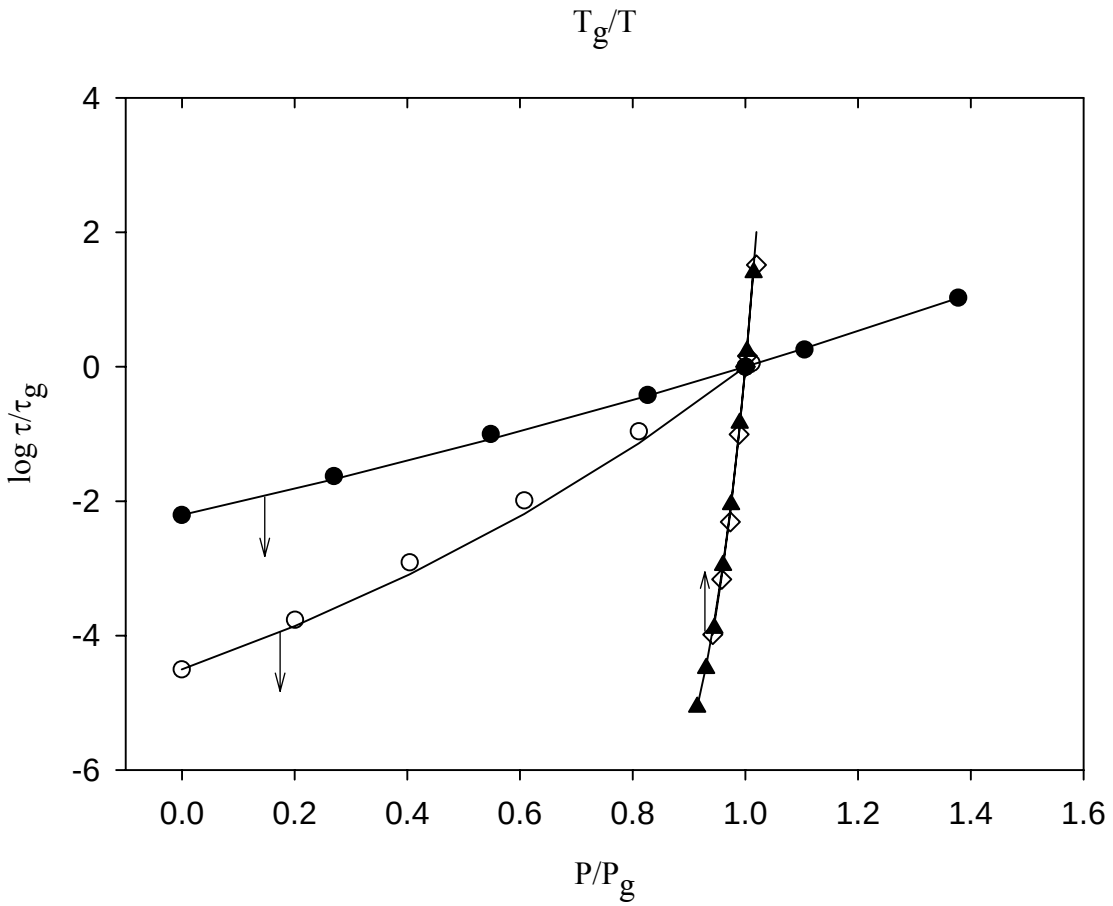

Figure 8 Predicted log τ/τ_g for DGEB vs. experimental data at T = 267 K (●), T = 279 K (○), P = 500 bar (▲), and P = 1000 bar (◇). The lines represent the prediction using the parameter v, (Table 1), and, in the constant pressure data, the parameter h = 4.00 x 10^{-20} J. The uncertainty in the prediction, resulting from the uncertainty in the parameters v and h, is smaller than the symbol size. The defined point at log $\tau_{f*}/\tau_g = 0$ at P/P_g or $T_g/T = 1$ has been added to the data sets.

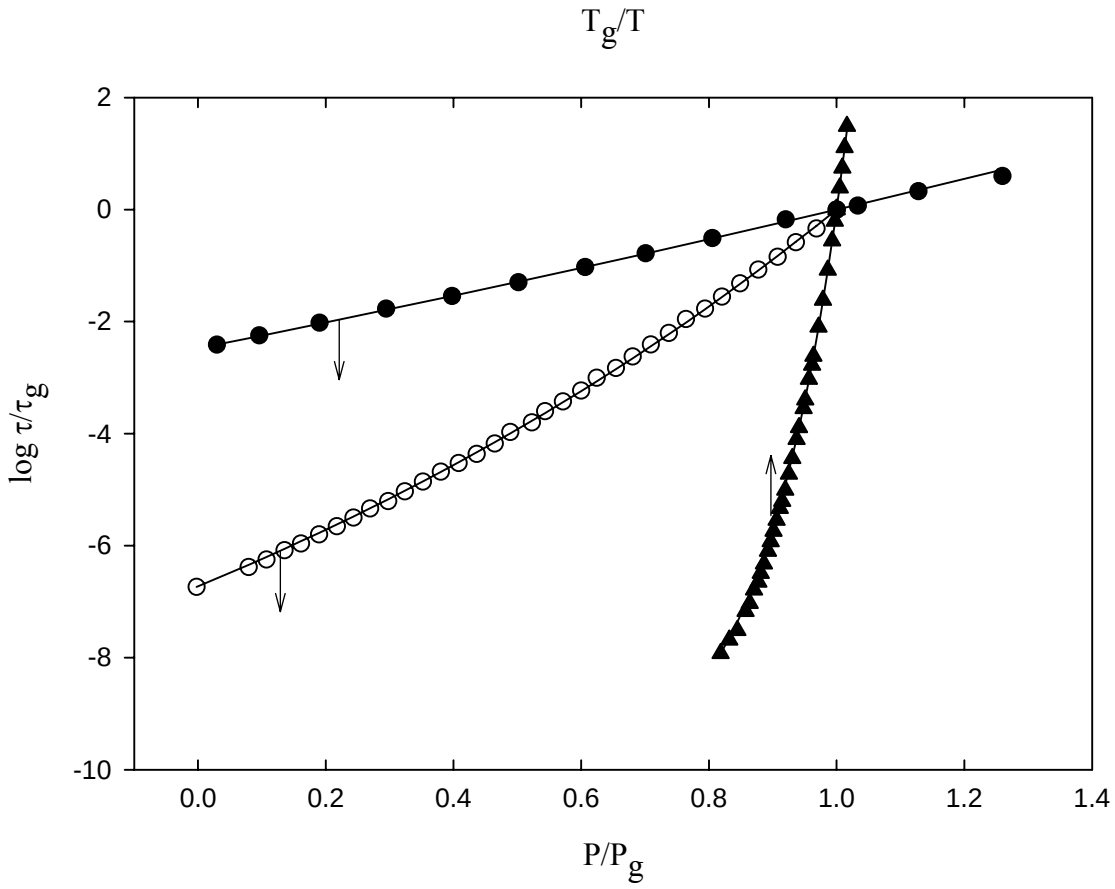

Figure 9 Predicted log τ/τ_g for PGEC vs. experimental data at T = 274.5 K (●), T = 303.4 K (○), and P = 0.1 MPa (▲). The lines represent the prediction with the parameter v, (Table 1), and in the constant pressure case, the parameter $h = 2.84 \times 10^{-20}$ J. The uncertainty in the prediction, resulting from the uncertainty in the v and h, is less than the symbol size. The defined point at log $\tau_{f^*}/\tau_g = 0$ at P/P_g or $T_g/T = 1$ has been added to the data sets.

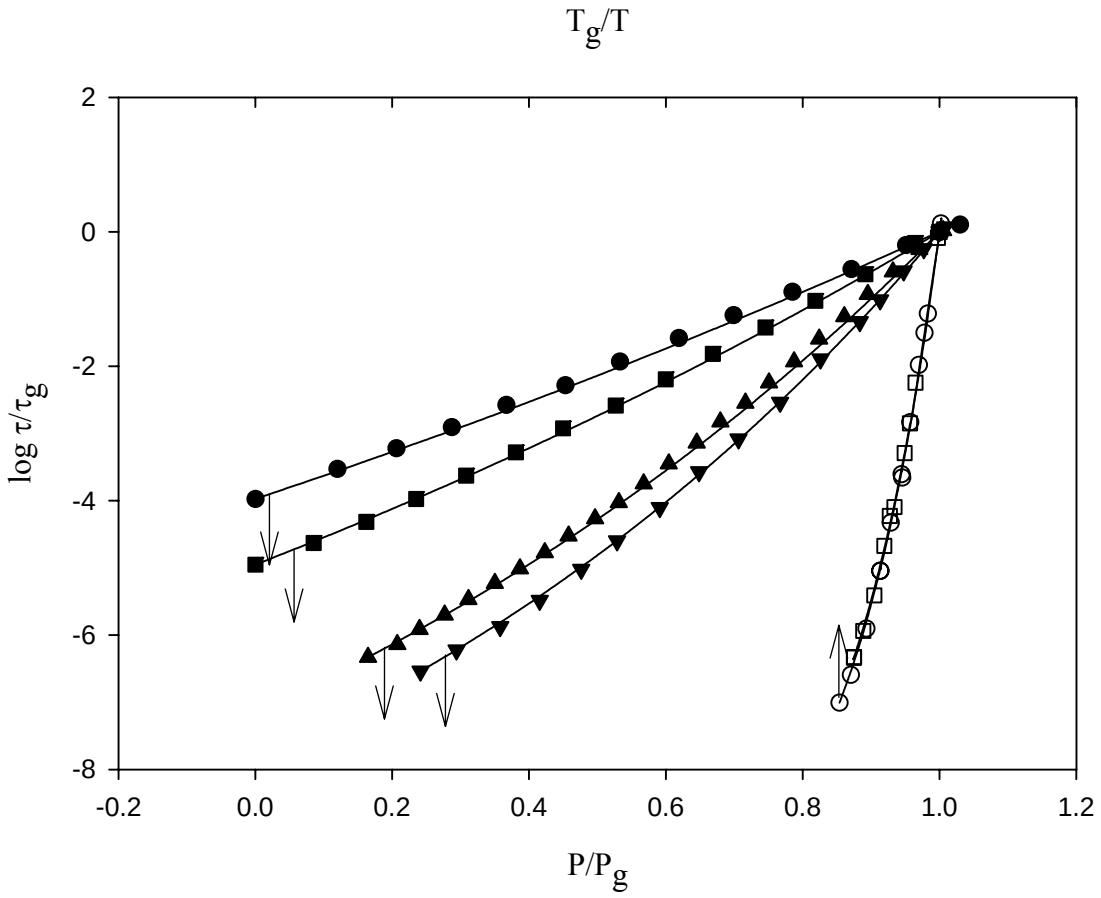

Figure 10 Predicted log τ/τ_g for PMTS vs. experimental data at T = 277 K (●), T = 283 K (■), T = 303 K (▲), T = 313 K (▼), P = 50 MPa (○), and P = 100 MPa (□). The lines represent the prediction with the parameter v, (Table 1), and in the constant pressure cases, the parameter h = 2.73 x 10^{-20} J. The uncertainty in the prediction, resulting from the uncertainty in v and h, is less than the symbol size. The defined point at log $\tau_{f^*}/\tau_g = 0$ at P/P_g or $T_g/T = 1$ has been added to the data sets.

4.6 Determination of the Parameter *h* and Prediction of Dielectric Relaxation at Other Pressure Conditions

Data at constant pressure and varying temperature were also available, so Eq. (36) was fitted to these data to determine *h* for PGEC, DGEB, and PMTS. Considering *h* a constant, Eq. (36) was applied to predict log τ/τ_g at a new pressure, given T_g, T_{f^*}, and log τ_{f^*}/τ_g at that pressure. Data at P = 250 bar were fitted to Eq. (36) for DGEB, with a resulting value of Φ_g = 69000 ± 48000, which gave $h = 4.00 \times 10^{-20}$ J. This *h*, as well as *v* for DGEB from Table 1, were used to predict log τ/τ_g at two other conditions, P = 500 and 1000 bar. Figure 8 shows that the predictions are quite good, confirming that *h* and *v* are both independent of pressure and temperature. The plots of T_g/T versus log τ/τ_g for P = 500 bar and P = 1000 bar overlap because the contribution of the term $P_g v$ in Eq. (36) is an order of magnitude less than *h* (whereas $h = 4.00 \times 10^{-20}$, for P = 500 bar, $P_g v = 1.21 \times 10^{-21}$ and for P = 1000 bar, $P_g v = 2.42 \times 10^{-21}$). In the case of PGEC, data at P = 95.5 MPa were fitted to Eq. (36) after first determining T_g via a fit of the data to that equation, to obtain Φ_g = 2610 ± 470, which yields $h = 2.94 \times 10^{-20}$ J. The resulting *h* value together with *v* from Table 1 were then used to predict log τ/τ_g at P = 0.1 MPa. Figure 9 shows this prediction is also quite good. For PMTS, data at P = 0.1 MPa were fitted to Eq. (36), with a resulting value of Φ_g = 2001 ± 470, which gave $h = 2.73 \times 10^{-20}$ J. This *h*, as well as *v* for PMTS from Table 1, were used to predict log τ/τ_g at two other conditions, P = 50 and 100 MPa. Figure 10 shows that the predictions are quite good, confirming that *h* and *v* are both independent of pressure and temperature. The plots of T_g/T versus log τ/τ_g for P = 50 MPa and P = 100 MPa overlap because the contribution of the term $P_g v$ in Eq. (36) is an order of magnitude less than *h* (whereas $h = 2.73 \times 10^{-20}$, for P = 50 MPa, $P_g v = 1.20 \times 10^{-21}$ and for P = 100 MPa, $P_g v = 2.40 \times 10^{-21}$). For DGEB at P = 250 bar a slight linear extrapolation of the literature data was required to determine T_g. To determine T_g for PMTS at P = 100 MPa, a linear interpolation of a T_g versus P_g plot was employed.

While the uncertainty of Φ_g is large in the DGEB and PGEC cases, the impact on h is small. For DGEB, the maximum value of Φ_g gives $h = 4.19 \times 10^{-20}$ J and the minimum value gives $h = 3.57 \times 10^{-20}$ J. For PGEC, the maximum value of h, due to uncertainty in Φ_g, is $h = 3.01 \times 10^{-20}$ J and the minimum value is $h = 2.88 \times 10^{-20}$ J.

4.7 Application to Polymethylphenylsiloxane

Polymethylphenylsiloxane, PMPS, a compound similar in structure to PMTS, was also evaluated. While data at $T = 293$ K were not available for this compound, data at several other temperatures were found in the literature.[49] Using data at $T = 253$ K, a value of $v = 2.48 \times 10^{-29}$ m^3 was determined. This value is very close to that found for PMTS, ($v = 2.40 \times 10^{-29}$ m^3), which may have been expected given the two compounds' chemical similarities. Given this value of v, predictions of log τ/τ_g versus P/P_g at two other temperatures were made, $T = 263$ K and $T = 273$ K. Figure 11 shows that a constant value of v succeeded in predicting log τ/τ_g at these two temperatures.

4.8 Application to 1,1'-di(*p*-methoxyphenyl)cyclohexane

Another compound, not included in Table 1, but for which a fair amount of dielectric relaxation data at various temperatures and pressures is available, is BMPC, 1,1'-di(*p*–methoxyphenyl)cyclohexane.[52] For this compound at $T = 283.55$K, a fit of Eq. (35) gave $\psi_g = 1.382 \pm 0.175$, resulting in $v = 0.793 \times 10^{-29}$ m^3. The defined point log $\tau_{f*}/\tau_g = 0$ at $P/P_g = 1$ was added to the data set prior to performing the regression. Data for BMPC at $P = 60$MPa were fitted to Eq. (36), to obtain $\Phi_g = 48.3 \pm 49$, giving $h = 1.36 \times 10^{-20}$ J. The great uncertainty in Φ_g is likely because the data set is small (four points). If the maximum value of h is calculated, from $\Phi_g = 97.3$, the result is $h = 1.62 \times 10^{-20}$ J, a difference of ~ 20%. These values of v and h were used to predict log τ/τ_g at two other conditions, $P = 180$ MPa and $T = 265.85$K. Graphs of predicted versus experimental values of log τ/τ_g are shown in Fig. 12.

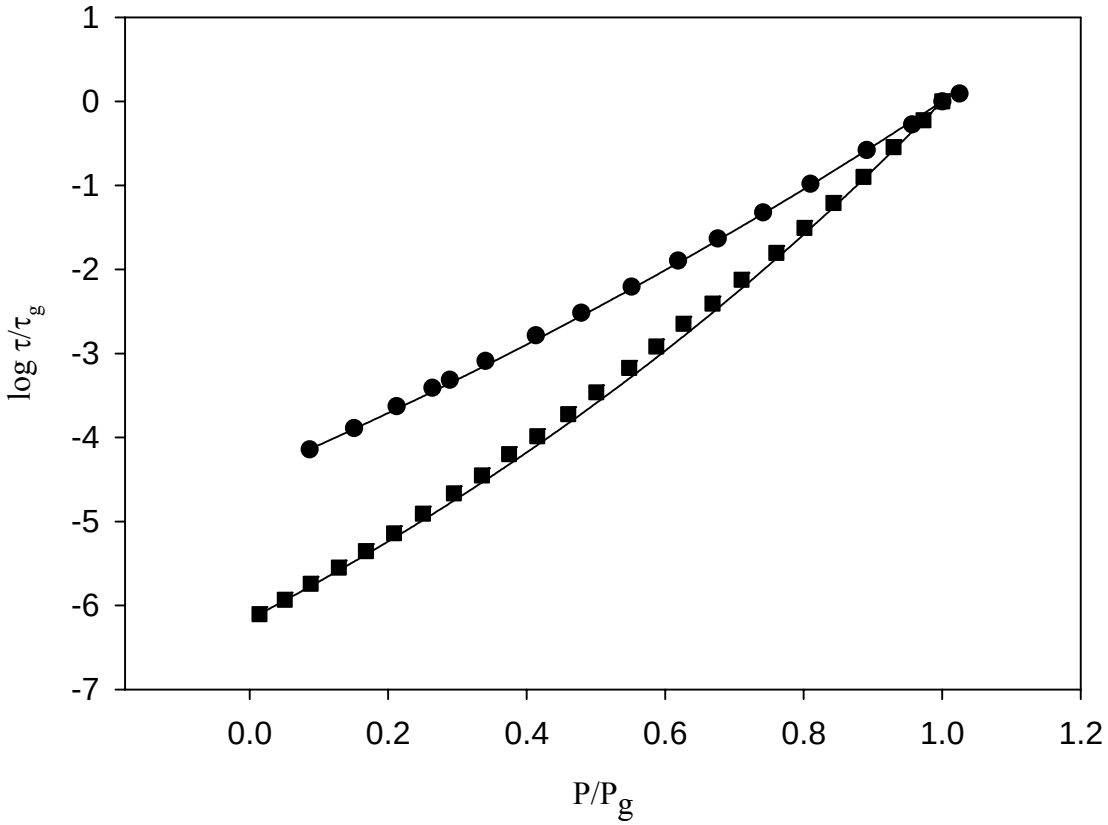

Figure 11 Predicted log τ/τ_g for PMPS vs. experimental data at T = 263 K (●) and T = 273 K (■). The lines represent the prediction with the parameter v = 2.48 x 10^{-29} m^3. The defined point at log $\tau_{f^*}/\tau_g = 0$ at $P/P_g = 1$ has been added to the data sets.

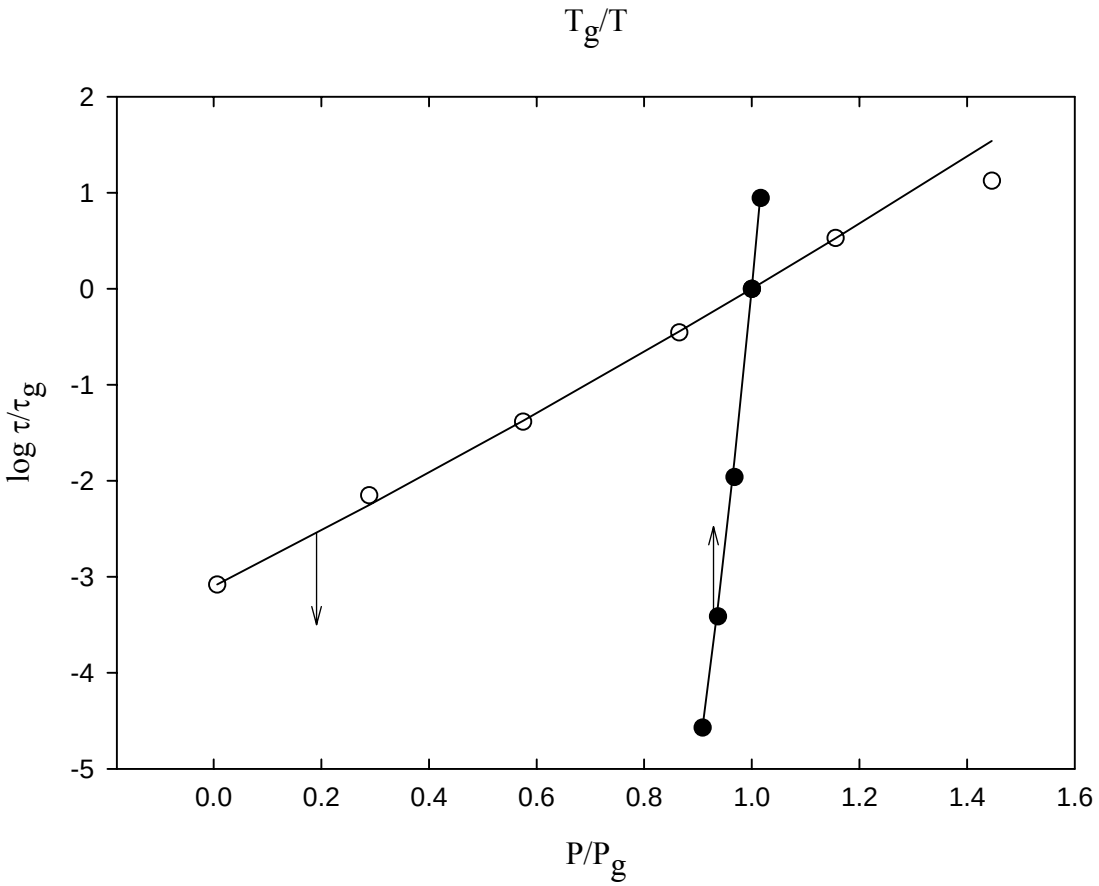

Figure 12 Predicted log τ/τ_g for BMPC vs. experimental data at P = 180 MPa (●) and T = 265.85 K (○). The lines represent the prediction with the parameter v = 0.793 x 10^{-29} m^3 and in the constant pressure case, the parameter h = 1.36 x 10^{-20} J. The defined point at log τ_{f^*}/τ_g = 0 at P/P_g or T_g/T = 1 has been added to the data sets. Uncertainty in the prediction resulting from the uncertainty in the parameters v and h is less than the size of the symbols.

4.9 Relationship of T_g to P (or of P_g to T)

A disadvantage of the VFTH equation is that it specifies a linear relation of T_g to P (or of P_g to T), whereas the experimental data for some compounds indicate a nonlinear relation.[49] Rearranging Eq. (23b) to solve for T_g as a function of P_g yields:

$$T_g = [(h + P_g v)/k_B] \{\ln[(1/b)\ln(\tau_g/\alpha)]\}^{-1} \quad (37)$$

If α and b are not constant, then the relationship of T_g to P_g may be nonlinear. Solving for α and b in terms of τ_{f*}, τ_g, Φ_{f*} and Φ_g yields:

$$b = \ln(\tau_{f*}/\tau_g) /(\Phi_{f*} - \Phi_g) \quad (38)$$

and

$$\ln(\alpha) = \ln(\tau_g) - \ln(\tau_{f*}/\tau_g) /(\Phi_{f*} /\Phi_g - 1) \quad (39a)$$

or

$$\alpha = \tau_g (\tau_{f*}/\tau_g)^{1/ (1 - \Phi f* /\Phi g)} \quad (39b)$$

This indicates that the parameters α and b vary with τ_{f*}, which in general is not constant for different experimental data sets, and also depend on pressure and temperature, which determine Φ_{f*} and Φ_g. Table 3 gives values of $\ln(\alpha)$ and b calculated from Eqs. (38) and (39) as well as values determined via regression of data to Eq. (23b). Generally good agreement between the regressed values of $\ln(\alpha)$ and b and the calculated values is seen. This indicates that $\ln(\alpha)$ and b depend on the selection of the fluid and the glass states, as given by P_g, P_{f*}, $\log \tau_{f*}$, $\log \tau_g$, T_g, and T_{f*}.

4.10 Validation of Linear Relation of $\ln \tau$ to Φ and Determination of α and b

Once h and v are known, Φ can be calculated at any pressure and temperature. It was thus possible to validate Eq. (23b) by plotting $\ln \tau$ vs. Φ, showing that this relation is linear. Figure 13 demonstrates this linear relation for PGEC at P = 95.5 MPa and at T = 293.5 K. The experimental data for DGEB and BMPC include many different sets of pressure and

Table 3 Parameters ln(α) and *b* evaluated for experimental data[a, b] for BMPC (1,1'-di(*p*–methoxyphenyl cyclohexane) and DGEB (diglycidal ether of bisphenol A) by regression with Eq. (23b), using *v* and *h* parameters as determined previously, and compared to ln(α) and *b* as calculated from Eqs. (38) and (39a) (designated with the subscript c).

Chemical	*T* (K)		*P* (MPa)	ln(α)	$\ln(\alpha)_c$	*b*	b_c	$-\log \tau_{f*}/\tau_g$	Φ_{f*}	Φ_g
BMPC	258.2	var.	45.7	46.8	0.948	0.973	1.16	45.4	48.1	
BMPC	265.9	var.	48.0	51.6	1.01	1.06	3.08	40.7	47.2	
BMPC	283.6	var.	47.5	47.0	1.07	1.06	4.41	34.9	44.6	
BMPC	297.7	var.	45.7	N/A	1.06	N/A	4.51	33.2	N/A	
BMPC	var.	180	36.0	35.9	0.817	0.821	4.57	31.0	43.8	
BMPC	var.	100	35.2	36.2	0.750	0.776	4.50	33.2	46.6	
BMPC	var.	60	36.2	36.3	0.757	0.761	3.69	36.5	47.7	
BMPC	var.	20	36.8	37.7	0.750	0.772	3.73	37.8	48.9	
DGEB	var.	100	18.5	19.2	0.000262	0.000282	3.98	35 700	68 300	
DGEB	var.	50	19.0	19.0	0.000276	0.000276	5.0	26 500	68 700	
DGEB	var.	25	19.4	19.1	0.000280	0.000277	5.02	27 100	68 800	
DGEB	267	var.	19.4	19.7	0.000280	0.000283	2.21	51 600	69 500	
DGEB	279	var.	18.9	19.2	0.000272	0.000272	4.50	32 300	70 400	
DGEB	293	var.	18.2	18.3	0.000250	0.000254	5.03	26 600	72 100	

[a]Reference 52.
[b]Reference 92.

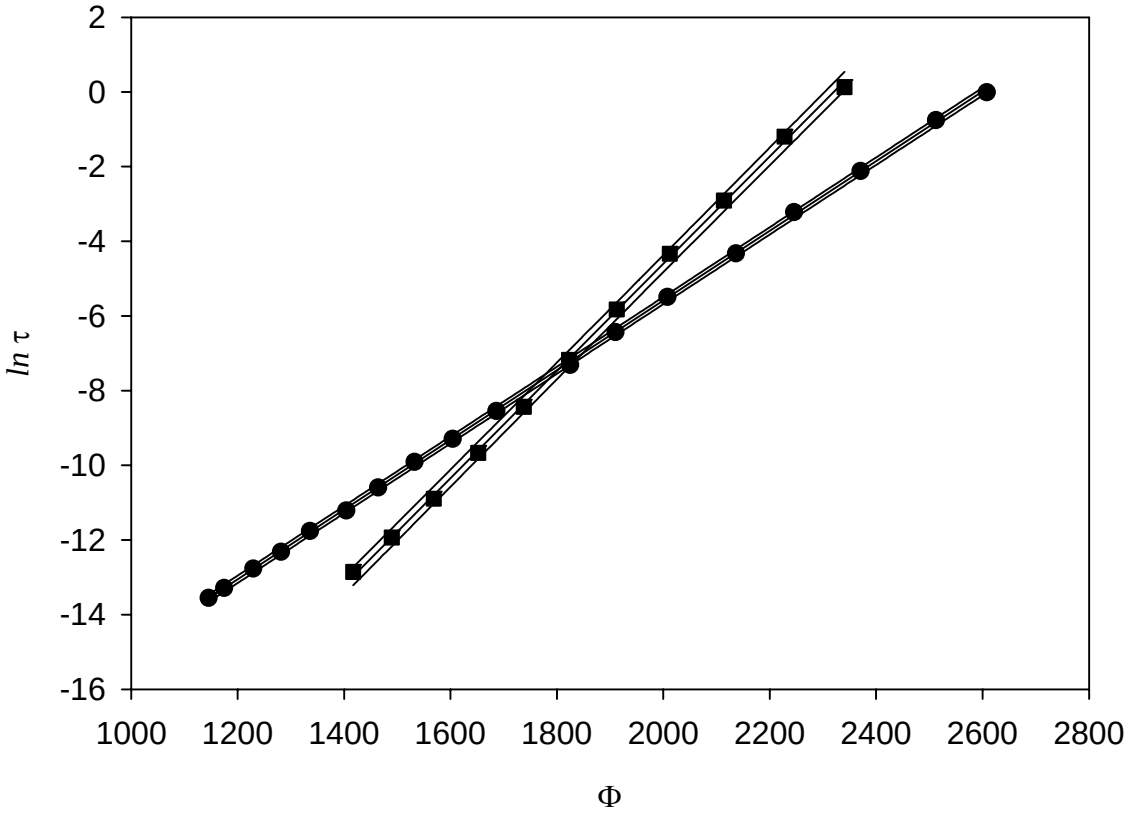

Figure 13 Graph of ln τ vs. Φ for PGEC at P = 95.5 MPa (●) and at T = 293.5 K (■). Lines indicate the predictions and their 95% prediction intervals. Φ has been calculated using the value of parameter v given in Table 1 and the parameter h = 2.94 x 10^{-20} J.

temperature conditions. For these compounds, multiple plots of ln τ vs. Φ could be made at the various temperature and pressure conditions, and the parameters α and b calculated by a linear fit to the data (Table 3). For DGEB, α and b are nearly constant across a range of temperatures and pressures, but for BMPC more variability in these parameters is seen.

4.11 Application to Orthoterphenyl

For OTP, data at P = 0.1 MPa could be fitted only by VFTH parameters for one portion, and a power law relation for another segment.[24] Figure 14 shows that with only one set of parameters in the current model, Eq. (35) agrees with OTP data at T = 275 K and Eq. (36) agrees with data at P = 0.1 MPa. To determine P_g at T = 275 K, it was necessary to extrapolate from the data available by fitting to Eq. (35). The parameter obtained from the T = 275 K data set, $\psi_g = 0.814 \pm 0.021$, leading to $v = -0.782 \times 10^{-29}$ m^3, was used to predict log τ/τ_g at T = 268 K. The negative value of v relates to the relative magnitudes of v_m and v_c. The data set for T = 268 K did not include the point at which log $\tau/\tau_g = 0$, so an extrapolation using Eq. (35) was performed to obtain P_g. The predicted data points demonstrate good agreement with experimental data. The parameter obtained from the P = 0.1 MPa data set, $\Phi_g = 595 \pm 147$, leading to $h = 2.21 \times 10^{-20}$ J, was tested against data at P = 25 MPa from the literature[26] and the result is also shown in Fig. 14. To determine T_g at P= 25 MPa, it was necessary to extrapolate from the data by fitting to Eq. (36). Again, reasonably good agreement with the experimental values was obtained. In Fig. 14, the prediction uncertainties, due to the uncertainties in v and h, are less than the symbol size.

4.12 Conclusion

The cluster kinetics model has been demonstrated to successfully model a variety of glassformers. The compounds successfully modeled have varying molecular weights, from polymers to small molecules, as well as fragilities from linear (Arrhenius) behavior to more

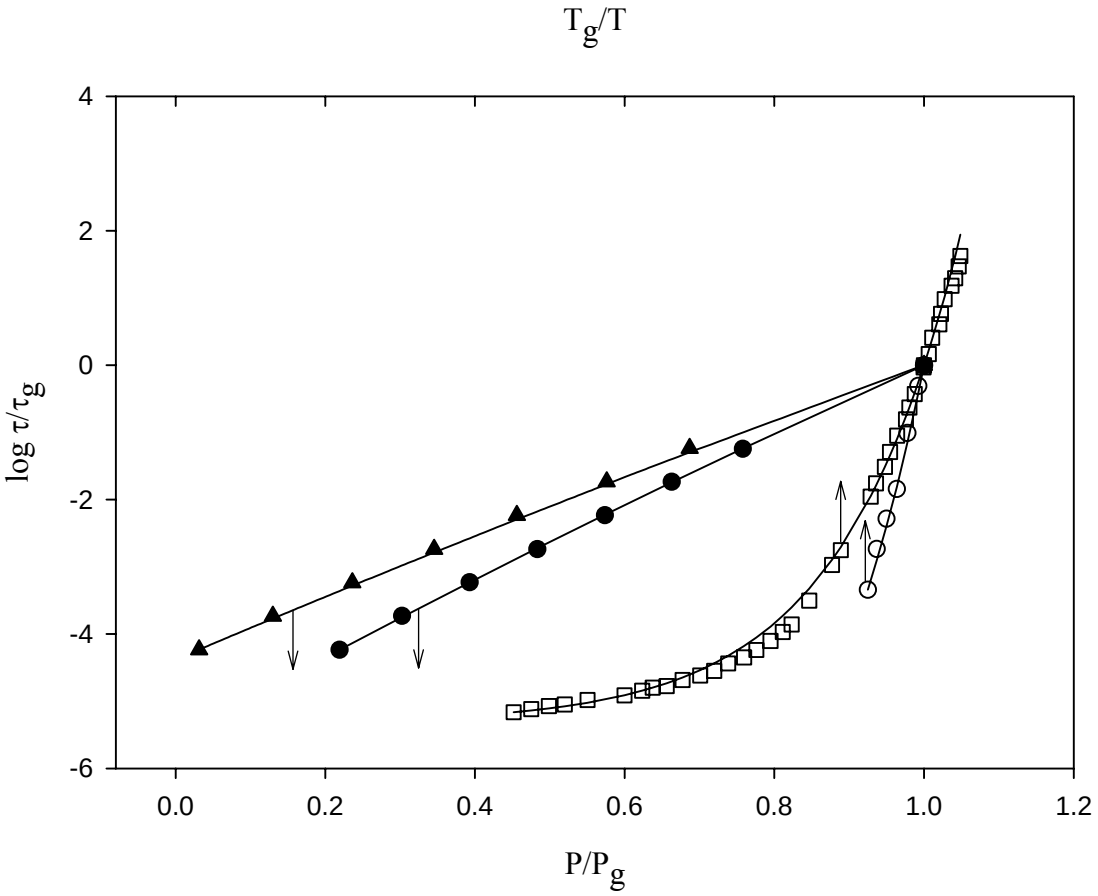

Figure 14 Experimental data for OTP: scaled dielectric relaxation times versus scaled pressure at two temperatures (● = 275 K and ▲ = 268 K) and versus scaled temperature at two pressures (□ = 0.1 MPa and ○ = 25 MPa) [24,26]. For $T = 275$ K and $P = 0.1$ MPa, the lines represent fits to Eqs. (20) and (21), respectively. For $T = 268$ K and $P = 25$ MPa, the lines show the predicted scaled dielectric relaxation values, with the parameter $v = -0.782 \times 10^{-29}$ m^3 as determined from the $T = 275$ K data fit and the parameter $h = 2.21 \times 10^{-20}$ J as determined from the $P = 0.1$ MPa data fit. The defined point at log $\tau_{f*}/\tau_g = 0$ at P/P_g or $T_g/T = 1$ has been added to the data sets. The uncertainty in the predictions, based on the uncertainty in v and h, is less than the symbol size.

fragile behavior. In addition, the range of experimental data for pressure, temperature, and relaxation time was quite broad, including pressures and temperatures above and below the dielectric glass transition, which was taken at $\tau = 1$ second. The relaxation times varied over nearly twelve decades. The parameters h and v have been demonstrated to be invariant to pressure and temperature[64]; parameters determined at one set of conditions could be applied at other temperatures and pressures to predict the dielectric relaxation, given T_g, P_g, T_{f^*}, P_{f^*}, and log τ_{f^*}/τ_g at the new conditions. This is evidence that h and v are properties of the compound, and not merely fitting parameters, and have physical meaning as the difference of activation energy and activation volumes differences. In addition, it was shown that the form of the model allows for a non-linear relationship of T_g to P_g, and vice versa, which is in accord with actual behavior seen in the published literature. The cluster kinetics model has thus met the goals of broad applicability and ease of use.

CHAPTER 5
APPLICATION OF CLUSTER KINETICS MODEL TO BINARY MIXTURES OF GLASSFORMERS EXHIBITING A SINGLE DIELECTRIC RELAXATION IN RESPONSE TO TEMPERATURE OR PRESSURE

5.1 Introduction

The operative definition of a binary mixture of glassformers for the purposes of this chapter requires that the two components each be glassformers, and that the blend or mixture be well-mixed. Compared to pure compounds, binary mixtures of glassformers present additional dynamic complexities. Although a number of models relating dielectric relaxation or viscosity to temperature and pressure have been developed to describe pure compounds (see Chapter 1), developing models to fit data for binary mixtures of glassformers is an area of active research[95-100]. Some treatments have simply used pure component glass transition models to fit mixture data[101-107]. This approach, however, raises the question of how to interpret the fitting parameters and how to relate them to properties of mixture components. For binary mixtures with a single response of dielectric relaxation to temperature or pressure, only one study[108] has used model parameters determined from pure component data to predict mixture behavior. In this chapter, a cluster kinetics model developed in Chapter 3 for pure compounds is extended to well-mixed binary mixtures of glassformers exhibiting a single dialectic relaxation versus temperature or pressure. A mixing relation for the h and v parameters is proposed, and mixture relaxation times calculated which are then compared to experimental data. Statistical analysis is applied to determine goodness of fit between the predicted and experimental values.

5.2 Mixing Relation

The proposition that underlies the approach taken here is that the parameters h and v for binary mixtures with a single measurable dielectric relaxation response to temperature can be determined by assuming that the cluster association-dissociation process is more important than any specific interactions in determining relaxation behavior. For an ideal, athermal solution[100,109,110], the following relation applies to any thermodynamic property (here designated as Y):

$$Y_{mix} = x_A Y_A + x_B Y_B \tag{40}$$

where Y_{mix} and Y_A and Y_B represent the thermodynamic property of the mixture and the mixture components, respectively, and x_A and x_B are the respective mole fractions. Considering h and v to be properties of the components of the mixture, Eq. (40) can be applied to these parameters as shown below:

$$h_{mix} = x_A h_A + x_B h_B \tag{41}$$

and

$$v_{mix} = x_A v_A + x_B v_B \tag{42}$$

Subscripts A and B indicate the two components of a binary mixture of glassformers whereas the subscript mix designates a mixture property. The quantities x_A and x_B are mole fractions, although sometimes weight fractions are used. Equation (40) has been recently used in applications of the Adam-Gibbs theory to binary mixtures of glassformers.[100,109,110]

5.3 Application to a Sorbitol and Glycerol Mixture

The relations Eqs. (41) and (42) have been tested for several binary mixtures of glassformers having a single measurable dielectric relaxation time at each temperature. First, h and v for the pure components of the mixture must be determined, which requires dielectric relaxation data versus temperature and pressure for the separate components of the mixture.

Data are available for sorbitol and glycerol to determine v values from dielectric relaxation data versus pressure[5,111] by regressing the experimental data with Eq. (35), given $\log_{10}(\tau_{f*}/\tau_g)$, P_{f*}, and P_g. Each so-determined value of ψ_g provides v, given P_g and T. The dielectric glass transition pressure, P_g, is defined as the pressure at which the dielectric relaxation equals one second. Once v is known, a second data set of dielectric relaxation times versus temperature[112,113] is regressed with Eq. (36) to determine Φ_g, given $\log_{10}(\tau_{f*}/\tau_g)$, T_{f*}, and T_g. Once Φ_g is known, and given v determined previously, as well as T_g and P, h can be calculated.

For pure sorbitol[111], Eq. (35) yielded $\psi_g = 1.015 \pm 0.195$. The value of v and the goodness of fit R^2 are given in Table 4. The parameter v is associated with the pressure effects on dielectric relaxation, and for ambient pressure, is generally negligible. A slight linear extrapolation was employed to determine P_g at a temperature of 286.4 K. Regression with Eq. (36) of a second data set[113] yielded $\Phi_g = 486.1 \pm 126.9$. The associated value of h and its range are given in Table 4. Despite the uncertainty in Φ_g, calculation of the dielectric relaxation is based upon differences of Φ_g, which tends to cancel the impact of any errors. In addition, the exponential form of Φ_g yields a much smaller range for h (Table 4). Similarly for pure glycerol[5], by Eq. (35) the nine available data points yielded $\psi_g = 2.116 \pm 0.414$. The associated values of v are given in Table 4. By linear interpolation, P_g was determined at a temperature of 230.6 K. Equation (36) with a second data set of 10 points[112] yielded $\Phi_g = 9.477 \pm 1.59$. The associated value of h and its range are given in Table 4. Parameters h and v for sorbitol and glycerol differ (by nearly an order of magnitude in the case of v), indicating that their dielectric relaxation behaviors versus temperature or pressure differ, quite significantly in the case of pressure. Mixtures of sorbitol and glycerol are known to exhibit

Table 4 For the sorbitol-glycerol mixture[a], parameters h_{mix} and v_{mix} were evaluated for 7 compositions according to Eqs. (41) and (42), respectively. The mole fraction of sorbitol is x_s. Ranges of h_{mix} were calculated from upper and lower values of h for mixture components. Values of P_g and T_g were determined by linear interpolation at $\tau = 1$ second of experimental data[a - e] (except when designated by an *, indicating a slight linear extrapolation of the experimental data). Values of T_g were determined from ambient pressure experimental data. Experimental data also supplied values of $\log_{10}(\tau_{f*}/\tau_g)$. R^2 values were determined by comparison of calculated dielectric relaxation times for the mixture with the experimental data. For pure components[b - e], $h_{mix} = h$ and $v_{mix} = v$, R^2 values reflect the goodness of fit of Eqs. (35) and (36), and ranges are from the standard error of the regression. Note: Amb = Ambient.

x_s	0.0	0.11	0.25	0.34	0.43	0.54	0.67	0.82	1.0
h_{mix} 10^{-20}J	0.62	0.81	1.05	1.20	1.36	1.54	1.77	2.02	2.33
Range	0.57-0.67	0.75-0.86	0.98-1.10	1.13-1.26	1.28-1.42	1.46-1.61	1.68-1.84	1.92-2.10	2.22-2.42
v_{mix} $10^{-31}m^3$	25.6	23.0	19.6	17.5	15.3	12.7	9.60	6.02	1.72
T_g K	200.4	204.9	215.6	224.8	231.4	241.5	254.4	265.8	272.8
$\log_{10}(\tau_{f*}/\tau_g)$	-0.85 (*h*) -4.75 (*v*)	-5.94	-5.85	-4.16	-4.98	-2.34	-2.31	-3.07	-10.56 (*h*) -3.44 (*v*)
R^2	0.997 (*h*) 0.9998 (*v*)	0.9999	0.9994	0.9986	0.9951	0.9988	0.9984	0.9969	0.9973 (*h*) 0.995 (*v*)
P_g GPa	0.932	Amb.	Amb.	Amb.	Amb.	Amb.	Amb.	Amb.	0.342*

[a]Reference 102.
[b-e]References 5,111 - 113

hydrogen bonding[114], so this mixture is a good choice to determine if clustering controls the relaxation such that specific interactions can be neglected in calculating relaxation behavior. It has been suggested[115,116] that hydrogen-bonding is necessary for a binary polymer mixture to exhibit a single dielectric relaxation response to temperature instead of two. As application of the cluster kinetics model to these binary mixtures with a single relaxation treats the components as a single entity, hydrogen-bonding may coordinate the two components such that they can be considered equivalent to a monomer.

For Eqs. (41) and (42), the mixture parameters are displayed in Table 4 for seven different compositions of the sorbitol and glycerol mixture[102]. The ranges were calculated from the upper and lower bounds of h for sorbitol and glycerol. With h_{mix} and v_{mix} given, the dielectric relaxation at the various mixture compositions versus temperature can be calculated, once mixture dielectric glass transition temperature and dielectric relaxation and temperature at non-glass conditions ($\log_{10}(\tau_{f^*}/\tau_g)$ and T_{f^*}) are known. All T_g values (at ambient pressure) in Table 4 were determined via linear interpolation of the experimental data at $\tau = 1$ second.

Figure 15 is a plot of dielectric relaxation versus temperature for four of the sorbitol and glycerol mixtures. Experimental data are designated by symbols and calculated values by lines. The R^2 statistic (Table 4), which measures how well the calculated dielectric relaxation times reproduce the experimental data, indicates good agreement with the experimental data by Eqs. (35) and (36).

Figure 16 shows a plot of dielectric relaxation versus temperature for the remaining three compositions of the sorbitol and glycerol mixture. The R^2 values (Table 4) again demonstrate agreement between calculated dielectric relaxation times and experimental values by Eqs. (35) and (36).

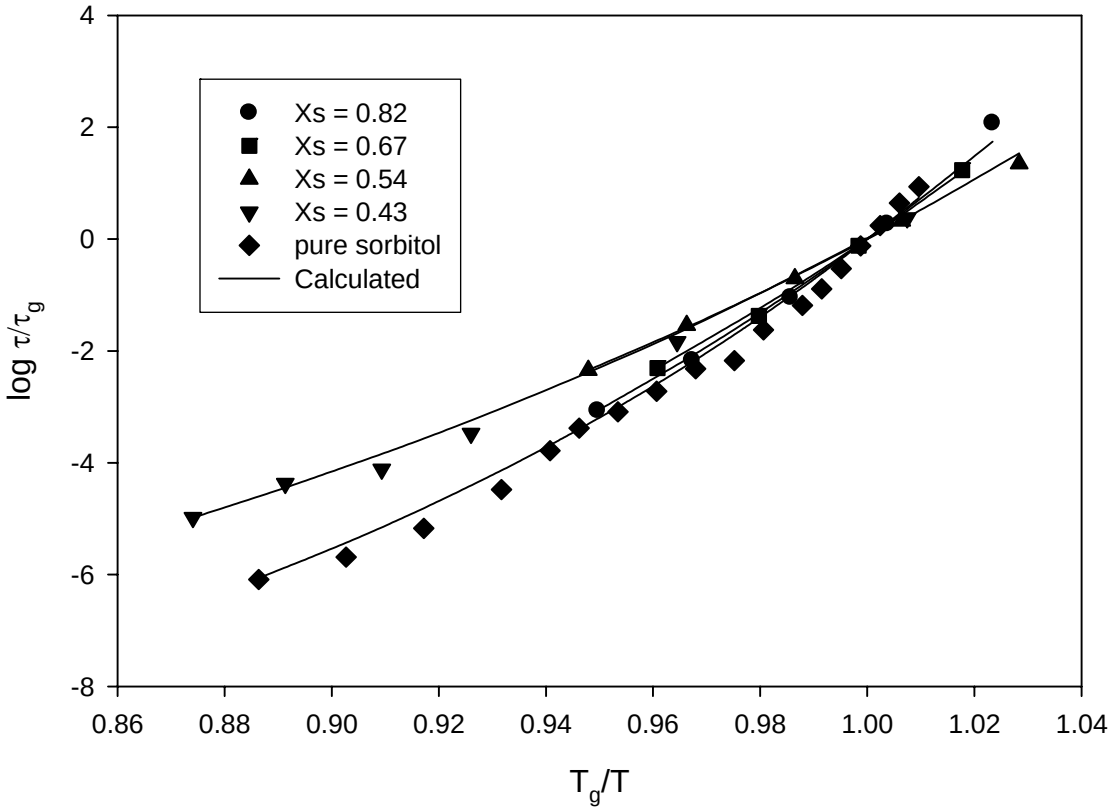

Figure 15 Dielectric relaxation time versus scaled temperature for four sorbitol-glycerol mixtures and for pure sorbitol. Experimental data are designated by symbols, x_s = 1.0 (◆), x_s = 0.82 (●), x_s = 0.67 (■), x_s = 0.54 (▲) and x_s = 0.43 (▼), calculated values (and regression of pure sorbitol data) by solid lines.

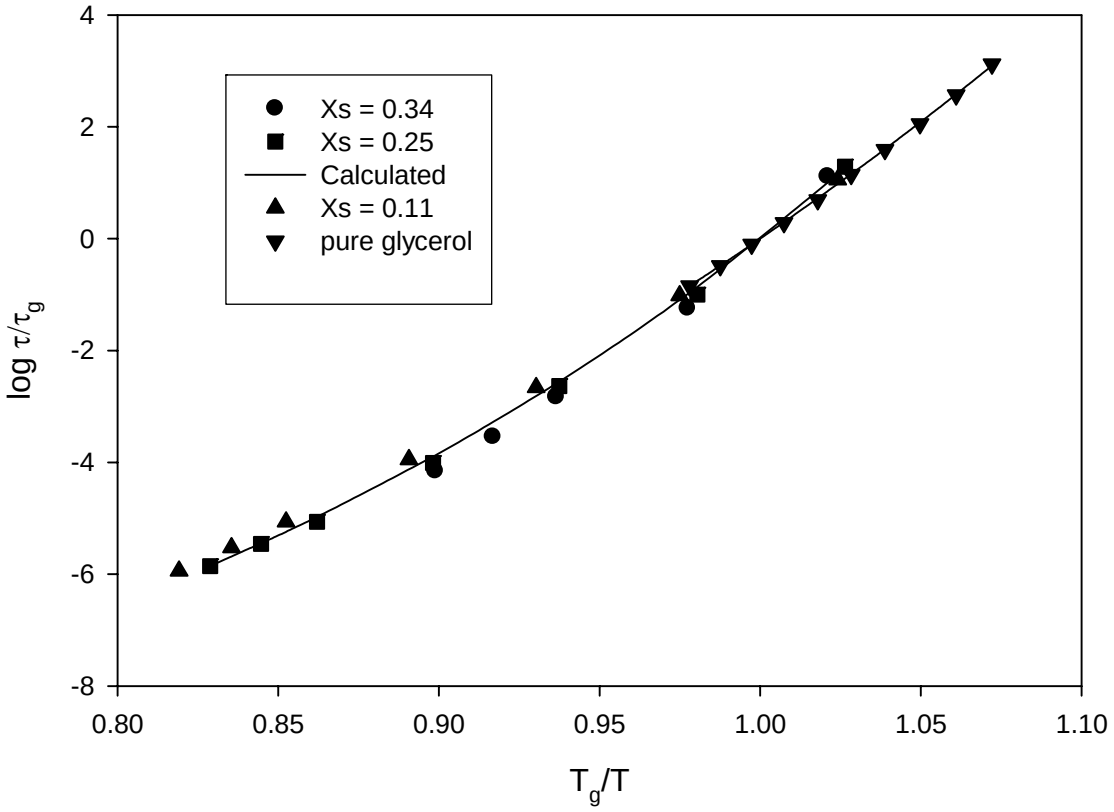

Figure 16 Dielectric relaxation time versus scaled temperature for three sorbitol-glycerol mixtures and for pure glycerol. Experimental data are designated by symbols, x_s = 0.34 (●), x_s = 0.25 (■), x_s = 0.11 (▲), and x_s = 0.0 (▼), calculated values (and regression of pure glycerol data) by solid lines.

If the upper and lower bounds on h_{mix} (Table 4) are used to calculate $\log_{10}(\tau/\tau_g)$, the result differs from that shown in Figs. 15 and 16 only at most in the second decimal place. Both Figs. 15 and 16 show that the dielectric relaxation behavior of the mixture changes with composition, which is expected since the components of the mixture have different relaxation behaviors, as evidenced by their differing values of h and v as noted previously.

5.4 Application to a Mixture of Sorbitol with Xylitol

Additional data for a second mixture containing sorbitol, this time mixed with xylitol, are available.[117, 114] This mixture also exhibits hydrogen bonding[114], which aids in assessing the effect of specific interactions in mixture dielectric relaxation behavior. Because constant temperature and constant pressure data are not available for xylitol, independently determining h and v for this component is not possible. However, a single parameter, $h_p = h + P\,v$, where P is ambient pressure, can be determined from constant ambient pressure data, which is available.[118]

To determine h_p for xylitol, dielectric relaxation data versus temperature at ambient pressure[118] is regressed with a modified version of Eq. (36), shown below as Eq. (43):

$$\log_{10}(\tau/\tau_g) = [(\Phi_g^{\,Tg/T} - \Phi_g)/(\,(\Phi_g^{\,Tg/Tf^*} - \Phi_g)]\,\log_{10}(\tau_{f^*}/\tau_g). \qquad (43)$$

where $\Phi_g = \exp(h_p/k_B T_g)$. Equation (43) is the same as Eq. (36), except that Φ_g has been re-defined in terms of h_p instead of h and v. Given T_g, T_{f^*}, and $\log_{10}(\tau_{f^*}/\tau_g)$, regressing experimental data with Eq. (43) gives a value of Φ_g and then h_p. The dielectric glass transition temperature is defined as before, equivalent to the temperature at which the dielectric relaxation equals one second. The value of Φ_g by Eq. (43) for literature xylitol data[118] is 139.5 ± 14.5. The associated value of h_p and its range are given in Table 5. For sorbitol, since h and v have previously been determined to be $v = 1.72 \times 10^{-31}$ m^3 and $h = 2.33 \times 10^{-20}$ J, h_p can simply be calculated by the definition given above, with ambient pressure, P

Table 5 Parameter $h_{p\text{-}mix}$ was evaluated for 3 compositions of a sorbitol-xylitol mixture,[a, b] by Eq. (41). The mole fraction of xylitol is x_x. Ranges of $h_{p\text{-}mix}$ were calculated from upper and lower values of h_p for mixture components. Values of T_g were determined by linear interpolation at $\tau = 1$ second of ambient pressure experimental data[a - c]. Experimental data also supplied values of $\log_{10}(\tau_{f*}/\tau_g)$. R^2 values were determined by comparison of calculated dielectric relaxation times for the mixture with the experimental data. For pure xylitol[c], $h_{p\text{-}mix} = h_p$, R^2 values reflect the goodness of fit of Eq. (43), and ranges are from the standard error of the regression.

x_x	0.0	0.3	0.5	0.7	1.0
$h_{p\text{-}mix}$ /10^{-20} J	2.33	2.15	2.03	1.91	1.73
range	2.22 – 2.42	2.06 – 2.23	1.96 – 2.10	1.85 – 1.97	1.69 – 1.77
T_g/K	272.8	265.5	262.7	257.9	253.8
$\log_{10}(\tau_{f*}/\tau_g)$	-10.56	-8.76	-9.01	-8.92	-9.23
R^2	0.9973	0.9959	0.9968	0.9974	0.9988

[a]Reference 117.
[b]Reference 114.
[c]Reference 118.

= 101325 Pa; applying this calculation yields h_p = 2.33 x 10^{-20} J. The contribution of the *v* term in h_p is thus negligible at ambient pressure, as mentioned previously. This dominance of *h* over *v,* particularly at low pressure, has been reported in Chapter 4 with other compounds. Because their h_p values differ by only 25 percent, it is expected that mixtures of sorbitol and xylitol of varying compositions would differ less in their dielectric relaxation response to temperature than the sorbitol-glycerol mixtures, where the values of h_p calculated from *h* and *v* for the pure compounds differ more (h_p for sorbitol is 2.33 x 10^{-20} J and for glycerol, 6.22 x 10^{-21} J). Applying the relation given in Eq. (41) by replacing *h* with h_p, mixture parameters for three different compositions of the sorbitol and xylitol mixture (Table 5) were determined. The mole fraction of xylitol in the mixture is x_x.[114,117] The ranges for $h_{p\text{-}mix}$, derived from upper and lower bounds of h_p for sorbitol and xylitol, are rather narrow and any difference in calculated values of $\log_{10}(\tau/\tau_g)$ is negligible.

With $h_{p\text{-}mix}$ determined, the dielectric relaxation at the various mixture compositions versus temperature can be calculated, once mixture dielectric glass transition temperature and dielectric relaxation and temperature at non-glass conditions ($\log_{10}(\tau_{f*}/\tau_g$ and T_{f*}) are known. Dielectric glass transition temperatures for the mixtures are given in Table 5. All data sets were at ambient pressure, and T_g values were determined by linear interpolation of the experimental data at τ = 1 second. Figure 17, a plot of experimental and calculated dielectric relaxation versus temperature for the three sorbitol and xylitol mixtures[114,117] and for pure sorbitol and xylitol, shows the dielectric relaxation response to temperature varies less across the composition range for the sorbitol-xylitol mixture than for the sorbitol-glycerol mixture. All the data sets for the sorbitol-glycerol and sorbitol-xylitol mixtures include data for $\log_{10}(\tau/\tau_g)$ at T_g/T = 0.96, where the difference between the largest and smallest values of $\log_{10}(\tau/\tau_g)$ for the sorbitol and glycerol mixture is 0.92, whereas it is only 0.07 for the sorbitol and

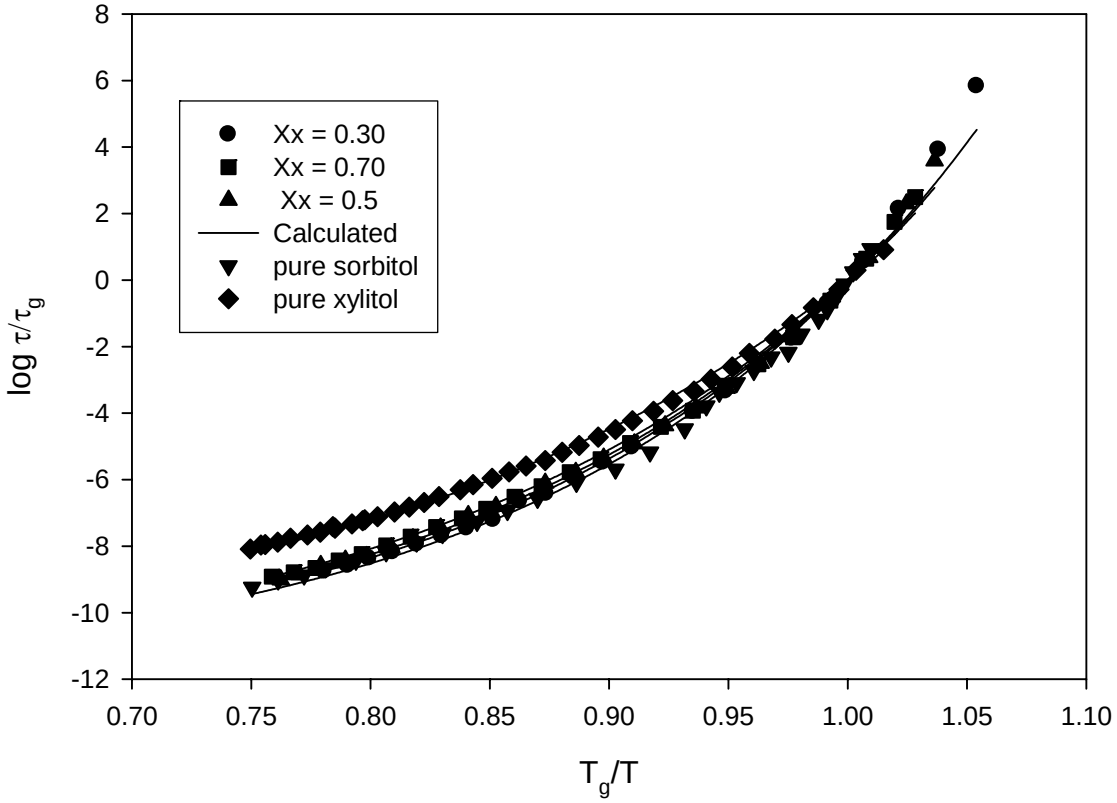

Figure 17 Dielectric relaxation time versus temperature for sorbitol-xylitol mixtures and for pure sorbitol and xylitol. Experimental data are designated by symbols x_x = 0.0 (▼), x_x = 0.3 (●), x_x = 0.5 (■), x_x = 0.7 (▲), and x_x = 1.0 (◆), calculated values (and regression of pure sorbitol and xylitol data) by solid lines.

xylitol mixture. This demonstrates that dielectric relaxation for the sorbitol and xylitol mixture varies less across the composition range for the mixture than does the sorbitol and glycerol mixture, as expected given that h_p for sorbitol is closer to that of xylitol than to the h_p value for glycerol. The R^2 statistic (Table 5) indicates agreement of the calculated dielectric relaxation with the experimental data when Eq. (43) is applied.

5.5 Application to a Polychloroepihydrin and Polyvinylmethylether Mixture

Data for a third mixture, of two polymers, containing polychloroepihydrin (PECH) and polyvinylmethylether (PVME), are also available[14]. As was the case for xylitol, constant temperature and constant pressure data are not available for the components of this mixture, so h_p is determined instead of h and v. PECH data at ambient pressure[14] regressed with Eq. (43) yield $\Phi_g = 10496.6 \pm 7364$. The associated value of h_p and its range are given in Table 6. Regressing the PVME data at ambient pressure[14] with Eq. (43) yields $\Phi_g = 6278.5 \pm 3481$. The associated value of h_p and its range are given in Table 6. On the basis of their almost equal h_p values, as well as their nearly identical T_g values, it is expected that mixtures of PECH and PVME of varying compositions will have very similar dielectric relaxation responses to temperature.

Most polymer mixtures exhibit two distinct dielectric relaxations versus temperature, one for each component. Due to the nearly identical glass transition temperatures of the two components, the PECH and PVME mixture has but a single relaxation time. Mixture parameters were determined according to Eq. (41) by replacing h with h_p for three different compositions of the PECH and PVME mixture, as shown in Table 6. Equation (43) was applied in this case using weight fraction instead of mole fraction, which cannot be calculated from the data given[14]. The values of $h_{p\text{-}mix}$ vary little across the composition range of the PECH and PVME mixture (with a maximum difference of 0.1×10^{-20} J across the

Table 6 Parameter $h_{p\text{-}mix}$ was evaluated for 3 compositions of a PECH-PVME mixture[a] according to Eq. (41). The weight fraction of PECH is x_{PECH}. Ranges of $h_{p\text{-}mix}$ were calculated from upper and lower values of h_p for mixture components. Values of T_g were determined by linear interpolation at $\tau = 1$ second of ambient pressure experimental data[a]. Experimental data also supplied values of $\log_{10}(\tau_{f*}/\tau_g)$. R^2 values were determined by comparison of calculated dielectric relaxation times for the mixture with the experimental data. For pure components[a], $h_{p\text{-}mix} = h_p$, R^2 values reflect the goodness of fit of Eq. (43), and ranges are from the standard error of the regression.

x_{PECH}	0.0	0.2	0.5	0.8	1.0
$h_{p\text{-}mix}/10^{-20}$ J	3.03	3.06	3.12	3.16	3.20
range	2.75 – 3.18	2.76 – 3.22	2.77 – 3.29	2.78 – 3.35	2.79 – 3.39
T_g (K)	250.8	252.1	253.5	252.9	250.7
$\log_{10}(\tau_{f*}/\tau_g)$	-3.74	-4.02	-3.92	-3.64	-3.81
R^2	0.9996	0.9997	0.9994	0.9994	0.9994

[a]Reference 14.

composition range). They are also not very different from the pure component values calculated from the data given[14]. The ranges of $h_{p\text{-}mix,}$ resulting from the upper and lower bounds of h_p for PECH and PVME, are narrow, such that any difference in the calculated $\log_{10}(\tau/\tau_g)$ is negligible (i.e. in second decimal place). Dielectric T_g (determined at τ = 1 second) for each mixture is given in Table 6. Anomalously, the values of the mixture dielectric T_g are not intermediate to the values of the pure components' dielectric $T_{g.}$, but since the proposed model (Eqs. (35) and (36)) uses mixture values of T_g and P_g, there is no impact of this anomalous behavior on the application of the model equations. Whatever specific interactions may cause the anomalous T_g, the inference of this work is that clustering behavior outweighs these interactions, or possibly that these interactions are reflected entirely in the value of T_g or other mixture data used in the prediction. For the three PECH and PVME mixtures, Figure 18 shows that the dielectric relaxation response to temperature varies little across the composition range. At $T_g/T = 0.96$, the variance in $\log_{10}(\tau/\tau_g)$ across the composition range is only 0.1. Agreement between calculated dielectric relaxation and experimental data was excellent. This is not surprising, given that the h_p values of the pure components are not that different from each other.

5.6 Conclusion

Dielectric relaxation times for three binary mixtures of glassformers were calculated by combining pure component data according to Eqs. (41) and (42). Only this simple mixing relation and mixture values for dielectric T_g, T_{f*}, and $\log_{10}(\tau_{f*}/\tau_g)$ are needed to calculate the relaxation behavior of a binary mixture with a single relaxation time. For three mixtures of glassformers exhibiting a single dielectric relaxation vs. temperature, the proposed model works well, but further testing with experimental data is warranted. Although the pressure variance of dielectric relaxation was not specifically examined in this work, the proposed

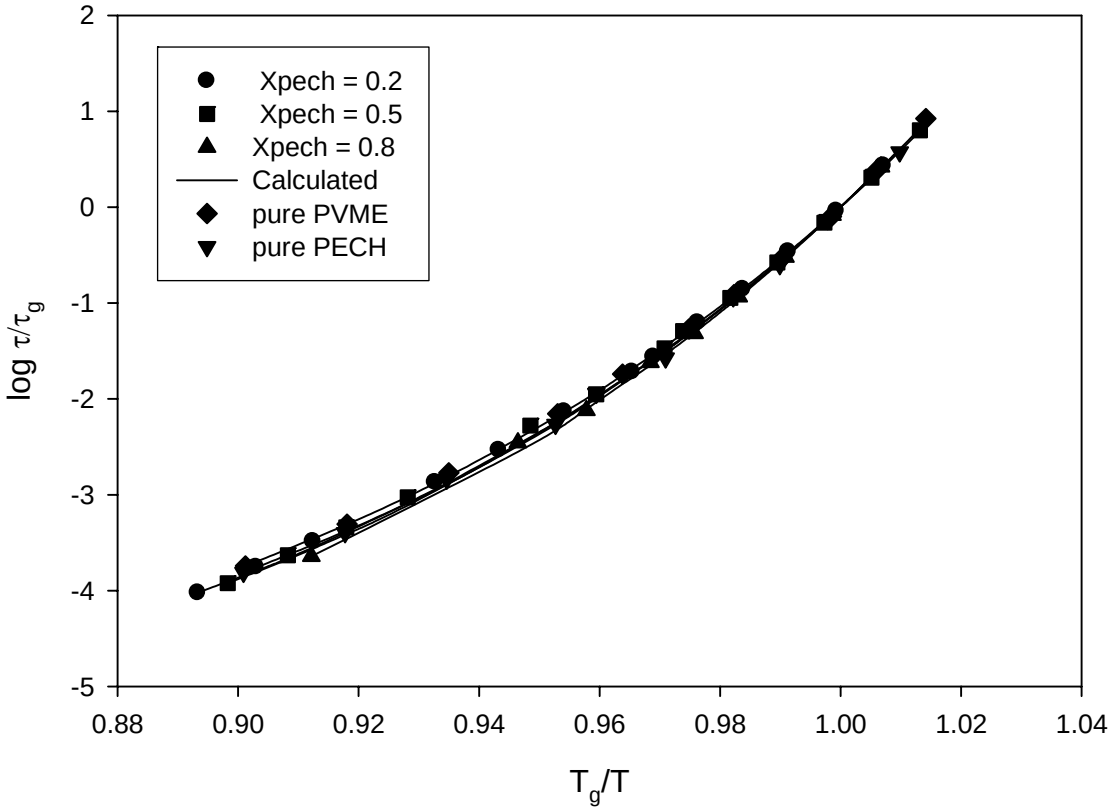

Figure 18 Dielectric relaxation time versus temperature for PECH-PVME mixtures and for pure PECH and PVME. Experimental data are designated by symbols x_{PECH} = 0.0 (▼), x_{PECH} = 0.2 (●), x_{PECH} = 0.5 (■), x_{PECH} = 0.8 (▲), and x_{PECH} = 1.0 (◆), calculated values (and regression of pure PECH and PVME data) by solid lines.

method, based on cluster kinetics, allows for calculation of viscosity or dielectric relaxation versus temperature or pressure. That this simple mixing relation may be used to calculate mixture h and v (or h_p) supports the idea that these are properties of the fluid, and not merely fitting parameters.

CHAPTER 6
APPLICATION OF THE CLUSTER KINETICS MODEL TO BINARY GLASSFORMER MIXTURES EXHIBITING TWO DISTINCT DIELECTRIC RELAXATIONS IN RESPONSE TO TEMPERATURE

6.1 Introduction

The definition of a glassformer mixture for this chapter is the same as in the preceding chapter, two glassformers that are combined in such a way as to be well-mixed. Mixtures of polymers are important both industrially and for basic scientific research into changes in dynamic behavior of glassformers upon mixing. Compositions of polymer blends are varied industrially to fine-tune the properties of the blend for specific applications. The ability to predict blend segmental relaxation behavior is therefore of great significance. Segmental relaxation is related to the glass transition[21], and is commonly measured and studied.

Glassformer mixtures are frequently dynamically heterogeneous and exhibit distinct segmental relaxations for each component[109,119,120]. In the previous chapter, binary glassformer mixtures exhibiting only a single measurable relaxation in response to temperature or pressure were examined. Here, the more common case of two measurable relaxations in a binary mixture of glassformers is treated. The observed dynamic heterogeneities in mixtures are thought to result from local composition differences[119]. Even for a binary glassformer mixture that is well-mixed at a molecular level, two distinct dielectric relaxations in response to changing temperature can often be detected and are related to local composition differences[109,119]. The two relaxations in a binary mixture, however, are different from the relaxation behavior of the pure components, typically either speeding up or slowing down relative to the pure behavior[120,121].

Two main theories have been applied to model these local composition heterogeneities: (1) thermally-induced concentration fluctuations; and (2) self-concentration effects[119,122]. Both theories are combined with various models relating dielectric relaxation and temperature[100,109,119,121] , such as Vogel-Fulcher-Tammann-Hesse[23], Adam-Gibbs[54], Donth[123] or Lodge-MacLeish[95] . While some success has been achieved, no one theory and model combination has been demonstrated to predict mixture behavior in all cases. The objective of this chapter is to show that a cluster kinetics model can predict dielectric relaxation of a glassformer component in a binary mixture without recourse to either theory. The clustering behavior, however, can be interpreted in terms of concentration fluctuations and self-concentration effects.

6.2 Background

Various authors have found that certain parameters of other models, such as the VFTH equation, are invariant to mixture composition.[107,119] In some cases, the relaxation behavior of a compound in various compositions of a mixture and its pure behavior (versus temperature) could be superposed after imposing a temperature shift.[122,124] This, however, is not the most common case, and was applied for NMR relaxation and normal mode relaxation data, respectively. Each of these cases, and indeed the very fact that the two components of a binary glassformer mixture relax independently, lead one to think that they can and should be treated independently[125]. The objective of this chapter is to extend the cluster kinetics model to binary mixtures having two relaxations in response to temperature or pressure. Having determined the cluster kinetics model parameters from pure component data, one can then predict dielectric relaxation times for the same component in a mixture. If h and v for the pure compound are applied to the compound in a binary mixture exhibiting two relaxations, then the assumption must be that the

compound exhibits a decided preference to cluster with itself, or clusters with the other compound in the mixture to such a limited extent that h and v for the pure compound can still be applied. Since it is understood that the relaxation of the component in the mixture differs from the pure behavior, using the pure component v and h will require that this difference be accounted for in other parameters of the model. Therefore, the application of the cluster kinetics model to mixtures also requires knowing the T_g of the component in the mixture, as well as a fluid data point (i.e. τ_{f*} and T_{f*}) for that component in the mixture. Thus, while each component is treated independently from the other, the mixing effects are accounted for in the component dielectric glass transition temperature and a component fluid data point. Earlier attempts[107,119] to use a similar approach with other models have had mixed results. For the data tested here the method is successful.

The basic concept that underlies this approach is that glassformer behavior in a mixture is essentially unchanged from its pure state behavior, insofar as the parameters h and v are concerned. The impact of the second mixture component is reflected in the change in dielectric glass transition temperature and of the fluid dielectric relaxation time for a given component of the mixture. An explanation is based on the different environment of the component (i.e., it is no longer surrounded by itself only). However, if the components act independently, then their relaxation behavior (defined as how the dielectric relaxation changes with temperature and pressure) should remain unchanged, even though the absolute value of the dielectric relaxation at a given temperature is altered. In the context of the cluster kinetics model, this implies that h and v (or h_p) remain unchanged from the pure component values.

6.3 Method

For a binary mixture of glassformers with two relaxations versus temperature, the value of h_p, a property of the compound, is first determined from pure component relaxation literature data by regression with Eq. (43). Then, given the dielectric glass transition temperature of that component in the mixture, as well as the fluid temperature and dielectric relaxation time of the component in the mixture, h_p is used to calculate the dielectric relaxation time of the component in the mixture, again using Eq. (43). The dielectric glass transition temperature is defined as the temperature at which $\log \tau = 0$. This calculated relaxation is compared to the actual measured relaxation of the component in the mixture as given in the literature, by calculating an R^2 that indicates how well the prediction matches the experimental data.

6.4 Application to Experimental Data

The above procedure has been attempted for four binary mixtures of glassformers: PoClS(poly(*o*-chlorostyrene)) and PS (polystyrene)[109], and PVME (polyvinylmethylether) and PS[119]; P2CS (poly (2-chlorostyrene)) and PVME[125]; P(CHA-*stat*-BMA) (poly-cyclohexylacrylate-*stat*-butylmethacrylate) and PS[119].

The cluster kinetics model, as originally conceived, is a two-state model (see Eq. (44) below):

$$\log_{10}(\tau/\tau_2) = [(\Phi_2^{\,T2/T} - \Phi_2)/(\,(\Phi_2^{\,T2/T1} - \Phi_2)]\,\log_{10}(\tau_1/\tau_2) \qquad (44)$$

where $\Phi_2 = \exp(h_p/k_B T_2)$.

In Eq. (43), the two states are expressed as glass and fluid. However, any two states could be used, as shown in Eq. (44). State 1 is equivalent to the fluid condition (i.e. the highest temperature data point in a constant pressure data set) in applications in this work. For two of the compositions of the PoClS and PS mixture[109], the data set did not include the

point at which log τ = 0. For those two compositions (25 and 50 wt%), the lowest temperature, T_2, was used in place of T_g (in Eq. (44)) while the dielectric relaxation corresponding to that temperature, τ_2, was used in place of τ_g. For the PVME component in the P2CS and PVME mixture[125], the mixture data set does not include the point at which log τ = 0, so Eq. (44) was used to calculate log τ for PVME in this mixture. Two compositions of a fourth mixture, of P(CHA-*stat*-BMA) with PS[119] were also analyzed using this approach. For this mixture, h_p was also determined by Eq. (44).

Given pure component data, one could calculate dielectric relaxation for both components of the binary mixtures of glassformers; however, data for both components were not available in all cases. For the PoClS and PS mixture[109], data for PS in the mixture were not given, so only the PoClS component is examined. For the PS and PVME mixture[119], only the PVME component's pure data and relaxation behavior in the mixture are available. Note that the molecular weight of the PS in the PS and PVME mixture is not the same as the PS in the PoClS and PS mixture, and thus the same h_p could not be used, as h_p is a function of molecular weight for a polymer. For the P(CHA-*stat*-BMA) and PS mixture[119], data were supplied for pure P(CHA-*stat*-BMA) only. For the P2CS and PVME blend[125], data for both pure components and their mixture behavior are given. As with the two mixtures containing PS, the two mixtures containing PVME represent different molecular weights for that component.

6.5 Poly(*o*-chlorostyrene) and Polystyrene Mixture Data

For the PoClS and PS mixture[109], three compositions were examined: 25, 50, and 75 wt% PoClS in PS. Eq. (43) was used as described above to determine $h_p = 4.67 \times 10^{-20}$ J for pure PoClS. Pure component values of T_g, T_{f*}, and $\log_{10}(\tau_{f*}/\tau_g)$ for PoClS used to determine h_p are given in Table 7, as well as the value of R^2 for the regression. Figure 19

Table 7 Dielectric relaxation was calculated for PoClS in 3 compositions of a PoClS and PS mixture[a] according to Eq. (43) (for pure PoClS and 75 wt % mixture) or Eq. (44) (for 25 and 50 wt% mixtures), based on the pure component h_p value for PoClS of 4.67 x 10^{-20} J. Values of T_g were determined by linear interpolation at $\tau = 1$ second for ambient pressure experimental data[a]. Values of T_2 were the lowest temperature in an ambient pressure experimental data[a]. Experimental data also supplied values of $\log_{10}(\tau_{f*}/\tau_g)$ and T_{f*} or $\log_{10}(\tau_1/\tau_2)$ and T_1 . R^2 values were determined by comparison of calculated dielectric relaxation times for PoClS in the mixture with experimental data, except for pure PoClS, where R^2 is a measure of the goodness of fit of Eq. (43) to experimental data.

$wt\%_{PoClS}$	25	50	75	100
T_g or T_2 (K)	329.76	190.42	189.15	402.41
T_{f*} or T_1 (K)	380.28	212.04	203.01	445.50
$\log_{10}(\tau_{f*}/\tau_g)$ or $\log_{10}(\tau_1/\tau_2)$	-4.22	-4.22	-3.09	-4.99
R^2	0.9894	0.9992	0.9910	0.9986

[a]Reference 109.

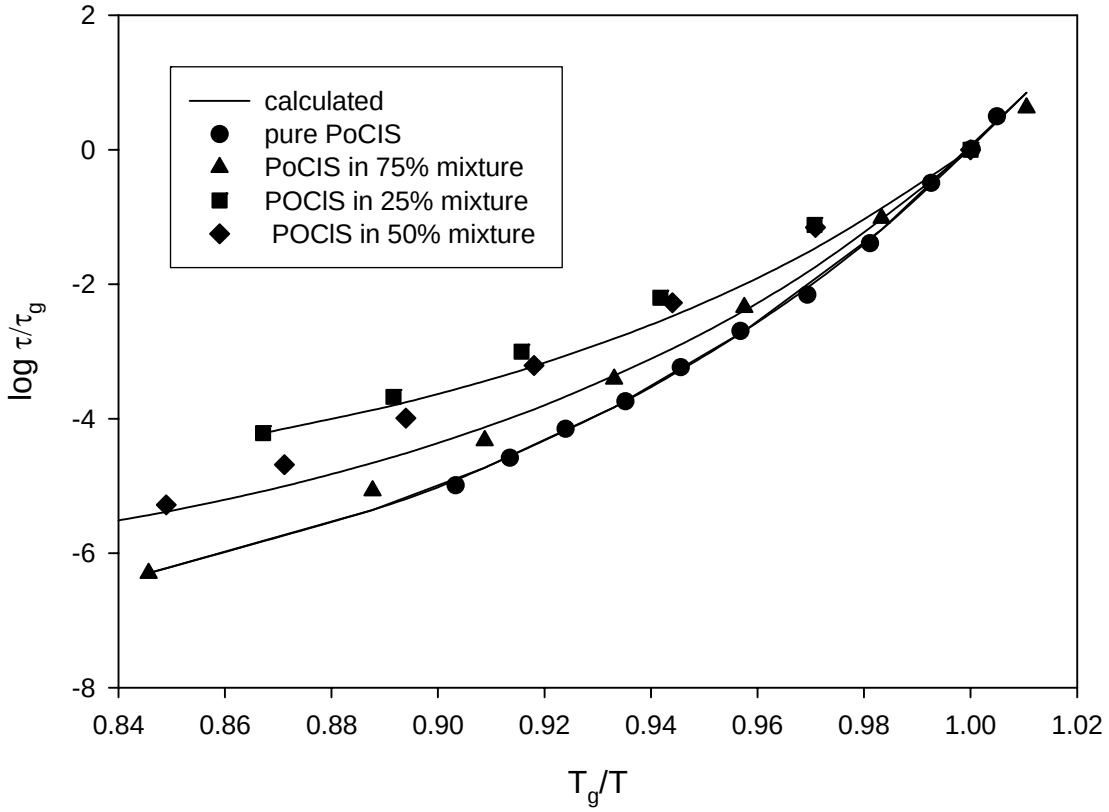

Figure 19 Plot of temperature dependence of relaxation time showing experimental data for pure PoClS (●), PoClS relaxation in 25wt% PoClS and PS mixture (■), in 50wt% PoClS and PS mixture (◆), and in 75 wt% PoClS and PS mixture (▲). Lines are fits of experimental data for pure PoClS, and calculated dielectric relaxation times for mixtures.

shows the experimental data for pure PoClS, and calculations of Eq. (43). For the 25 and 50 wt% PoClS mixtures, Eq. (44) was employed to calculate the dielectric relaxation of PoClS in the mixtures. For the 75 wt% PoClS mixture, Eq. (43) was used to calculate the dielectric relaxation for PoClS in the mixture. Table 7 and Fig. 19 show results for these calculations, and Table 7 lists experimental data (T_g, T_{f*}, and $\log_{10}(\tau_{f*}/\tau_g)$ or T_2, T_1, and $\log_{10}(\tau_1/\tau_2)$) used in the calculations. Data for this mixture spans the range from a concentration low in PoClS to one high in PoClS, with dielectric relaxation behavior visibly (in Fig. 19) changing through this range. Predictions for all cases using pure PoClS h_p gave good agreement with literature data.

6.6 Polyvinylmethylether and Polystyrene Mixture Data

Two compositions of the PVME and PS mixture were available[119], 50 wt% and 65 wt% PVME in PS. Eq. (43) was used to determine h_p = 1.90 x 10^{-20} J for pure PVME. Pure component values of T_g, T_{f*}, and $\log_{10}(\tau_{f*}/\tau_g)$ for PVME used to determine h_p are given in Table 8, as well as the value of R^2 for the regression. To obtain this value of h_p, one data point that appeared to be an outlier was eliminated from the experimental data set. Figure 20 shows the experimental data for pure PVME, and model values of Eq. (43). For the 50 and 65 wt% PVME mixtures, the dielectric relaxation of the PVME in the mixture was calculated by Eq. (43), with the pure component h_p. Figure 20 shows both the experimental data and the calculated values, while Table 8 lists the data (T_g, T_{f*}, and $\log_{10}(\tau_{f*}/\tau_g)$) used in the calculation and the values of R^2 achieved. Figure 20 also shows that the dielectric relaxation behavior of the two mixtures is markedly different, even though their compositions do not change nearly as much as the previous mixture examined, PoClS and PS. Nonetheless, pure PVME h_p once again gives good agreement with literature data.

Table 8 Dielectric relaxation was calculated for PVME in 2 compositions of a PVME and PS mixture[a] according to Eq. (43), based on the pure component h_p value for PVME of 1.90 x 10^{-20} J. Values of T_g were determined by linear interpolation at τ = 1 second for ambient pressure experimental data (except where denoted by * where a slight linear extrapolation was used to determine T_g) [a]. Experimental data also supplied values of $\log_{10}(\tau_{f*}/\tau_g)$ and T_{f*}. R^2 values were determined by comparison of calculated dielectric relaxation times for the PVME in the mixture with the experimental data, except for pure PVME, where R^2 is a measure of the goodness of fit of Eq. (43) to experimental data.

$wt\%_{PVME}$	50	65	100
T_g (K)	271.96	275.55	256.15
T_{f*} (K)	440.49	378.13	390.90
$\log_{10}(\tau_{f*}/\tau_g)$	-10.43	-3.19	-9.55
R^2	0.9972	0.9963	0.9973

[a]Reference 119.

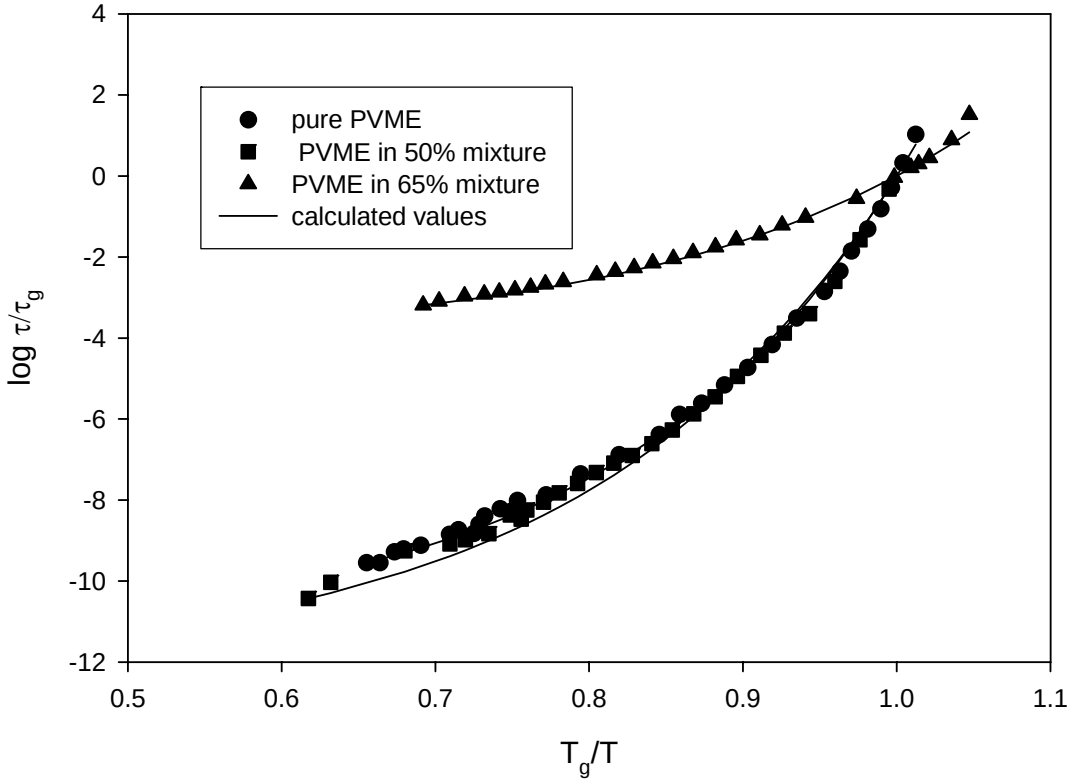

Figure 20 Plot of temperature dependence of relaxation time showing experimental data for pure PVME (●) PVME relaxation in 50 wt% PVME and PS mixture (■), and PVME relaxation in 65 wt% PVME and PS mixture (▲). Solid lines are fits of experimental data for pure PVME, and calculated dielectric relaxation times for mixtures.

6.7 Poly(2-chlorostyrene) and Polyvinylmethylether Mixture Data

A single blend of P2CS and PVME was available for analysis[125]. Eq. (43) was used to determine h_p = 3.13 x 10^{-20} J for pure P2CS. Pure component values of T_g, T_{f^*}, and $\log_{10}(\tau_{f^*}/\tau_g)$ for P2CS used to determine h_p are given in Table 9, as well as the value of R^2 for the regression. Figure 21 shows the experimental data for pure P2CS, and values calculated by Eq. (43). For the blend with PVME, the dielectric relaxation was calculated using Eq. (43) and the pure component h_p. Figure 21 shows both the experimental data and the calculated values, Table 9 lists the experimental data used in the calculation (T_g, T_{f^*}, and $\log_{10}(\tau_{f^*}/\tau_g)$), and the value of R^2 achieved. As can be seen in Fig. 21, the calculated dielectric relaxation deviates from the experimental values at higher values of T_g/T. Comparing the pure component data for P2CS and that for the P2CS in the blend, note that the pure component data does not cover the region of higher T_g/T. Likely the behavior of P2CS is this region was not captured by the pure component data set and thus is not reflected in the h_p determined. This is the explanation for the poor fit in this region. Since the mixture data set is broader, using it to determine h_p for P2CS would give a better result. Accordingly, the experimental data for P2CS in the mixture was regressed with Eq. (43) to find h_p = -1.55 x 10^{-21} J. This value of h_p was then employed, with pure component experimental values for T_g, T_{f^*}, and $\log_{10}(\tau_{f^*}/\tau_g)$, using Eq. (43) to calculate the dielectric relaxation for the pure P2CS. Results for this approach can also be seen in Fig. 21 as dashed lines. Data used in the calculation (values of T_g, T_{f^*}, and $\log_{10}(\tau_{f^*}/\tau_g)$) and resultant R^2 values are given in Table 9. This approach, a reversal of the method described above in that mixture data is used to determine h_p which is then employed to predict pure component dielectric relaxation, works well in this case.

Table 9 Left-most two columns: Dielectric relaxation was calculated for P2CS in a blend of PVME and P2CS[a] according to Eq. (43), based on the pure component h_p value for P2CS of 3.13 x 10^{-20} J. Right-most two columns: Dielectric relaxation was calculated for pure P2CS[a] according to Eq. (43), based on the blend h_p value for P2CS in PVME of -1.55 x 10^{-21} J. Values of T_g were determined by linear interpolation at $\tau = 1$ second of ambient pressure experimental data. Experimental data also supplied values of $\log_{10}(\tau_{f*}/\tau_g)$ and T_{f*}. R^2 values were determined by comparison of calculated dielectric relaxation times for the P2CS in the mixture (column 1) and for the pure P2CS (column 4) with the experimental data. For the blend P2CS and pure P2CS, (columns 2 and 3), R^2 is a measure of the goodness of fit of Eq. (43) to experimental data.

	Pure, regressed	blend, predicted	pure, predicted	blend, regressed
T_g (K)	392.69	303.96	392.69	303.96
T_{f*} (K)	444.34	348.50	444.34	348.5
$\log_{10}(\tau_{f*}/\tau_g)$	-5.23	-3.92	-5.23	-3.92
R^2	0.9990	0.9274	0.9859	0.9986

[a]Reference 125.

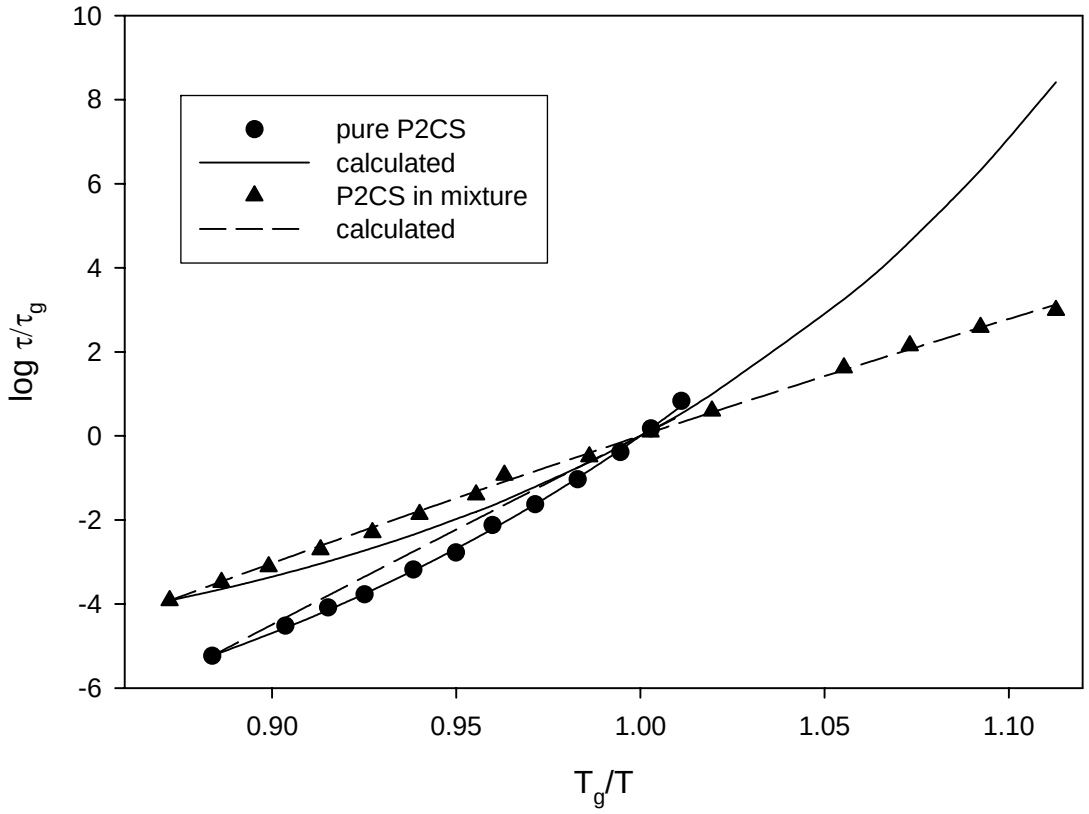

Figure 21 Plot of temperature dependence of relaxation time showing experimental data for pure P2CS (●) and P2CS relaxation in a mixture with PVME (▲). Solid lines are fits of experimental data for pure P2CS, and calculated dielectric relaxation for the mixture. Dashed lines are fits of experimental data for P2CS in the blend, and calculated dielectric relaxation times for pure P2CS.

Since the mixture data set is broader, it gives a more accurate value of h_p which is capable of predicting the pure component dielectric relaxation vs. temperature.

Eq. (43) was used to determine $h_p = 2.39 \times 10^{-20}$ J for the pure PVME used in the blend with P2CS. Figure 22 shows the experimental data for pure PVME, and values calculated by Eq. (43). Table 10 lists experimental data for T_g, T_{f^*}, and $\log_{10}(\tau_{f^*}/\tau_g)$ used in the regression and the R^2 value for the fit. For the blend with P2CS, Eq. (44) was applied to calculate the dielectric relaxation of PVME in the mixture, from the pure component h_p. Figure 22 shows both the experimental data and the calculated values. Table 10 lists the experimental data (for T_2, T_1, and $\log_{10}(\tau_1/\tau_2)$) used in the calculation as well as the resultant R^2 values. Two of the experimental data points were omitted in this exercise, as they appeared anomalous (i.e. they indicated that relaxation time did not change with decreasing temperature). The relaxation behavior of the PVME in the mixture differs from the pure behavior (see Fig. 22), as the shape of the dielectric relaxation vs. scaled temperature curves are not the same. Good agreement between literature data and prediction is still achieved, however.

6.8 Poly-cyclohexylacrylate-*stat*-butylmethacrylate and Polystyrene Mixture Data

Two compositions of the P(CHA-*stat*-BMA) and PS mixture were available[119], 50 wt% and 70 wt% P(CHA-*stat*-BMA) in PS. The pure P(CHA-*stat*-BMA) experimental data were regressed with Eq. (44) to obtain $h_p = 2.25 \times 10^{-20}$ J. Figure 23 shows the experimental data for pure P(CHA-*stat*-BMA), and model values of Eq. (44). Table 11 lists experimental data for T_2, T_1, and $\log_{10}(\tau_1/\tau_2)$ used in the regression, as well as the goodness of fit, R^2. For the 50 and 70 wt% P(CHA-*stat*-BMA) mixtures, the dielectric relaxation of the P(CHA-*stat*-BMA) in the mixture was calculated by Eq. (44), using pure component h_p. Figure 23 shows both the experimental data and the calculated

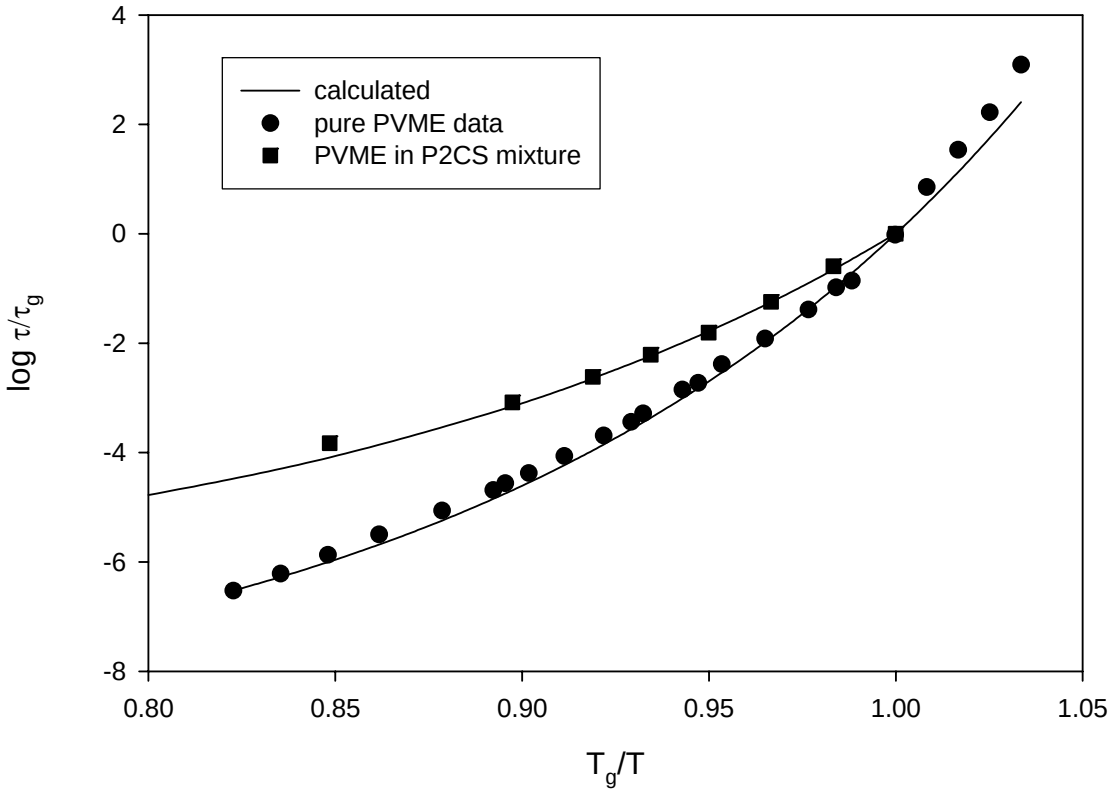

Figure 22 Plot of temperature dependence of relaxation time showing experimental data for pure PVME (●) and PVME relaxation in a blend with P2CS (■). Solid lines are fits of experimental data for pure PVME, and calculated dielectric relaxation times for the blend.

Table 10 Dielectric relaxation was calculated for PVME in a blend of PVME and P2CS[a] according to Eq. (43) or Eq. (44), based on the pure component h_p value for PVME of 2.39 x 10^{-20} J. The value of T_g for the pure PVME was determined by linear interpolation at $\tau = 1$ second for ambient pressure experimental data. The value of T_2 represents the lowest temperature data point in an ambient pressure experimental data set for the PVME in the blend. Experimental data also supplied values of $\log_{10}(\tau_{f*}/\tau_g)$ and T_{f*} $\log_{10}(\tau_1/\tau_2)$ and T_1. R^2 values were determined by comparison of calculated dielectric relaxation times for the PVME in the mixture with the experimental data. For pure PVME, R^2 is a measure of the goodness of fit of Eq. (43) to experimental data.

	pure, regressed	blend, predicted
T_g or T_2 (K)	250.35	283.24
T_{f*} or T_1 (K)	304.29	354.74
$\log_{10}(\tau_{f*}/\tau_g)$ or $\log_{10}(\tau_1/\tau_2)$	-6.52	-4.80
R^2	0.9921	0.9975

[a]Reference 125.

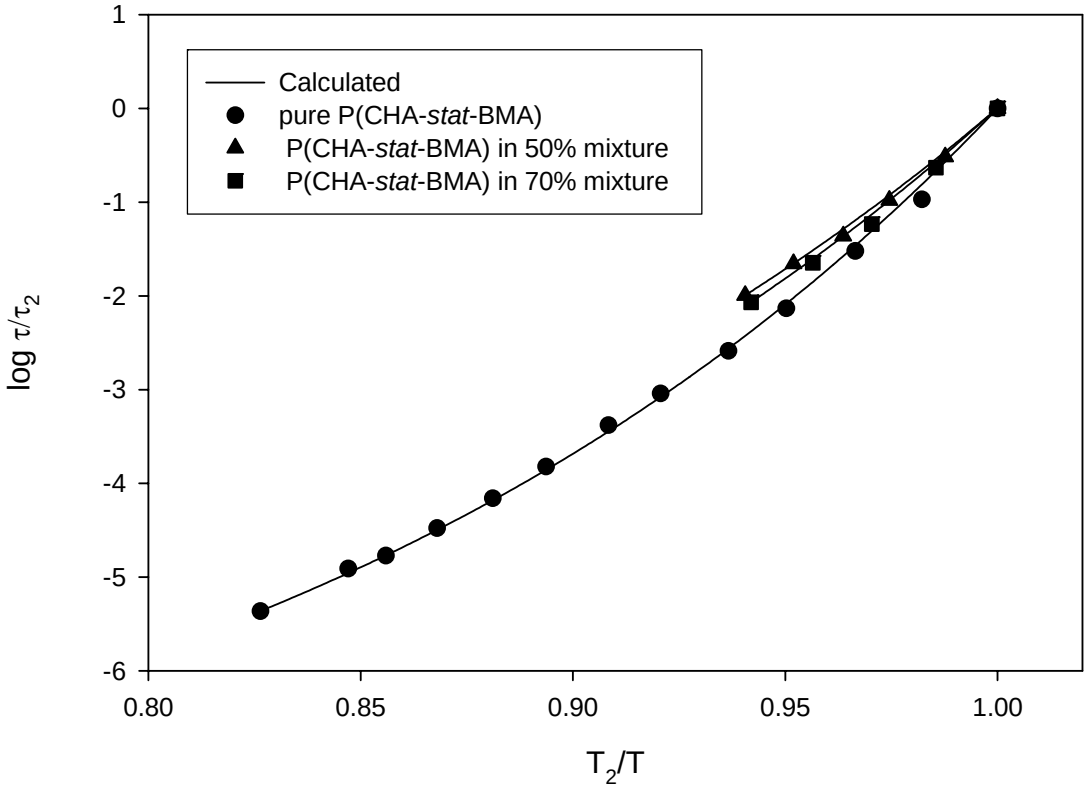

Figure 23 Plot of temperature dependence of relaxation time showing experimental data for pure P(CHA-*stat*-BMA) (●), P(CHA-*stat*-BMA) relaxation in 50 wt% P(CHA-*stat*-BMA) and PS mixture (▲), and in 70 wt% P(CHA-*stat*-BMA) and PS mixture (■). Lines are fits of experimental data for pure P(CHA-*stat*-BMA), and calculated dielectric relaxation times for mixtures.

Table 11 Dielectric relaxation was calculated for the P(CHA-*stat*-BMA) component in two compositions of a P(CHA-*stat*-BMA) and PS mixture[a] according to Eq. (44), based on the pure component h_p value for P(CHA-*stat*-BMA) of 2.25 x 10^{-20} J. Values of T_2 represent the lowest temperature data point in an ambient pressure experimental data set[a]. Experimental data also supplied values of $\log_{10}(\tau_1/\tau_2)$ and T_1. R^2 values were determined by comparison of calculated dielectric relaxation times for the P(CHA-*stat*-BMA) in the mixture with the experimental data, except for pure P(CHA-*stat*-BMA), where R^2 is a measure of the goodness of fit of Eq. (44) to experimental data.

$wt\%_{P(\text{CHA-}stat\text{-BMA})}$	50	70	100
T_2 (K)	332.96	323.40	297.75
T_1 (K)	354.01	343.33	360.30
$\log_{10}(\tau_1/\tau_2)$	-2.00	-2.07	-5.36
R^2	0.9979	0.9971	0.9987

[a]Reference 119.

values. Table 11 lists the experimental data (for T_2, T_1, and $\log_{10}(\tau_1/\tau_2)$) used in the calculation and the resultant R^2 values. For these two mixtures, the basic shape of the dielectric relaxation vs. scaled temperature curve appears the same as for the pure component, only offset (see Fig. 23). Predictions of the cluster kinetics model give good agreement with literature data in each case.

6.9 Conclusion

The cluster kinetics model approach, using pure component values of h_p with limited mixture data (two data points, the highest temperature and either the lowest temperature or the dielectric glass transition point), predicts mixture component behavior over a range of temperatures, mixture compositions (25 – 75%) and dielectric relaxations (-10.4 – 0.9). This has been demonstrated for a range of dielectric relaxation behaviors vs. scaled temperature, both where the component behavior is very similar to the pure behavior, and where it differs markedly. The method was tested for four binary glassformer mixtures. When the key parameter (h_p) can be determined accurately by a sufficiently large pure-component data set, the method proved reliable for available mixture data sets. The principal weakness is the need for some mixture data, at least two data points. Thus, the method is not fully predictive based solely on pure component data.

CHAPTER 7
APPLICATION OF THE CLUSTER KINETICS MODEL TO GLASSFORMERS IN SOLUTION

7.1 Introduction

For the purpose of this work, a glassformer solution is defined as occurring whenever a glassformer is dissolved in another component, whether the solvent is a glassformer itself or not, forming a well-mixed solution. Polymer solutions, where both solvent and solute are frequently glassformers, are important both industrially and for basic scientific research into changes in dynamic behavior of glassformers upon dissolution. Polymer solutions, while not frequently applied industrially, provide a representation for molecular processes in living organisms[126], and thus prediction of their properties is important. Segmental relaxation is commonly measured and studied in glassformer solutions.

The segmental relaxation of a glassformer in solution has been used to extrapolate a model parameter for pure solute[100], which was then used to describe relaxation of that component in a mixture. In addition, in a solution of polyvinylacrylate in toluene[127], a constant value of one of the VFTH parameters could be used to describe experimental data for the pure component as well as the component in solution. So, it would seem that the behavior of a glassformer in solution may be similar to its behavior in a mixture, the subject of the previous chapter. Whether the solute glassformer is relaxing independently of the solvent is a point of contention, however, since only one relaxation is measured for a glassformer in solution, and some studies indicate that the solute and solvent move cooperatively.[21,128] In this study the solute is treated independently in a quantitative

manner. The objective of the chapter is to show that a cluster kinetics model can predict dielectric relaxation of a glassformer in solution.

7.2 Background

Recent work has used glassformer solution data to predict behavior in a glassformer mixture[100]. Thus, since binary mixture behavior and solution behavior can be related, at least in one case, they are treated here with a common approach. As in the previous chapter, having determined the cluster kinetics model parameters from pure component data, one can then predict dielectric relaxation times for the same component in solution. If h and v for the pure compound are applied to the compound in solution, then the assumption must be that the compound exhibits a decided preference to cluster with itself, or clusters with the solvent to such a limited extent that h and v for the pure compound can still be applied. Since it is understood that the relaxation of the component in solution differs from the pure behavior, using the pure component v and h will require that this difference be accounted for in other parameters of the model. Therefore, the application of the cluster kinetics model to solutions also requires knowing the T_g of the solution as well as a fluid data point (i.e. τ_{f*} and T_{f*}) for the solution. Thus, while the solute is treated independently from the solvent, the dissolution effects are accounted for in the solution dielectric glass transition temperature and a solution fluid data point. For the data tested here this method is successful.

The concept underlying this approach is that glassformer behavior in solution is essentially unchanged from its pure state behavior, insofar as the parameters h and v are concerned. The impact of the solute is reflected in the change in dielectric glass transition temperature and of the fluid dielectric relaxation time for the solution. An explanation is based on the different environment of the component (i.e., it is no longer

surrounded by itself only). However, if the solute acts independently of the solvent, then its relaxation behavior (defined as how the dielectric relaxation changes with temperature and pressure) should remain unchanged, even though the absolute value of the dielectric relaxation at a given temperature is altered. In the context of the cluster kinetics model, this implies that h and v (or h_p) remain unchanged from the pure component values.

7.3 Method

Similarly to the previous chapter, for a solution of a glassformer h_p is again determined from pure component literature data for the glassformer by regression with Eq. (43). Dielectric relaxation in solution is calculated using h_p, the solution dielectric glass transition temperature, and the solution fluid dielectric relaxation time and temperature by application of Eq. (43). This result is then compared to literature data for the solution, by calculating an R^2 that indicates how well the prediction matches the experimental data.

7.4 Application to Experimental Data

The above procedure has been attempted for four solutions of glassformers: PVME dissolved in toluene[100], aqueous *nPG* (*n*-propylene glycol)[129], aqueous glycerol[126], and aqueous propylene glycol (PG).[126] The cluster kinetics model, as originally conceived, is a two-state model (see Eq. (44) in the previous chapter). In Eq. (43), the two states are expressed as glass and fluid.

However, any two states could be used, as shown by Eq. (44). State 1 is equivalent to the fluid condition (i.e. the highest temperature data point in a constant pressure data set) in applications in this work. The fourth solution was examined using the two-state model, a 75 % solution of aqueous PG[126], although the value of h_p here was determined from T_g, T_{f*} and $\log_{10}(\tau_{f*}/\tau_g)$.

7.5 Solution Data for Polyvinylmethylether in Toluene

For a solution of polyvinylmethylether (PVME) dissolved in toluene[100], five compositions were examined: 50, 60, 70, 80, and 88 wt% PVME. Pure component data for the PVME in solution with toluene were regressed with Eq. (43) to obtain h_p = 2.13 x 10^{-20} J. Figures 24 and 25 both show the experimental data for pure PVME, and calculated values of Eq. (43). Table 12 lists the values for T_g, T_{f^*}, and $\log_{10}(\tau_{f^*}/\tau_g)$ in the regression and the goodness of fit, R^2. For all PVME solutions, experimental data for T_g, T_{f^*}, and $\log_{10}(\tau_{f^*}/\tau_g)$ employed in the calculations of dielectric relaxation by Eq. (43) are given in Table 12, as well as values of R^2. Figure 24 shows both the experimental data and the calculated values for the 50, 60 and 70 wt% PVME solutions. Results for the 80 and 88 wt% PVME solutions are shown in Fig. 25. Figure 25 indicates that solution behavior approaches pure PVME behavior at the more concentrated solutions, as might be expected. The cluster kinetics model effectively predicts concentrated solution dielectric relaxation behavior.

7.6 Aqueous *n*-Propylene Glycol Solution Data

Four aqueous *n*-propylene glycol (*nPG*) solutions were analyzed: 20, 30, 40, and 50 wt% *nPG*.[129] Pure component data for the *nPG* were regressed with Eq. (43) to obtain h_p = 1.38 x 10^{-20} J. Figures 26 and 27 show the experimental data for pure *nPG*, and values from Eq. (43). Table 13 lists the experimental values for T_g, T_{f^*}, and $\log_{10}(\tau_{f^*}/\tau_g)$ employed in the regression, as well as the goodness of fit, R^2. For all the *nPG* solutions, experimental data (for T_g, T_{f^*}, and $\log_{10}(\tau_{f^*}/\tau_g)$) used in Eq. (43) to calculate dielectric relaxation of the *nPG* in solution are given in Table 13. Figure 26 shows both the experimental data and the calculated values for the 20 and 30 wt% *nPG* solutions whereas Fig. 27 shows this information for the 40 and 50 wt% solutions. These

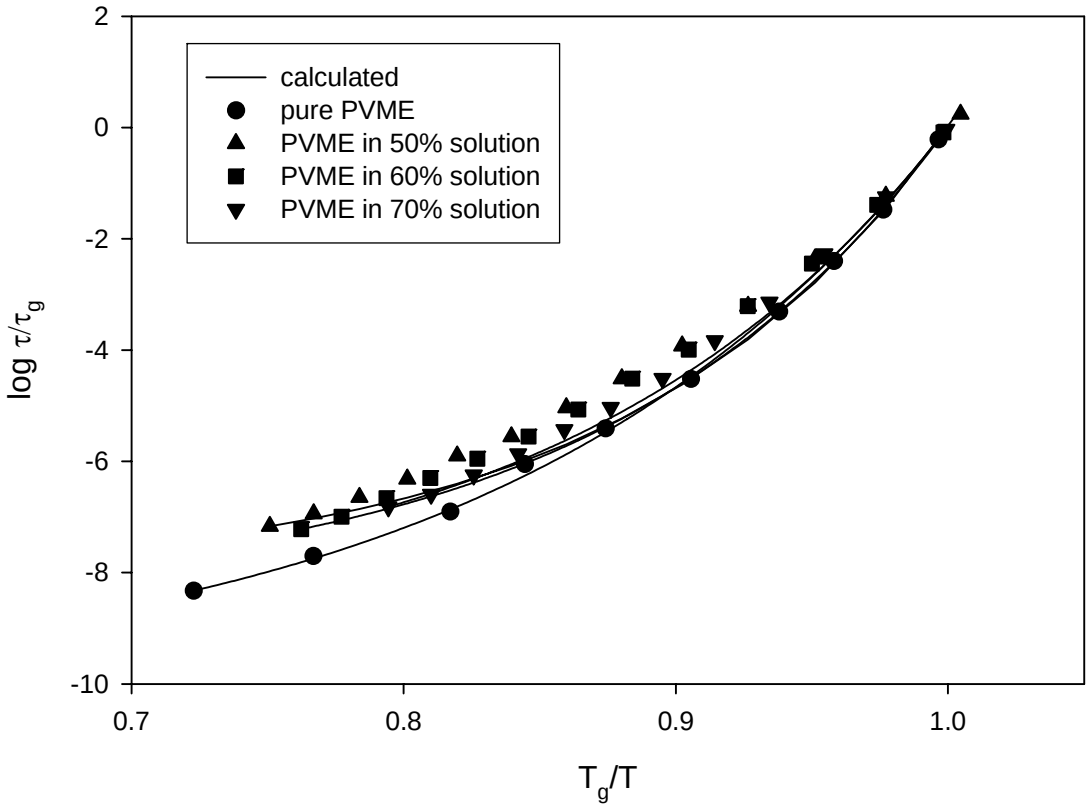

Figure 24 Plot of temperature dependence of relaxation time showing experimental data for pure PVME (●), PVME relaxation in 50 wt% PVME toluene solution (▲), PVME relaxation in 60 wt% PVME toluene solution(■), and PVME relaxation in 70 wt% PVME toluene solution. Lines are fits of experimental data for pure PVME, and calculated dielectric relaxation times for solutions.

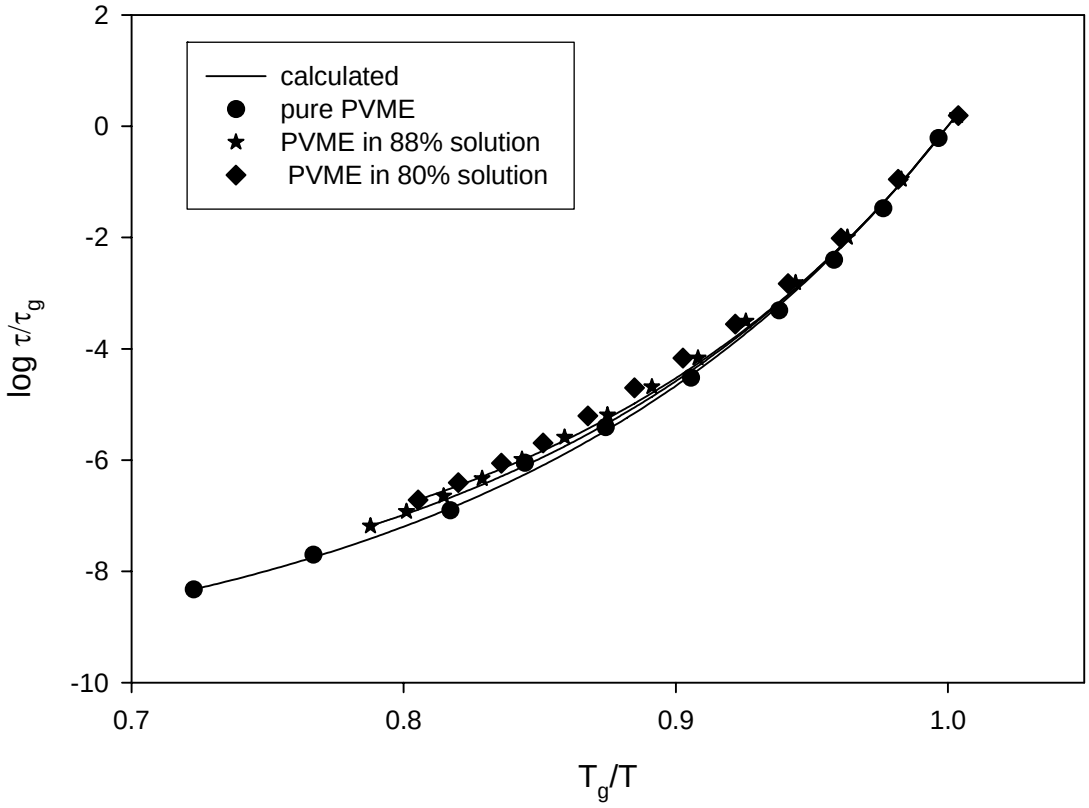

Figure 25 Plot of temperature dependence of relaxation time showing experimental data for pure PVME (●), PVME relaxation in 80 wt% PVME toluene solution (◆), and PVME relaxation in 88 wt% PVME toluene solution (★). Lines are fits of experimental data for pure PVME, and calculated dielectric relaxation times for solutions.

Table 12 Dielectric relaxation was calculated for PVME in five compositions of PVME and toluene solution[a] according to Eq. (43), with the pure component h_p value for PVME of 3.23 x 10^{-20} J. Values of T_g were determined by linear interpolation at τ = 1 second for ambient pressure experimental data[a] (except where indicated by an *, where an extrapolation of the experimental data was necessary). Experimental data also supplied values of $\log_{10}(\tau_{f*}/\tau_g)$ and T_{f*}. R^2 values were determined by comparison of calculated dielectric relaxation times for the PVME in the solution with the experimental data, except for pure PVME, where R^2 represents goodness of fit of Eq. (43) to experimental data.

$wt\%_{PVME}$	50	60	70	80	88	100
T_g (K)	178.67	192.68*	212.83	223.79	238.59	251.58
T_{f*} (K)	237.95	252.75	267.90	277.89	302.85	348.03
$\log_{10}(\tau_{f*}/\tau_g)$	-7.17	-7.22	-6.82	-6.72	-7.18	-8.32
R^2	0.9866	0.9907	0.9984	0.9978	0.9993	0.9988

[a]Reference 100.

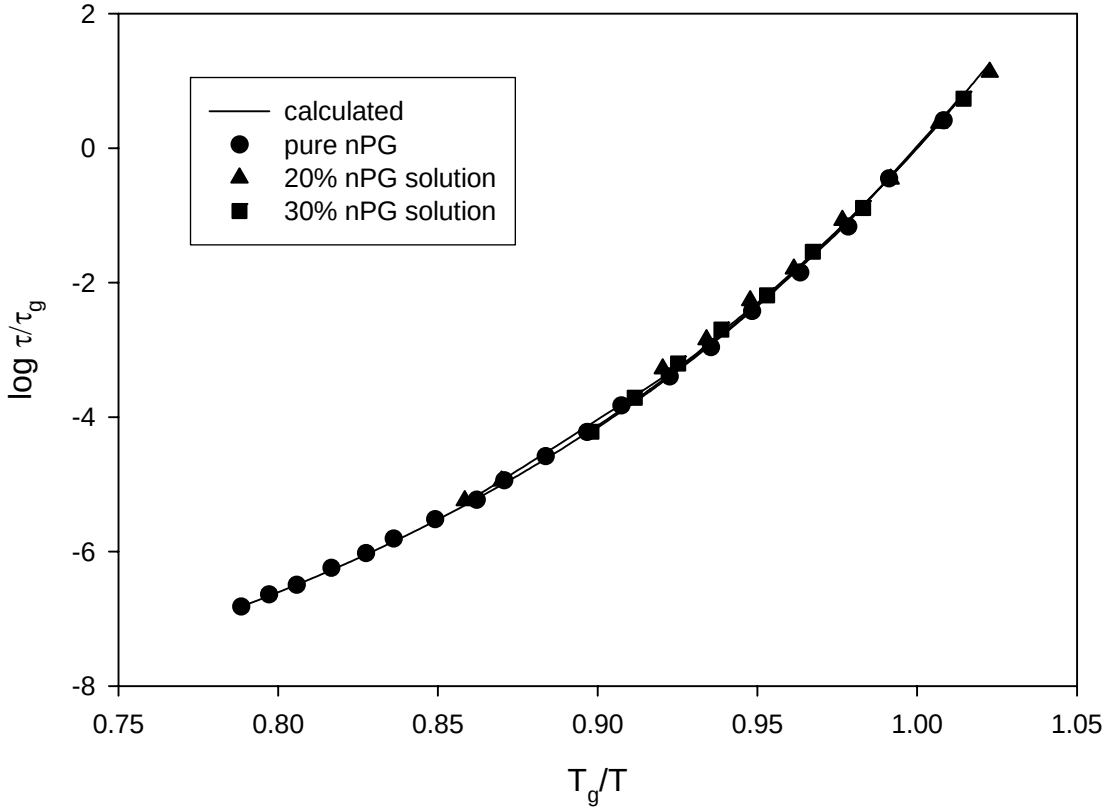

Figure 26 Plot of temperature dependence of relaxation time showing experimental data for pure *nPG* (●), *nPG* relaxation in 20 wt% aqueous *nPG* solution (▲), and *nPG* relaxation in 30 wt% aqueous *nPG* solution (■). Lines are fits of experimental data for pure *nPG*, and calculated dielectric relaxation times for solutions.

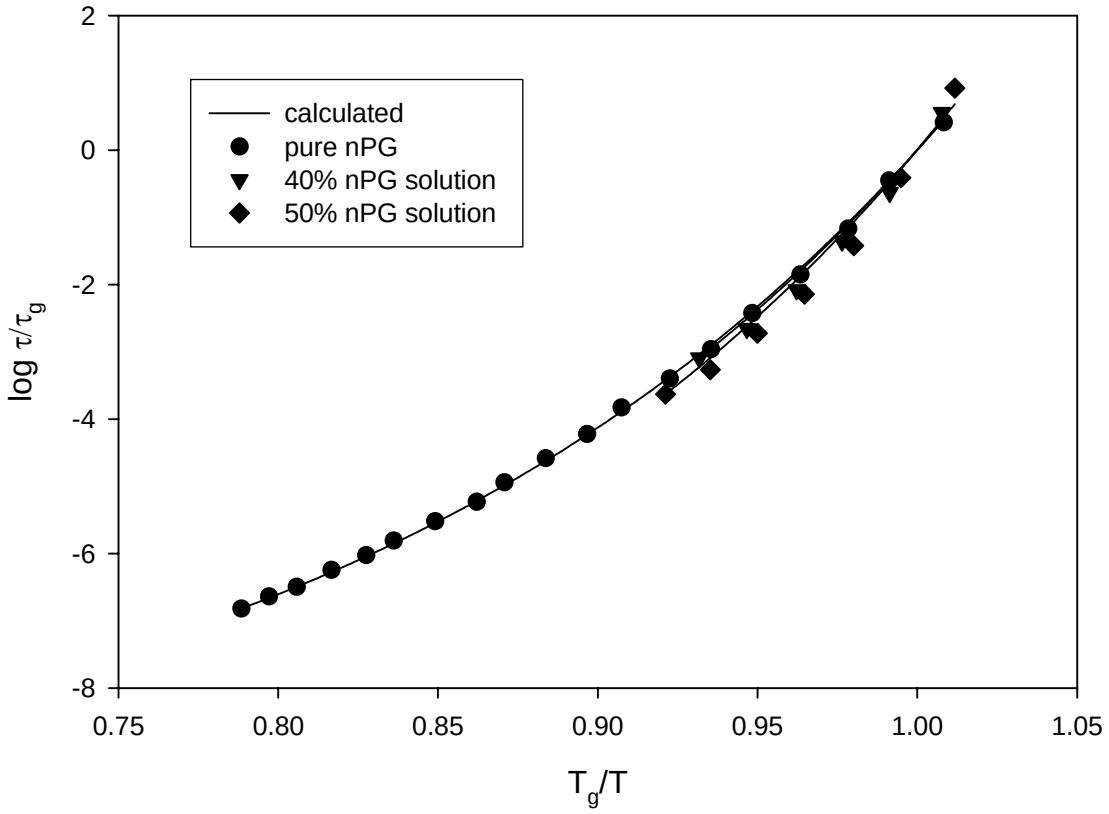

Figure 27 Plot of temperature dependence of relaxation time showing experimental data for pure *nPG* (●), *nPG* relaxation in 40 wt% aqueous *nPG* solution (▼), and *nPG* relaxation in 50 wt% *nPG* solution (◆). Lines are fits of experimental data for pure *nPG*, and calculated dielectric relaxation times for solutions.

Table 13 Dielectric relaxation was calculated for *nPG* in four compositions of an aqueous *nPG* solution[a] according to Eq. (43), based on the pure component h_p value for *nPG* of 1.38 x 10^{-20} J. Values of T_g were determined by linear interpolation at $\tau = 1$ second for ambient pressure experimental data[a]. Experimental data also supplied values of $\log_{10}(\tau_{f*}/\tau_g)$ and T_{f*}. R^2 values were determined by comparison of calculated dielectric relaxation times for the *nPG* in the solution with the experimental data, except for pure *nPG*, where R^2 represents goodness of fit of Eq. (43) to experimental data.

$wt\%_{nPG}$	20	30	40	50	100
T_g (K)	192.09	190.42	189.15	186.88	195.61
T_{f*} (K)	223.78	212.04	203.01	202.86	248.10
$\log_{10}(\tau_{f*}/\tau_g)$	-5.24	-4.22	-3.09	-3.63	-6.82
R^2	0.9989	0.9992	0.9910	0.9859	0.9996

[a]Reference 126.

solutions represent the more dilute solution case, versus the PVME in toluene case previously examined. Surprisingly, less change in dielectric relaxation behavior vs. the pure component behavior is apparent for these dilute solutions. Another anomaly that can be seen in Table 13 is that the more dilute solutions have a glass transition temperature closer to pure *nPG* than the more concentrated solutions, which is counterintuitive. However, since the cluster kinetics model uses the solution T_g directly, this anomaly does not prevent an accurate prediction. The cluster kinetics model predicts well in these cases, too.

7.7 Aqueous Glycerol Solution Data

For a solution of aqueous glycerol[126], data for five solutions were analyzed: 25, 33, 41.6, 50, and 75 wt% glycerol. Pure component data for the glycerol used in the aqueous solutions were regressed with Eq. (43) to obtain h_p = 8.88 x 10^{-21} J. Figures 28 and 29 show the experimental data for pure glycerol, and the fits of Eq. (43). Table 14 lists values of T_g, T_{f*}, and $\log_{10}(\tau_{f*}/\tau_g)$ used in the calculation. Figure 28 shows both the experimental data and the calculated values for the 25, 33, and 41.6 wt% aqueous glycerol solutions. Figure 29 shows the same information for the 50 and 75 wt% solutions. R^2 values for all solution compositions are also given in Table 14, indicating very good agreement of calculated dielectric relaxation with experimental data. Table 14 also lists values of T_g,T_{f*}, and $\log_{10}(\tau_{f*}/\tau_g)$ used in the calculations. These data sets essentially cover the range from more dilute to concentrated solutions of glycerol. Unlike the PVME in toluene, the more concentrated solutions do not appear (Fig. 29) to approach the pure glycerol relaxation behavior. The cluster kinetics model predicts relaxation behavior across the concentration range for this solution.

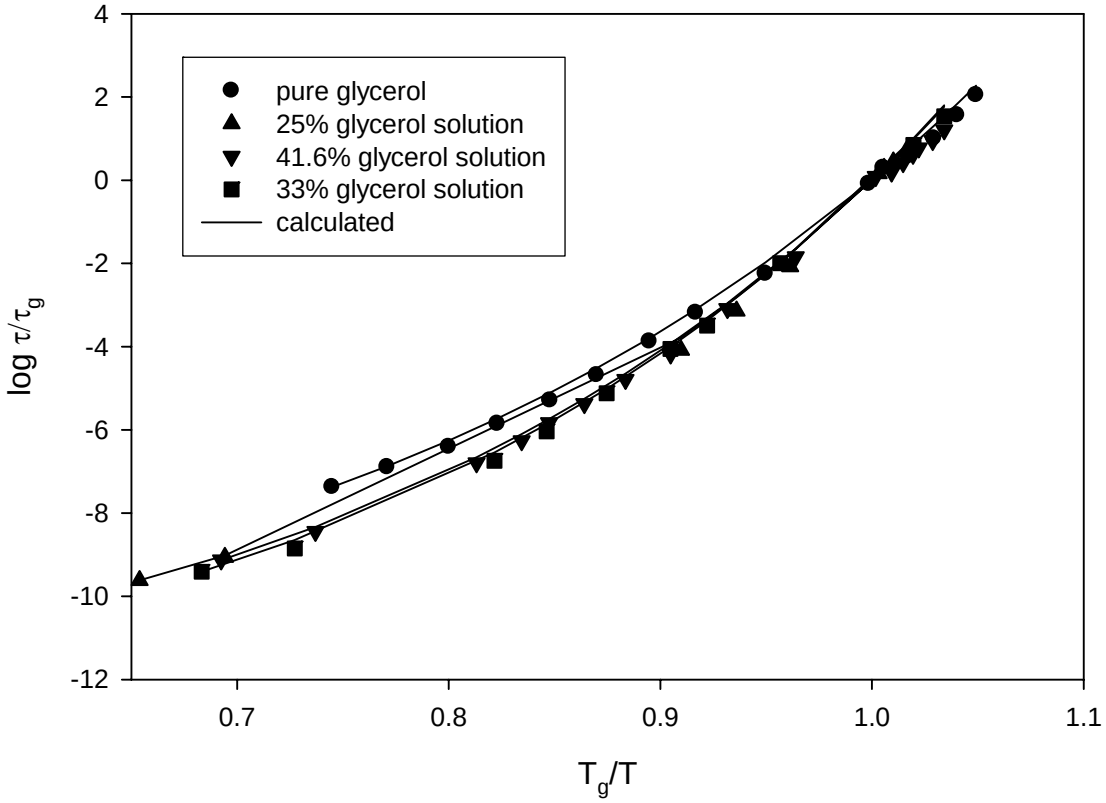

Figure 28 Plot of temperature dependence of relaxation time showing experimental data for pure glycerol (●), glycerol relaxation in 25 wt% aqueous glycerol solution (▲), glycerol relaxation in 33 wt% aqueous glycerol solution(■), and glycerol relaxation in 41.6 wt% aqueous glycerol solution (▼). Lines are fits of experimental data for pure glycerol, and calculated dielectric relaxation times for solutions.

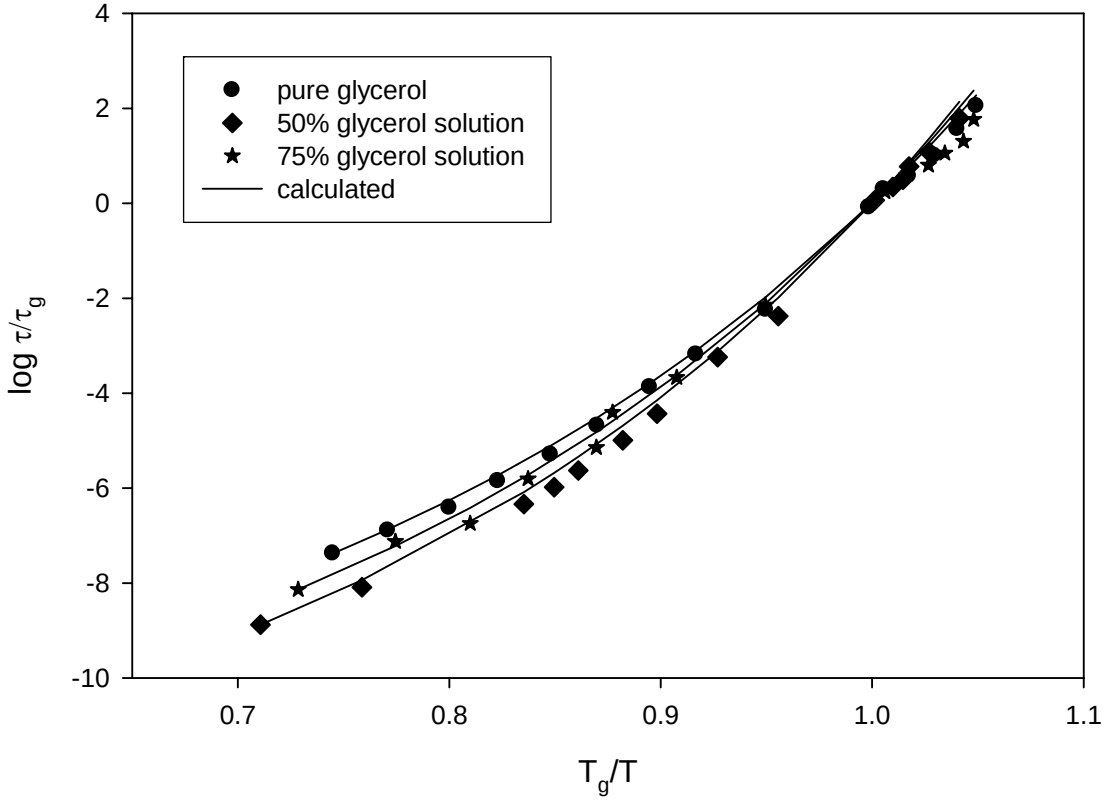

Figure 29 Plot of temperature dependence of relaxation time showing experimental data for pure glycerol (●), glycerol relaxation in 50 wt% aqueous glycerol solution (◆), and glycerol relaxation in 75 wt% aqueous glycerol solution (★). Lines are fits of experimental data for pure glycerol, and calculated dielectric relaxation times for solutions.

Table 14 Dielectric relaxation was calculated for glycerol in five compositions of an aqueous glycerol solution[a] according to Eq. (43), with the pure component values for glycerol of 8.88 x 10^{-21} J. Values of T_g were determined by linear interpolation at $\tau = 1$ second for ambient pressure experimental data[a]. Experimental data also supplied values of $\log_{10}(\tau_{f*}/\tau_g)$ and T_{f*}. R^2 values were determined by comparison of calculated dielectric relaxation times for the glycerol in the solution with the experimental data, except for pure glycerol, where R^2 represents the goodness of fit of Eq. (43) to experimental data.

$wt\%_{Glycerol}$	25	33	41.6	50	75	100
T_g (K)	172.51	180.27	182.7	188.56	192.81	196.92
T_{f*} (K)	263.82	263.83	263.86	265.31	264.65	264.36
$\log_{10}(\tau_{f*}/\tau_g)$	-9.61	-9.41	-9.13	-8.88	-8.14	-7.38
R^2	0.9988	0.9995	0.9991	0.9989	0.9961	0.9972

[a]Reference 126.

7.8 Aqueous Propylene Glycol Solution Data

For a solution of aqueous propylene glycol (PG)[126], data for a single solution (75 wt% PG) were analyzed. Pure component data for the PG were regressed with Eq. (43) to obtain $h_p = 9.36 \times 10^{-21}$ J. Figure 30 shows the experimental data for pure PG, and the fit of Eq. (43). Table 15 gives the experimental values for T_g, T_{f*}, and $\log_{10}(\tau_{f*}/\tau_g)$ used in the regression, as well as the goodness of fit, R^2. For the 75 wt% PG solution, with the pure component h_p, the dielectric relaxation of the PG in the solution was calculated by Eq. (44). Figure 30 shows both the experimental data and the calculated values. Table 15 lists the values of T_2, T_1, and $\log_{10}(\tau_1/\tau_2)$ used in the calculation. In this fairly concentrated solution, the dielectric relaxation behavior differs significantly from the pure component behavior (see Fig. 30). The cluster kinetics model nonetheless predicts solution behavior quite well.

7.9 Conclusion

The solutions examined above cover a broad range of compositions (from 20 to 88 wt%) as well as relaxation times (log τ from -9.6 to 1.8). In addition, the behaviors range from quite similar to pure component dielectric relaxation behavior vs. scaled temperature, to markedly different behavior. In all cases, the assumption that the dielectric relaxation behavior of the solute in the solution is unchanged from its pure state holds true. The cluster kinetics model approach, using pure component values of h_p with limited solution data (two data points, the highest temperature and either the lowest temperature or the dielectric glass transition point), predicts solution behavior over a range of temperatures and dielectric relaxations. The method was tested for four glassformer solutions and proved reliable for available solution data sets. The principal

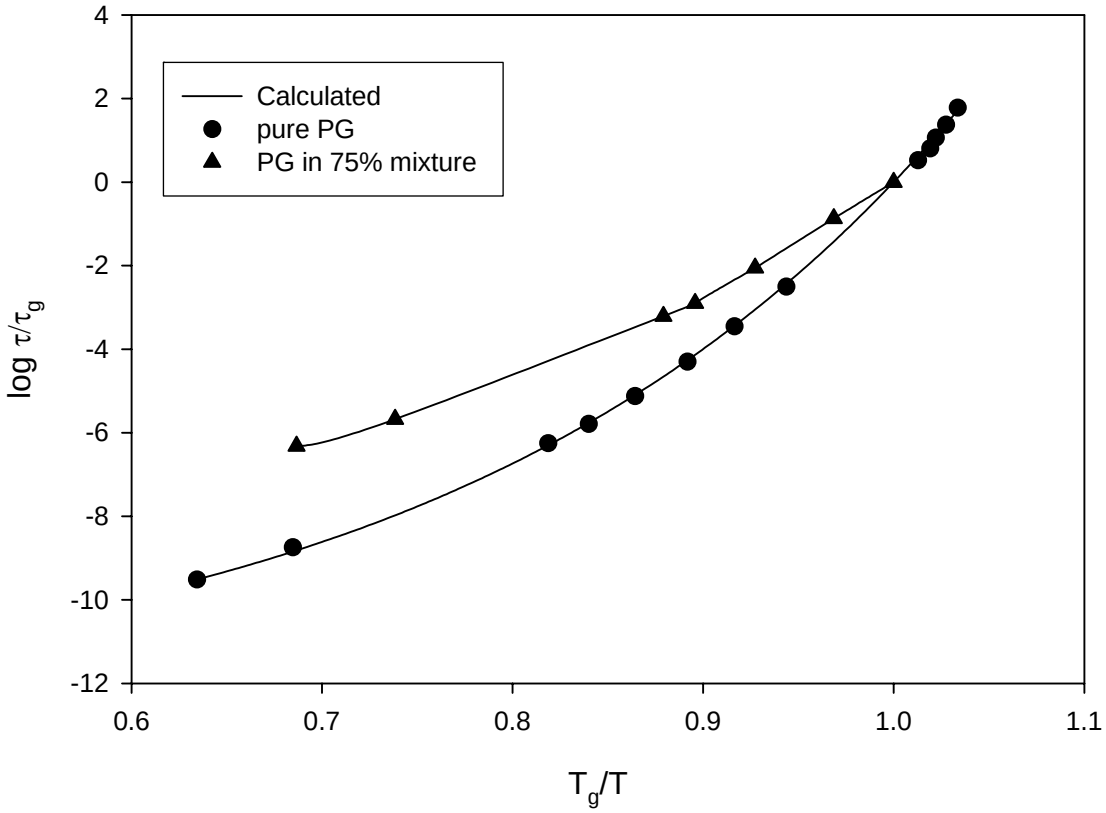

Figure 30 Plot of temperature dependence of relaxation time showing experimental data for pure PG (●) and PG relaxation in 75 wt% aqueous PG solution (▲). Lines are fits of experimental data for pure PG, and calculated dielectric relaxation times for the solution.

Table 15 Dielectric relaxation was calculated for PG in an aqueous solution according to Eq. (44), based on the pure component h_p value for PG of 9.36 x 10^{-21} J. The value of T_g for the pure PG was determined by linear interpolation at $\tau = 1$ second of ambient pressure experimental data. The value of T_2 represents the lowest temperature data point in an ambient pressure experimental data set for the PG in solution. Experimental data also supplied values of $\log_{10}(\tau_{f*}/\tau_g)$ and T_{f*} or $\log_{10}(\tau_1/\tau_2)$ and T_1. R^2 values were determined by comparison of calculated dielectric relaxation times for PG in solution with the experimental data. For pure PG, R^2 is a measure of the goodness of fit of Eq. (43) to experimental data.

$wt\%_{PG}$	75	100
T_g or T_2 (K)	191.7	177.71
T_{f*} or T_1 (K)	279.16	280.15
$\log_{10}(\tau_{f*}/\tau_g)$ or $\log_{10}(\tau_1/\tau_2)$	-6.32	-9.51
R^2	0.9996	0.9997

[a]Reference 126.

weakness is the need for some solution data, at least two data points. Thus, the method is not fully predictive based solely on pure component data.

CHAPTER 8
CONCLUSION

8.1 Conclusion

A cluster-kinetics model has been developed, based upon the concept that molecules cluster together as they approach the glass transition, and that this is the underlying physical phenomenon that explains glass formation. The model development made use of population balance equations for monomers and their clusters, which were solved for molar concentrations of monomers and clusters in terms of the rate coefficients. The rate coefficients of the reaction-like mechanisms that represent the cluster and monomer interactions were assumed independent of mass, and assumed to have transition state temperature and pressure dependence. The molar concentrations were then related to viscosity by the Turnbull-Cohen theory, resulting in a relation of temperature and pressure to viscosity or dielectric relaxation. The cluster kinetics model so developed has been shown to be applicable to wide variety of pure glassformers, including both small and large molecules and fragile and non-fragile compounds, as well as to glassformer mixtures, and solutions of glassformers. It has been successfully applied across a broad range of temperatures, pressures, and dielectric relaxation times. The cluster kinetics model is thus broadly applicable as a tool for explaining fundamental glass relaxation behavior and for interpreting experimental data. It is also fairly easy to apply, having only two parameters (h and v, the differences of activation energy and volume differences, respectively), meeting a goal of ready and straightforward applicability. The parameters h and v have been demonstrated to be invariant to pressure and temperature; parameters determined at one set of conditions could be applied at other temperatures and pressures to predict the dielectric relaxation at the new

conditions. This is evidence that h and v are properties of the compound, and not merely fitting parameters, and have physical meaning as the difference of activation energy and activation volumes differences. In addition, it was shown that the form of the model allows for a non-linear relationship of T_g to P_g, and vice versa, which is in accord with actual behavior seen in the published literature. Dielectric relaxation times for three binary mixtures of glassformers exhibiting a single dielectric relaxation vs. temperature or pressure were calculated by combining pure component cluster kinetics model parameters (h and v or h_p) according to a simple mixing relation. The cluster kinetics model approach, using pure component values of h_p with limited mixture data predicts mixture component behavior over a range of temperatures and dielectric relaxations for four binary mixtures exhibiting two distinct dielectric relaxations in response to temperature or pressure. The understanding underlying this approach to modeling of these mixtures is that the behavior of the component in the mixture is unchanged from the pure component as far as the cluster kinetics model equation parameters h and v *or* h_p are concerned, since these are properties of the compound. Successful predictions of dielectric relaxation time have been demonstrated for a range of dielectric relaxation behaviors vs. scaled temperature, both where the mixture component behavior is very similar to the pure behavior, and where it differs markedly. When the key parameter (h_p) can be determined accurately by a sufficiently large pure-component data set, the method proved reliable for available mixture data sets. A similar approach allowed use of the cluster kinetics model to predict glassformer solution dielectric relaxation for four solutions. The solutions examined covered a broad range of compositions as well as relaxation times. As in the mixture case, the solution behaviors ranged from quite similar to pure component dielectric relaxation behavior vs. scaled temperature to notably different behavior. In all cases, the assumption that the dielectric relaxation behavior of the solute in

the solution is unchanged from its pure state holds true. The cluster kinetics model approach, based on pure component values of h_p with limited mixture or solution data, predicts solution behavior over a range of temperatures and dielectric relaxations. The principal weakness of the cluster kinetics modeling approach for mixtures and solutions is the need for some mixture or solution data, at least two data points, these being necessary to take into account missing and dissolution effects. Thus, the method is not fully predictive based solely on pure component data.

REFERENCES

[1]T. Scopigno, G. Ruocco, F. Sette, and G. Monaco, Science **302**, 849 (2003).

[2]M.D. Ediger, Annu. Rev. Phys. Chem. **51**, 99 (2000).

[3]M.L. Falk, Science **318**, 1880 (2007).

[4]S. Sastry, Nature **409**, 164 (2001).

[5]S. Hensel-Bielowka, M. Paluch, J. Ziolo, and C.M. Roland, J. Phys. Chem. B **106**, 12459 (2002).

[6]J. Wiedersich, N.V. Surovtsev, and E. Rössler, J. Chem. Phys. **113**, 1143 (2000).

[7]S. Pawlus, R. Casalini, C.M. Roland, M. Paluch, S.J. Rzoska, and J. Ziolo, Phys. Rev. E 7**0**, 061501 (2004).

[8]P.G. Debenedetti and F.H. Stillinger, Nature **410**, 259 (2001).

[9]C.M. Roland, S. Hensel-Bielowka, M. Paluch, and R. Casalini, Rep. Prog. Phys. **68** 1405 (2005).

[10] C.A. Daniels, Polymers(CRC Press, Boca Raton, FL 1989).

[11]O.V. Mazurin, Glass Phys. Chem. **33,** 22 (2007).

[12]R.J. Seyler, Assignment of the Glass Transition (ASTM International, West Conshohocken, PA 1994).

[13]H.C. Andersen, PNAS **102**, 6686 (2005).

[14] A. Alegría, C. Elizetxea, I. Cendoya, and J. Colmenero, Macromolecules **28,** 8819 (1995).

[15]C.M. Roland, R. Casalini, P. Santangelo, M. Sekula, J. Ziolo, and M. Paluch, Macromolecules **36,** 4954 (2003).

[16]R. Casalini, M. Paluch, and C.M. Roland, J. Phys. Chem. A **107,** 2369 (2003).

[17] S.S.N. Murthy, J. Phys. Chem. **100,** 8508 (1996).

[18] C.M. Roland and R. Casalini, Macromolecules **36,** 1361 (2003).

[19] S.P. Andersson and O. Andersson, Macromolecules **31,** 2999 (1998).

[20] M. Paluch, M. Sekula, S. Pawlus, S.J. Rzoska, J. Ziolo, and C.M. Roland, Phys. Rev. Lett. **90,** 175702 (2003).

[21] S.H. Zhang and J. Runt, J. Polym. Sci., Part B: Polym. Phys. **42,** 3405 (2004).

[22] E. Donth, The Glass Transition, Relaxation Dynamics in Liquids and Disordered Materials (Springer Verlag, Berlin 2001).

[23]H. Vogel, Phys. Z. **22**, 645 (1921); G.S. Fulcher, J. Am. Chem. Soc. **8**, 339 (1923); G. Tammann and W. Hesse, Z. Anorg. Allg. Chem. **156**, 245 (1926).

[24]H. Leyser, A. Schulte, W. Doster, and W. Petry, Phys. Rev. E **51**, 5899 (1995).

[25] S. Pawlus, M. Paluch, M. Sekula, K.L. Ngai, S.J. Rzoska, and J. Ziolo, Phys. Rev. E **68,** 021503 (2003).

[26]G. Fytas, T. Dorfmüller, and C.H. Wang, J. Phys. Chem. **87,** 5041 (1983).

[27]M. Paluch, S. Pawlus, and C.M. Roland, Macromolecules **35**, 7338 (2002).

[28]G.P. Johari and E. Whalley, Faraday Symp. Chem. Soc. **6,** 23 (1972).

[29]M.H. Cohen and D. Turnbull, J. Chem. Phys. **31,** 1164 (1959).

[30]A.K. Doolittle and D.B. Doolittle, J. Appl. Phys. **28,** 901 (1957).

[31]G. Dlubek, D. Kilburn, and M.A. Alam, Electrochim. Acta **50,** 2351 (2005).

[32]R. Simha and T. Somcynsky Macromolecules **2,** 342 (1969).

[33]G. Dlubek, D. Kilburn, and M.A. Alam, Electrochim. Acta **49,** 5241(2004).

[34]G. Dlubek, J. Wawryszczuk, J. Pionteck, T. Gowrek, H. Kaspar, and K.H. Lochhass, Macromolecules **38,** 429 (2005).

[35]T. Pakula and J. Teicmann, Mater. Res. Soc. Symp. Proc. **455,** 211 (1997).

[36]T. Pakula, J. Mol. Liq. **86,** 109 (2000).

[37]K. Pasterny, M. Paluch, K. Grzybowka, and A. Grzybowski, J. Mol. Liq. **109,** 137 (2004).

[38]M.H. Cohen and G.S. Grest, Phys. Rev. B **20,** 1077 (1979).

[39]M.H. Cohen and G.S. Grest J. Non-Cryst. Solids **61/62,** 749 (1984).

[40]G.S. Grest and M.H. Cohen, Phys. Rev. B **21,** 4113 (1980).

[41]G.S. Grest and M.H. Cohen, Adv. Chem. Phys. **48,** 455 (1981).

[42]S. Corezzi, S. Capaccioli, R. Casalini, D. Fioretto, M. Paluch, and P.A. Rolla, Chem. Phys. Lett. **320,** 113 (2000).

[43]L. Comez, S. Corezzi, D. Fioretto, H. Kriegs, A. Best, and W. Steffen, Phys. Rev. E **70,** 011504 (2004).

[44]M. Paluch, R. Casalini, and C.M. Roland, Phys. Rev. E **67,** 021508, (2003).

[45]J.T. Bendler and M.F. Schlesinger, J. Mol. Liq. **36,** 37 (1987).

[46]J.T. Bendler and M.F. Schlesinger, J. Stat. Phys. **53,** 531 (1988).

[47]J.T. Bendler, J.J. Fontanella, and M.F. Schlesinger, Phys. Rev. Lett. **87,** 195503 (2001).

[48]M. Paluch, S. Hensel-Bielowka, and T. Psurek, J. Chem. Phys. **113,** 4374 (2000).

[49]M. Paluch, C.M. Roland, and S. Pawlus, J. Chem. Phys. **116,** 10932 (2002).

[50]M. Paluch and C.M. Roland, J. Non-Cryst. Solids **316,** 413 (2003).

[51]I. Avramov, J. Non-Cryst. Solids **262,** 258 (2000).

[52]A. Patkowski, J. Gapiński, and G. Meier, Colloid Polym. Sci. **282**, 874 (2004).

[53]R. Casalini and C.M. Roland, Phys. Rev. B **71,** 014210 (2005).

[54]G. Adam and J.H. Gibbs, J. Chem. Phys. **43,** 139 (1965).

[55]R. Casalini, S. Capaccioli, M. Lucchesi, P.A. Rolla, and S. Corezzi, Phys. Rev. E **63,** 031207 (2001).

[56]C.A. Angell, J. Cond. Matter Phys. **12,** 6463 (2000).

[57]K.L. Ngai, J. Phys. Chem. B **103,** 5895 (1999).

[58]M. Goldstein, Phys. Rev. B **71,** 136201 (2005).

[59]D. Prevosto, M. Lucchesi, S. Capaccioli, R. Casalini, and P.A. Rolla, Phys. Rev. B **71,** 136202 (2005).

[60]W.C.K. Poon, J. Phys.: Condens. Matter **14,** R859 (2002).

[61]T.G. Smagala and B.J. McCoy, Chem. Eng. Sci. **61,** 3 (2005).

[62]A. Zucca, D.L. Marchisio, A.A. Barresi, and R.O. Fox, Chem. Eng. Sci. **61,** 87 (2006).

[63]G. Madras and B.J. McCoy, J. Crystal Growth **279,** 466 (2005).

[64]E. L. Haseltine, J.B. Rawlings, and J. Yin, Comp. Chem. Eng. **29,** 675 (2005).

[65]Y.P. Jeon and B.J. McCoy, Physical Review E **72,** 037104 (2005).

[66]G. Madras and B.J. McCoy, Handbook of Breakage (Elsevier, Amsterdam 2007).

[67]G. Madras and B.J. McCoy, Chem. Eng. Sci. **62,** 5257 (2007).

[68]J. Yang, B.J. McCoy, and G. Madras, J. Chem. Phys. **124,** 024713 (2006).

[69]D.M. Himmelblau and K.B. Bischoff, Process Analysis and Simulation – Deterministic Systems (John Wiley & Sons, New York 1968).

[70]K.N. Pham, A.M. Puertas, J. Bergenholtz, S.U. Egelhaaf, A. Moussaïd, P.N. Pusey, A.B. Schofield, M.E. Cates, M. Fuchs, and W.C.K. Poon, Science **296,** 104 (2002).

[71]C.A. Angell, B.E. Richards, and V. Velikov, J. Phys.: Condens. Matter **11,** A75 (1999).

[72]B.J. McCoy, J. Phys. Chem. Solids **63**, 1967 (2002).

[73]J.P.K. Doye, D.J. Wales, F.H.M. Zetterling, and M. Dzugutov, J. Chem. Phys. **118**, 2792 (2003).

[74]M. Dzugutov, S.I. Simdyankin, and F.H.M. Zetterling, Phys. Rev. Lett. **89**, 195701 (2002).

[75]P. Sandkühler, J. Sefcik, and M. Morbidelli, J. Phys. Chem. B **108**, 20105 (2004).

[76]P. Sandkühler, J. Sefcik, and M. Morbidelli, Langmuir **21**, 2062 (2005).

[77]M. Goldstein, J. Phys. Chem. B Lett. **110**, 9772 (2006).

[78]L. Berthier, G. Biroli, J.P. Bouchaud, L.Cipelleti, D. El Masri, D. L'Hôte, F. Ladieu, and M. Pierno, Science **310**, 1797 (2005).

[79]B.J. McCoy and G. Madras, J. Colloid Interface Sci. **201**, 200 (1998).

[80]D.J. Lacks, Phys. Rev. Lett**. 80**, 5385 (1998).

[81]D. Frenkel, Science **296,** 65 (2002).

[82]D.L. Malandro and D.J. Lacks, J. Chem. Phys. **107,** 5804 (1997).

[83]R.D. Mountain, *Supercooled Liquids – Advances and Novel Applications, ACS Symposium Series No. 676*, **676**, 122 (1997).

[84]M.G. Evans and M. Polanyi, Trans. Faraday Society **34**, 11 (1938).

[85]K. Jacobs, D. Zaziski, E.C. Scher, A.B. Herhold, and A.P. Alivisatos, Science **293**, 1803 (2001).

[86]P.G. Debenedetti, Metastable Liquids—Concepts and Principles (Princeton University Press, Princeton 1996).

[87]D. Turnbull and M.H. Cohen, J. Chem. Phys. **34**, 120 (1961).

[88]A.K. Doolittle, J. Appl. Phys. **22**, 1471 (1951).

[89]C.A. Angell, Science **267**, 1924 (1995).

[90]R. Casalini, S. Capaccioli, S. Presto, M. Lucchesi, P.A. Rolla, S. Corezzi, and M. Paluch, IEEE Trans. Dialect. El. In. **8,** 395 (2001).

[91]M. Paluch, M. Sekula, S. Maślanka, K. Mańczyk, W.W. Sulkowski, S.J. Rzoska, and J. Ziolo, J. Chem. Phys. **120,** 2020 (2004).

[92]M. Paluch, J. Gapiński, A. Patkowski, and E.W. Fischer, J. Chem. Phys**. 114,** 8048 (2001).

[93]C.M. Roland, T. Psurek, S. Pawlus, and M. Paluch, J. Polym. Sci., Part B: Polym. Phys. **41,** 3047 (2003).

[94]S.J. Rzoska, M. Paluch, S. Pawlus, A. Drozd–Rzoska, J. Ziolo, J. Jadzyn, K. Czuprynski, and R. Dabrowski, Phys. Rev. E **68**, 031705 (2003).

[95]T.P. Lodge and T.C.B. McCleish, Macromolecules **33**, 5278 (2000).

[96]S.K. Kumar, R.H. Colby, S.H. Anastasiadis, and G. Fytas, J. Chem. Phys. **105**, 3777 (1996).

[97]C.M. Roland, S. Capaccioli, M. Lucchesi, and R. Casalini, J. Chem. Phys. **120**, 10640 (2004).

[98]G. Katana, E.W. Fischer, Th. Hack, V. Abetz, and F. Kremer, Macromolecules **28**, 2714 (1995).

[99]E. Leroy, A. Alegría, and J. Colmenero, Macromolecules **36**, 7280 (2003).

[100]G.A. Schwartz, D. Cangialosi, A. Alegría, and J. Colmenero, J. Chem. Phys. **124**, 154904 (2006).

[101]W. Huang and R. Richert, J. Chem. Phys. **124**, 164510 (2006).

[102]K. Duvvuri and R. Richert, J. Phys. Chem. B **108**, 10451 (2004).

[103]C. Svanberg, R. Bergman, P. Jacobsson and L. Börjesson, Phys. Rev. B **66**, 054304 (2002).

[104]A.R.E. Brás, M.T. Viciosa, C.M. Rodrigues, C.J. Dias, and M. Dionísio, Phys. Rev. E **73**, 061709 (2006).

[105]S.H. Zhang, R. Casalini, J. Runt, and C.M. Roland, Macromolecules **36**, 9917 (2003).

[106]K. Mpoukouvalas, G. Floudas, S.H. Zhang, and J. Runt, Macromolecules **38**, 552 (2005).

[107]I. Cendoya, A. Alegría, J.M. Alberdi, J. Colmenero, H. Grimm, D. Richter, and B. Frick, Macromolecules **32**, 4065 (1999).

[108]K.L. Ngai and S. Capaccioli, J. Phys. Chem. B **108**, 11118 (2004).

[109]D. Cangialosi, G.A. Schwartz, A. Alegría and J. Colmenero, J. Chem. Phys. **123,** 144908 (2005).

[110]D. Cangialosi, A. Alegría, and J. Colmenero, Macromolecules **39,** 7149 (2006).

[111]M. Paluch, S. Hensel-Bielowka, R. Casalini, and C.M. Roland, J. Chem. Phys. **116,** 9839 (2002).

[112]K. Schröter and E. Donth, J. Chem. Phys. **113,** 9101 (2000).

[113]A. Faivre, G. Niquet, M. Maglione, J. Fornazero, J.F. Jal, and L. David, Euro. Phys. J. B **10,** 277 (1999).

[114]Y. Yomogida, A. Minoguchi, and R. Nozaki, Phys. Rev. E **73,** 041510 (2006).

[115] S.H. Zhang, P.C. Painter and J. Runt, Macromolecules **35**, 8478 (2002).

[116]S.H. Zhang, P.C. Painter and J. Runt, Macromolecules **35**, 9403 (2002).

[117]A. Minoguchi, K. Kitai, and R. Nozaki, Phys. Rev. E **68**, 031501 (2003).

[118]M. Paluch, C.M. Roland, S. Pawlus, J. Ziolo, and K.L. Ngai, Phys. Rev. Let. **91,** 115701 (2003).

[119] Y. He, T.R. Lutz, and M.D. Ediger, J. Chem. Phys. **119,** 9956 (2003).

[120] R. Pérez Aparicio, A. Arbe, J. Colmenero, B. Frick, L. Willner, D. Richter, and L.J. Fetters, Macromolecules **39,** 1060 (2006).

[121] S. Kamath, R.H. Colby, S.K. Kumar, K. Karatasos, G. Floudas, G. Fytas, and J.E.L. Roovers, J. Chem. Phys. **111,** 6121 (1999).

[122] Y. Hirose, O. Urakawa, and K. Adachi, Macromolecules **36,** 3699 (2003).

[123] E.J. Donth, Relaxation and Thermodynamics in Polymers (Akademie Verlag, Berlin 1992).

[124]B. Min, X. Qiu, M.D. Ediger, M. Pitsikalis, and N. Hadjichristidis, Macromolecules **34**, 4466 (2001).

[125] C.M. Roland, K.J. McGrath, and R. Casalini, Macromolecules **39,** 3581 (2006).

[126] S.S.N. Murthy, J. Phys. Chem. B **104,** 6955 (2000).

[127] M. Yada, M. Nakazawa, O. Urakawa, Y. Morishima, and K. Adachi, Macromolecules **33**, 3368 (2000).

[128] S. Sudo, M. Shimomera, K. Kanari, N. Shinyashiki, and S. Yagihara, J. Chem. Phys. **124**, 044901 (2006).

[129] S. Cerveny, G.A. Schwartz, A. Alegría, R. Bergman, and J. Swenson, J. Chem. Phys. **124**, 194501 (2006).

APPENDIX:
ADDITIONAL DETAILS RELATED TO CHAPTER 3 MODEL DEVELOPMENT

A.1 Explanation of Terms

The terms in Eqs. (11) and (12) in Chapter 3 can be related to Eqs. (9) and (10) (the reaction-like mechanisms) in that same chapter. Those equations are re-written here for reference as Eqs. (A1) and (A2):

$$\boldsymbol{C}(x) + \boldsymbol{M}(x_m) \underset{k_d}{\overset{k_g}{\leftrightarrows}} \boldsymbol{C}(x + x_m), \tag{A1}$$

$$\boldsymbol{C}(x) + \boldsymbol{C}(x') \underset{k_b}{\overset{k_a}{\leftrightarrows}} \boldsymbol{C}(x + x'). \tag{A2}$$

The cluster and monomer balances are also re-written here for reference, as Eqs. (A3) and (A4):

$$\partial c/\partial t = -k_g c\int_o^{\infty} m(x')dx' + k_g\int_o^{x} c(x\text{-}x')m(x')dx' - k_d\, c + k_d\int_x^{\infty} c(x')\,\delta[x\text{-}(x'\text{-}x_m)]\,dx' -$$

$$2k_a c\int_o^{\infty} c(x')dx' + k_a\int_o^{x} c(x')c(x\text{-}x')dx' - k_b\, c + 2k_b\int_x^{\infty} c(x')dx'/x' + I\,\delta(x\text{-}x^*) \tag{A3}$$

$$\partial m/\partial t = -k_g m(x)\int_o^{\infty} c(x')dx' + k_d\int_x^{\infty} c(x')\,\delta(x\text{-}x_m)dx' - I\delta(x-x^*)x^*/x_m. \tag{A4}$$

Beginning first with the cluster balance, the terms in Eq. (A3) are:

Term1: $-k_g c\int_o^{\infty} m(x')dx'$

Term 1 proceeds from the loss of clusters due to the forward reaction in Eq. (A1). In this formulation, the cluster can react with any monomer, represented by the integral from zero to

infinity. Note that the integral term is just the definition of the zeroth moment for the monomer.

Term2: $k_g \int_0^x c(x\text{-}x')m(x')dx'$

Term 2 proceeds from the gain of clusters due to the forward reaction in Eq. (A1). In this formulation, the reaction is re-written as:

$$\boldsymbol{C}(x\text{-}\ x') + \boldsymbol{M}(x') \xrightarrow{k_g} \boldsymbol{C}(x) \qquad \text{(A5)}$$

because the balance of interest is over the clusters produced, not those lost. The range of the integral stems from the observation that while x' is a distribution of sizes, it may only take a value lower than x.

Term 3: $-k_d\, c$

results from the loss of clusters due to the reverse reaction in Eq. (A1). To obtain this result, the reaction is re-written as:

$$\boldsymbol{C}(x) \xrightarrow{k_d} \boldsymbol{C}(x\text{-}\ x') + \boldsymbol{M}(x') \qquad \text{(A6)}$$

Term 4: $k_d \int_x^\infty c(x')\ \delta[x\text{-}(x'\text{-}x_m)]\ dx'$

Term 4 proceeds from the gain of clusters due to the reverse reaction in Eq. (A1). The δ portion of the term signifies that the resultant cluster is always of size $(x' - x_m)$ (see Eq. (A9) below). The limits of integration require that x' be no less than x. The provenance of these limits can be seen if the reaction is re-written as:

$$\boldsymbol{C}(x') \xrightarrow{k_d} \boldsymbol{C}(x) + \boldsymbol{M}(x'\text{-}\ x) \qquad \text{(A8)}$$

The reaction is can also be re-written as:

$$\boldsymbol{C}(x') \xrightarrow{k_d} \boldsymbol{C}(x' - x_m) + \boldsymbol{M}(x_m) \qquad \text{(A9)}$$

which shows more clearly the resultant cluster size.

Term 5: $-2k_a c\int_0^{\infty} c(x')dx'$

represents the loss of cluster due to the forward reaction in Eq. (A2). Two clusters are lost, thus the number 2 in the term. The clusters may have any size, therefore the integral is from zero to infinity.

Term 6: $k_a\int_0^{x} c(x')c(x-x')dx'$

accounts for the gain of clusters due to the forward reaction in Eq. (A2). To obtain this formulation, the reaction is re-written as:

$$\boldsymbol{C}(x- x') + \boldsymbol{C}(x') \xrightarrow{k_a} \boldsymbol{C}(x). \qquad \text{(A10)}$$

Note that x' cannot exceed x, thus the limits of integration are from zero to x.

Term 7: $-k_b\, c$

This term represents loss of clusters due to the reverse reaction in Eq. (A2) To obtain this result, the reaction is re-written as:

$$\boldsymbol{C}(x) \xrightarrow{k_b} \boldsymbol{C}(x') + \boldsymbol{C}(x- x'). \qquad \text{(A8)}$$

Term 8: $2k_b\int_x^{\infty} c(x')dx'/x'$

represents cluster gain via the reverse reaction in Eq. (A2). The number two appears in this term because two clusters are created each time a single cluster breaks apart. The $(1/x')$ portion of the term is a random breakage kernel, used because the cluster can break apart

randomly, creating two clusters of various sizes. To obtain this formulation, the reaction is re-written as:

$$\boldsymbol{C}(x') \xrightarrow{k_b} \boldsymbol{C}(x) + \boldsymbol{C}(x'- x). \qquad \text{(A9)}$$

Note that x' is a distribution of sizes, but must always be greater than x, thus the limits of integration shown. The final term in Eq. (A3) is related to nucleation.

Examining the terms in the monomer balance (Eq. (A4)) gives:

Term 1: $-k_g m(x)\int_0^{\infty} c(x')dx'$

which represents loss of monomer due to the forward reaction in Eq. (A1). The limits of integration reflect the monomer reacting with the full distribution of cluster sizes.

Term 2: $k_d\int_x^{\infty} c(x')\,\delta(x-x_m)dx'$

represents gain of monomer due to the reverse reaction in Eq. (A1). The δ indicates that a monomer of size x_m always results from the break up of the cluster. Re-writing the reaction as:

$$\boldsymbol{C}(x') \xrightarrow{k_d} \boldsymbol{M}(x) + \boldsymbol{C}(x' - x). \qquad \text{(A11)}$$

shows why the limits of integration are from x to infinity. This reaction can also be written as:

$$\boldsymbol{C}(x') \xrightarrow{k_d} \boldsymbol{M}(x_m) + \boldsymbol{C}(x' - x_m). \qquad \text{(A12)}$$

which shows more clearly that a monomer of size x_m always results from the breaking apart of the cluster. The final term in Eq. (A4) represents nucleation.

As described in Chapter 3, Eqs. (A3) and (A4) can be converted to moment forms by the application of Eq. (13). The resultant moment equations are re-written here for reference as Eqs. (A13) and (A14):

$$dc^{(n)}/dt = -(k_d + k_g m^{(0)})c^{(n)} + \sum_{j=0}^{n} ({}^{n}_{j})\, x_m^{n-j}\, c^{(j)}[(-1)^{n-j} k_d + k_g m^{(0)}] - 2k_a c^{(0)} c^{(n)} +$$

$$k_a \sum_{j=0}^{n} ({}^{n}_{j})\, c^{(j)}\, c^{(n-j)} - k_b c^{(n)} + 2k_b c^{(n)}/(n+1) + I\, x^{*n} \qquad \text{(A13)}$$

and

$$dm^{(n)}/dt = [k_d\, x_m{}^n - k_g m^{(n)}]c^{(0)} - I\, x^{*n} x^*/x_m \qquad \text{(A14)}$$

A.2 Explanation of terms in moment equations

Each term in Eqs. (A13) and (A14) results from applying the operation $\int_0^\infty [\,]\, x^n\, dx$. However, some of the terms require additional mathematical manipulation to obtain the final form shown in Eqs. (A13) and (A14). Here those terms that are not straightforward will be explained. The terms immediately below refer to the values from the previous section of this Appendix for the cluster balance.

Term 2:

Applying the moment operation:

$$k_g \int_0^\infty x^n dx \int_0^x c(x-x')m(x')dx'$$

Reversing the order of integration:

$$k_g \int_0^\infty m(x')dx' \int_{x'}^\infty c(x-x')\, x^n dx$$

Let $y = x\text{-}x'$ and $dy = dx$ and substitute in

$$k_g \int_0^\infty m(x')dx' \int_0^\infty c(y)(y+x')^n\, dy$$

Let $(y+x')^n = \sum_{j=0}^{n} ({}^{n}_{j})\, y^{n-j}\, x'^{\,j}$ and substitute where $({}^{n}_{j})$ are the binomial expansion

coefficients. Note that the summation is taken outside the integral.

$$k_g \sum_{j=0}^{n} \binom{n}{j} \int_0^{\infty} m(x')\, x'^{j}\, dx' \int_0^{\infty} c(y)\, y^{n-j}\, dy$$

where $m^{(j)} = \int_0^{\infty} m(x')\, x'^{j}\, dx'$ and $c^{(n-j)} = \int_0^{\infty} c(y)\, y^{n-j}\, dy$

Rewriting gives the final form seen in Eq. (A13):

$$k_g \sum_{j=0}^{n} \binom{n}{j} m^{(j)}\, c^{(n-j)}$$

Term 4

Applying the moment operation

$$k_d \int_0^{\infty} x^n dx \int_X^{\infty} c(x')\delta[x - (x' - x_m)]dx'$$

Reversing the order of integration:

$$k_d \int_0^{\infty} c(x')\, dx' \int_0^{x'} x^n\, \delta[x - (x' - x_m)]\, dx$$

The second integral can be solved because $x' > x' - x_m$ (so integrating past the spike); The second integral becomes $(x' - x_m)^n$.

Substitute this result and apply $(x' - x_m)^n = \sum_{j=0}^{n} \binom{n}{j} (-1)^j\, x'^{n-j}\, x_m^{\,j}$

$$k_d \sum_{j=0}^{n} \binom{n}{j} (-1)^j\, x_m^{\,j} \int_0^{\infty} c(x')\, x'^{n-j}\, dx'$$

where $c^{n-j} = \int_0^{\infty} c(x')\, x'^{n-j}\, dx'$

Note that the summation was taken outside integral.

The final value as shown in Eq. (A13) is:

$$k_d \sum_{j=0}^{n} \binom{n}{j} (-1)^j x_m^j c^{(n-j)}$$

Term 6

Applying the moment operation:

$$k_a \int_0^{\infty} x^n dx \int_0^{x} c(x')\, c(x - x')\, dx'$$

Reversing the order of integration:

$$k_a \int_0^{\infty} c(x')\, dx' \int_{x'}^{\infty} x^n\, c(x - x')\, dx$$

Define $(y+x')^n = \sum_{j=0}^{n} \binom{n}{j} y^{n-j} x'^{j}$ and substitute, taking the summation outside the integral:

$$k_a \sum_{j=0}^{n} \binom{n}{j} \int_0^{\infty} x'^{j}\, c(x')\, dx' \int_0^{\infty} c(y)\, y^{n-j}\, dy$$

where $c^{(j)} = \int_0^{\infty} x'^{j}\, c(x')\, dx'$ and $c^{(n-j)} = \int_0^{\infty} c(y)\, y^{n-j}\, dy$

Recognizing moments to get the final form shown in Eq. (A13:

$$k_a \sum_{j=0}^{n} \binom{n}{j} c^{(j)}\, c^{(n-j)}$$

Term 8

Applying the moment operation:

$$2\, k_b \int_0^{\infty} x^n dx \int_x^{\infty} c(x')\, (1 / x')\, dx'$$

Reversing the order of integration

$$2\,k_b \int_0^{\infty} c(x')\,(1/x')\,dx' \int_0^{x'} x^n\,dx$$

Now solving the second integral to obtain $\int_0^{x'} x^n\,dx = (x'^{n+1}) / (n+1)$ and

substituting,

$$2\,k_b \int_0^{\infty} c(x')\,(1/x')\,dx'\,(x'^{n+1}) / (n+1) = 2k_b / (n+1) \int_0^{\infty} c(x')\,x'^{n}\,dx'$$

Recognizing the moment gives the final form seen in Eq. (A13)

$$2k_b\,c^{(n)} / (n+1)$$

There is one term in the monomer balance that may not be sufficiently clear without additional explanation. The derivation of the final form of term 2 in the monomer balance is given below.

Term 2

Applying the moment operation

$$k_d \int_0^{\infty} x^n\,dx \int_x^{\infty} c(x')\,\delta(x - x_m)\,dx'$$

Reversing the order of integration

$$k_d \int_0^{\infty} c(x')\,dx' \int_0^{x'} x^n\,\delta(x - x_m)\,dx$$

Recognizing that $\int_0^{\infty} c(x')\,dx' = c^{(n)}$ and $\int_0^{x'} x^n\,\delta(x - x_m)\,dx = x_m{}^n$ and re-writing

gives the final form seen in Eq. (A14):

$$k_d \, c^{(n)}_{x_m} \, n$$

VITA

Lisa Ann Brenskelle graduated from Carnegie Mellon University in 1989 with the degrees of Bachelor of Science in Chemical Engineering, with an option in computer-aided control and design, and Bachelor of Arts in French, German, and Spanish. Her first position after college was in the research and development department of Ethyl Corporation at their Houston, Texas, plant site. She worked there for almost three years, doing a variety of projects, the largest and most time-consuming of which was a controls system upgrade. Lisa then moved on to a process controls engineer position with BOC Process Plants in New Jersey in 1992. She remained with BOC for nearly eight years, taking an applications engineer position with ExxonMobil Chemical in Baton Rouge, Louisiana, in 2000. Lisa initially began work part-time on a Master of Science degree in chemical engineering with Dr. Armando B. Corripio as her advisor at the Louisiana State University and Agricultural and Mechanical College in 2001, transitioning to the doctoral program in 2003 upon the retirement of Dr. Corripio, working with Dr. Benjamin J. McCoy She left ExxonMobil in 2003 and spent some time working on her doctoral studies full-time. After completion of the residency requirement at the university, Lisa returned to work in industry in 2005, taking a process controls engineering position with Marathon Oil Corporation in Garyville, Louisiana. At the same time, Dr. McCoy left the university and Dr. Martin A. Hjortsø agreed to become Lisa's advisor. Lisa has published two papers with Dr. McCoy, and a third has been submitted for publication, all in the Journal of Chemical Physics. She has also presented her work at three consecutive American Institute of Chemical Engineers conferences (2005, 2006, and 2007). Lisa remains employed with Marathon Oil today, although she now works in Houston, Texas, on a long-term temporary assignment.